12-2018

Impedance Sensing of Cancer Cells Directly on Sensory Bioscaffolds of Bioceramics Nanofibers

Hanan Alismail
University of Arkansas, Fayetteville

Impedance Sensing of Cancer Cells Directly on Sensory Bioscaffolds of Bioceramics Nanofibers

A dissertation submitted in partial fulfillment
of the requirement for the degree of
Doctor of Philosophy in Cell and Molecular Biology

by

Hanan Alismail
King Saud bin Abdul Aziz
Bachelor of Science in Clinical Laboratories, 2008
University of Arkansas
Master of Science in Cell and Molecular Biology, 2013

December 2018
University of Arkansas

This dissertation is approved for recommendation to the Graduate Council

_____
Z. Ryan Tian, Ph.D.
Dissertation Director

_____
Yuchun Du, Ph.D.
Committee Member

_____
Ralph Henry, Ph.D.
Committee Member

_____
David Paul, Ph.D.
Committee Member

_____
Radwan Alfaouri, Ph.D.
Committee Member

Abstract

Cancer cell research has been growing for decades. In the field of cancer pathology, there is an increasing and long-unmet need to develop a new technology for low-cost, rapid, sensitive, selective, label-free (i.e. direct), simple and reliable screening, diagnosis, and monitoring of live cancerous and normal cells in same (or similar) shape and size from the same anatomic region. For the first time based on an electrochemical impedance signal, the breast cancer and normal cells have been thus screened, diagnosed and monitored on a smart bioscaffold of entangled nanowires of bioceramics titanate. The bioscaffold was grown and self-assembled directly on the surface of implantable Ti-metal following a patent from Tian-lab, and characterized by means of SEM, XRD, etc. On the smart bioscaffold in aqueous solutions of phosphate buffer saline (PBS), human breast benign (MCF7) and aggressive (MDA-MB231) cancer cells, normal (MCF10A) cells, and colon cancer cells (HCT116) showed characteristic impedance highly different than that of the blank sensor. For two sets of mixtures each mixing the normal and cancer cells, the impedance signals have shifted linearly with the wide range of mixing ratios, showing the biosensor's selectivity and reliability. After being treated with glucose and chemotherapeutic drug (i.e. doxorubicin or DOX), different breast cancer cells showed different impedance signals from their difference in glucose metabolisms (i.e. Warburg Effect) and in resistances to the Dox, thus-fingerprinting the cells easily. Based on the nanostructure chemistry, impedance equivalent circuitry and cancer cell biology, it's the different cells surface binding on the nanowires, and different cancer cells metabolic wastes from the different treatments on the nanowires that changed the charge density on the scaffolding nanowire surface and in turn changed the impedance signals. This new sensor is believed generally expandable to quantifying and characterizing live cells and even biological tissues of different types in future.

Acknowledgements

I am heartily thankful to Dr. Tian, the thesis director and my academic father, whose encouragement, guidance, kindness, and support from the initial to the final level enabled me to develop a deep understanding of this subject. I highly appreciate his effort to give his best to all Ph.D. students in our group.

It is a pleasure to thank those who made this thesis possible, especially my thesis committee members: Dr. Du, Dr. Paul, Dr. Henry & Dr. Alfaouri, without their assistance, this degree would not have been successful. Special thanks to Dr. Paul for teaching me the equivalent circuitry and the impedance measurements. Thanks to Dr. Alfaouri for giving me the opportunity to work with him in the biophysics field and being able to contribute in a co-authored paper. I also thank Dr. Muldoon's and Dr. Shi's graduate students, Haley James and Zhijian Hu, for their help and assistance. I would like also to thank Dr. Zhou for her help in cell culture.

I would like to thank my passed away dad, Abdulaziz Alismail, for giving me his trust and life experience to persuade my successes and being proud of my accomplishments. Without my mom, Fawziyah Aljafari, encouragement, I would not have finished the degree. Many thanks to all my friends, Qusay, Asya, Parker, Seaab, Jacob, our lab members, and my cousin, Mashaeel Alismail, for supporting and encouraging me during my studies.

Lastly, I offer my regards and blessings to King Saud bin Abdulaziz University for health science who sponsored and supported me to pursue my Ph.D. degree

Dedication

This work is dedicated to all researchers past and present who have made extensive efforts to improve health care and diagnostics.

Table of Contents:

PART I **1**

Chapter 1. Introduction **1**

1.1 Overview of Current Cancer Diagnosis and Research **1**

1.2 The Importance and Motivation **2**

1.3 Dissertation Structure **2**

Chapter 2. Overview of Cell membrane and Metabolism **4**

2.1 Cell Structure and Its Function **4**

2.1.1 Cell membrane structure 4

2.1.2 Transportation across the biomembranes 5

2.2 Normal vs Cancer Cell Metabolism **7**

2.2.1 Normal cell metabolism 7

2.2.2 Warburg effect and cancer cell metabolic symbiosis 8

Chapter 3. Impedance Cell Biosensing Based on Nanomaterial **12**

3.1 Cell Biosensing Using Impedance **12**

3.2 Nanostructured Biomaterials and Biosensors **16**

3.2.1 Development of nanostructured biomaterials 16

3.2.2 Nanofibrous bioscaffolds as extracellular matrix analogues 17

3.3 TiO_2-Based Nanostructured Bioceramics **19**

3.3.1 Syntheses of TiO2 –based nanostructures 19

3.3.2 Commonly seen nanostructures and dimensions of TiO2- based bioceramics 20

3.3.3 Properties and applications of TiO2–based nanobioceramics 21

3.4 Biosensors Based on Nanowires **23**

3.4.1 Silicon nanowires for biosensing—the state-of-art at present 26

3.4.2 Titanate nanowires for biosensing—the game changer 28

Chapter 4. Major Methods for The Characterization 30

4.1 Power X-Ray Diffraction (PXRD) 30

4.2 Scanning Electron Microscopy (SEM) 31

4.3 Electrochemical Impedance Spectroscopy (EIS) 33

4.4 Randal's Equivalent Circuit 34

Part II 37

Chapter 5. Materials, Chemicals and Experimental 37

5.1 Materials and Chemicals 37

5.2 Experimental 38

5.2.1 TiO2- nanowire hydrothermal synthesis 38

5.2.2 The nanowire characterization 38

5.2.3 Bioimpedance cell sensing on the titanate nanowires 41

5.2.4 Microscopic visualization using Fluoresce staining 43

5.2.5 Error analysis 44

Chapter 6. Results and Discussions 45

6.1 Nanowire Characterization 45

6.1.1 X-ray diffraction (XRD) 45

6.1.2 Scanning electron microscope SEM 46

6.1.3 Point-of-Zero-Change (PZC) on H(Na)-Titanate 48

6.1.4 Impedance characterization for the titanate nanowires-entangled cell-nests 49

6.2 Impedance Sensing of Live Cell on the TiO_2-Nanowires. 51

6.2.1 Impedance test for breast cancer cell lines over the sensing time 52

6.2.2 1st impedance test for distinguishing breast cancer cells from colon cancer cells 59

6.2.3 Impedance test for breast cancer cell and normal cell lines in different mixing ratios 62

6.2.4 1st impedance test for the Warburg effect on breast cancer and colon cancer cell-lines 63

6.2.5 Impedance test for the temperature effect on the breast cancer cell lines at 37℃ 66

6.2.6 1st impedance test for the doxorubicin drug effect on the breast cancer cell lines 67

6.3 Checking the cell attachment under the optical microscope 70

Chapter 7. Conclusion 72

Chapter 8. Future work 74

References 75

List of Figures

Figure 2.1: Illustration of a cross section of cell membrane and its major components. 5

Figure 2.2: Schematic drawing of cancer cell metabolism (Warburg effect). 10

Figure 3.1: Illustration of electrical gradient across the cell membrane. 13

Figure 3.2: Schematic Illustration for common synthesis methods of nanostructured TiO_2. 20

Figure 3.3: Schematic diagram of TiO_2 of different dimensional structure. 21

Figure 3.4: Illustration of layered TiO_2 crystal structure 22

Figure 3.5: Schematic diagram of TiO_2 applications. 22

Figure 3.6: Schematic **i**llustration of a typical biosensor. 24

Figure 4.1: Bragg's Law illustration. 32

Figure 4.2: Schematic representation of the basic SEM components. 33

Figure 4.3: a) phase shift illustration between voltage and current. b) phase shift expressed as an angle between the real (Z_{RE}) and imaginary (Z_{IM}) parts of the complex impedance. 34

Figure 4.4: The equivalent circuit, with the nanowire induction (L), nanowire resistance (R_1), cell membrane capacitance (C_2), cell membrane resistance (R_2), intracellular matrix capacitance (C_1), intracellular matrix resistance (R_{CT}), and Warburg diffusion impedance (W_{01}). 36

Figure 5.1: Schematic illustration for TiO_2-Based nanowire hydrothermal synthesis process. 40

Figure 5.2: The autoclave chamber (left) and the Teflon liner (23mL) (right). 40

Figure 5.3: Schematic illustration for the set-up and corresponding equivalent circuitry. 42

Figure 6.1: The physical morphology of titanate after the hydrothermal treatment. 46

Figure 6.2: PXRD pattern for titanate nanowire pattern of a typical sample with the titanate nanowires on the Ti-metal after 24 hours of the hydrothermal treatment 47

Figure 6.3: A schematics for illustrating the change on the Ti-metal surface after the hydrothermal reaction, as supported by the SEM micrograph. 48

Figure 6.4: The SEM study on the nanowires from the growths over the 4, 8, and 12 hours. 48

Figure 6.5: The SEM characterization of the bioscaffolds on the typical sample from 8-hour hydrothermal synthesis. (a). The face-on view on the sample-top; (b). A tilt view. 49

Figure 6.6: Point of zero charge (Isoelectric point) for DDI washed titanate (TiO_2) nanowire from pH titration (1-12). 50

Figure 6.7: The impedance measurements of titanate surface corresponding to pH titration. 51

Figure 6.8: Illustration of surface deprotonation and protonation corresponding to the aqueous solution pH change. 52

Figure 6.9: Impedance vs Frequency for normal cells (MCF10A) in three-time sensing durations (25,35, and 45 minutes). The error bar reflects three repeats. 54

Figure 6.10: Impedance vs Frequency for benign cancer cells (MCF7) in three-time sensing durations (25,35, and 45 minutes). The error bar reflects three repeats. 55

Figure 6.11: Impedance vs Frequency for malignant breast cancer cells (MDA-MB231) three-time sensing durations (25,35, and 45 minutes). The error bar reflects the three repeats. 56

Figure 6.12: Impedance vs Frequency for three breast cancer cells (MCF10A, MCF7, MDA-MB231) in three-time duration (25,35, and 45 minutes). 57

Figure 6.13: Impedance test for normal cell and different cancer cell types. 61

Figure 6.14: Nyquist plot for TiO_2, normal (MCF10A), and three different cancer cell lines. 62

Figure 6.15: Nyquist plot for Titanium metal. 62

Figure 6.16: Impedance at 1 MHz for mixed sample. 64

Figure 6.17: (a) Impedance test for different cancer cell lines with no glucose in 1xPBS. (b) Impedance test for cancer cells compared to normal cell incubated with 1xPBS+ 5.5mM glucose. *P* value for MCF7 and MDA 231 is $< 10^{-80}$. 66

Figure 6.18: Impedance level of MCF7 and MDA 231 at 37℃ 67

Figure 6.19: Microscopic image to drug treated MCF7 in cell culture compared to control. 69

Figure 6.20: (a) Impedance test for MCF7 treated with DOX for 24 and 48 hours. (b) Impedance test for MCF7 treated with DOX for 24 hrs and then incubated with glucose for 35 minutes before performing the test. 70

Figure 6.21: Impedance test of MDA-MB231 treated with DOX for 24hours and being incubated with glucose before the test. 71

Figure 6.22: Optical microscopic images of the cells on bioscaffold. (a). without stain; (b). with fluorescent stain (b). 72

Figure 7.1: MCF7 characterization 74

Figure 7.2: MDA-MB231 characterization. 74

List of Tables

Table 4.1: Equivalent Circuitry Parameters. 36

Table 5.1: Regents for preparing SBF (pH7.40, 1L) 38

PART I

Chapter 1. Introduction

1.1 Overview of Current Cancer Diagnosis and Research

Breast cancer patients have been increasing in number causing a high health threat worldwide. According to the American Cancer Society, breast cancer is the most common non-cutaneous cancer in women in the US. Breast cancer has a 14% mortality rate among women and the rate is the second highest among all types of cancer.[1] Current diagnostic technology utilizes a combination of radiological, surgical, and pathologic assessments. Diagnosis of breast cancer is routinely done by mammogram, but it cannot distinguish between benign and malignant lesions. Mammogram also fails to detect 10% to 25% of breast cancers, because tumor detection is difficult in dense breast tissue.[2] A biopsy is also needed to confirm or role out cancer, and it requires significant sample preparation using bench top protocols. PCR and flow cytometry also have been used for detecting circulating cancer cells in the blood and may predict the survival rate.[3] However, both techniques require using specific tagging system and identifying particular markers, which may not be expressed in some cancer subpopulations. Also, they lead to cell destruction and loss of cell viability. Therefore, there is a high demand to solve this issue by developing further advanced technology to improve sensitivity and selectivity in breast cancer detection. The technology should also be simple, efficient, and inexpensive.

Recently, nanowire material has attracted attention as an excellent material to be used in biosensing technology. This is due to their unique properties of being semiconducting with high sensitivity to detect single molecule.[4] Titanium oxide (TiO_2)-based semiconductor nanowires can be grown on top of titanium metal and, in turn, it can be used as an electrode to sense cancer cells. These TiO_2 nanowires have a band gap between 1.8 and 4.1 eV. This range reflect a

semiconductor property making them unique from other nanowires by having the best sensitivity ranges.[123] Besides, TiO_2-nanowires are easily fabricated, highly biocompatible and chemically more stable.[5] Thus, TiO_2-nanowires are ideal for sensing purposes.

1.2 The Importance and Motivation

In this study, TiO_2 nanowires were used for the development of a label-free electrochemical biosensor on a bio-scaffold for direct detection of different live breast cancer cell lines (MCF7 and MDA-MB231) in *vitro*. Cancer cells exhibit altered local dielectric properties compared to normal cells.[40] They have different electrical conductance and capacitance, which can be measured by electrical impedance scanning (EIS). Therefore, these observations open a new direction toward using the electrochemical properties of cancer cells and apply them to help in developing a prognostic tool for future diagnostic technology. This new method also can be potentially used in various important applications in cancer screening and monitoring, which are doable in vitro at ultra-low-cost and in real-time.

1.3 Dissertation Structure

This dissertation consists of eight chapters. In chapter one, the introduction; it consists of a brief overview of current cancer diagnostic tool and the significance of this study within this field.

Chapter two, overview of cell membrane and cell metabolism, where it begins by explaining the function of the cells and the mass transfer across its biomembranes. The biomembranes structure and the surface charge influence on its functionality.

Chapter three, impedance cell biosensing based on nanomaterial, describes the history of using bioimpedance to determine the pathological tissue stage. Further, introducing nanomaterial and their applications in biosensing, specifically the TiO_2- nanowire that has been used in this research.

Chapter four, characterization methods, an introductory about the working principles of instruments being used in this project. Chapter five, materials and methods, a full explanation of the required chemicals, material and the instrumentation and the equivalent circuitry that has been used, which will be presented and thoroughly explained. In chapter six, results and discussion and the sensing of cells by TiO_2-nanowire and the interpretation of the results will be discussed in detail.

Chapter seven, summarize the experimental results and conclusion. Chapter eight, the future work; some projects are proposed to be conducted by any interested graduate student or researchers in this field.

Chapter 2. Overview of Cell membrane and Metabolism

2.1 Cell Structure and Its Function

2.1.1 Cell membrane structure

A cell is the smallest structural and functional biological system of an organism. It consists of cytoplasm and a nucleus surrounded by a plasma membrane. It can be classified into two categories: prokaryotic and eukaryotic. Prokaryotes can be distinguished by lacking a true nucleus such as in bacteria, where it can be found in animal, plant, and fungi cells. Cells differ in size and shapes, for example, bacteria are around 1-5 μm, while animal cells are around 10-100 μm in diameter. Cell membrane have the main role in transporting biomolecules across its plasma membrane, which is related to the ratio of surface area to the volume which is quite large [6].

The plasma membrane is the most common structure among cells, giving the cell its shape and protecting its organelles. Moreover, it controls the traffic of biomolecules and ions across it and it has an important role in initiating certain signaling pathways and cascades to activate or inhibit certain cells activity in response to the external environment. It composes of two (4-5 nm in thickness) phospholipids layers arranging them self by having the polar head groups directed toward the outer and the inner membrane surrounding polar solution such as water, while having the hydrophobic two fatty acids (nonpolar) tails imbedded within the interior of the membrane, thus exhibiting amphipathic nature (**Fig. 2.1**) [7]. The hydrocarbon chains play an essential role in maintaining cell fluidity and stability. Higher number of saturated chains (having single bonds) give more rigidity to the membrane, while kinks (double-bond between hydrocarbon chain will interfere with fatty acid packing resulting in a decrease in rigidity (increase the fluidity of the membrane). In general, biomembranes consists of different kind of phospholipids such as Phosphatidylcholine (lecithin) (PC), Phosphatidylethanolamine (cephalin) (PE), Phosphatidylserine (PS), Phosphatidylinositol (PI), and Sphingomyelin (SM). Moreover,

cell membrane contains glycolipids, cholesterol, and membrane proteins. Membrane proteins have an important role in transportation, attachment, recognition, and signal transactions. [6]

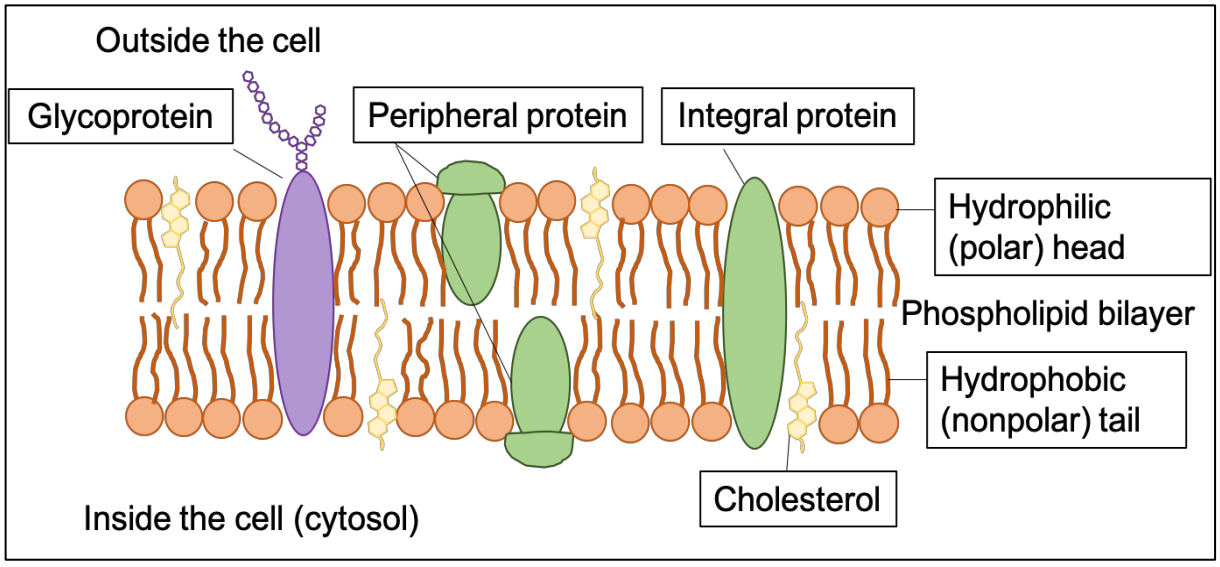

Figure 2.1: Illustration of a cross section of cell membrane and its major components.

2.1.2 Transportation across the biomembranes

The plasma membrane is responsible for maintaining the hemostasis of cell by creating a barrier separating the cell from the exterior environment and allowing specific biomolecules to bypass into the cell cytoplasm keeping specific concentration and composition.[8] Due to its dense hydrophobic core, the plasma membrane phospholipids bilayer is impermeable to water-soluble molecules and ions. Only gases, such as oxygen (O_2) and carbon dioxide (CO_2) along with small uncharged polar molecules, such as ethanol and urea can move freely by simple diffusion across the artificial pure phospholipid membrane or phospholipid mixed with cholesterol. These molecules can diffuse without the need of a protein carrier and thus no energy is consumed. Thus, the movement is down the chemical concentration gradient (the higher the concentration gradient of the substance, the faster the movement rate across the membrane). Ionic molecules

movement is controlled by electrochemical potential (gradient), which include both the concentration gradient and the charge gradient across the membrane.

Most cells' membranes have a negative potential, meaning that the outside of the membrane have higher potential than inside.[7] The excess in the negative charges inside the cell is due to the presence of the negatively charged proteins, even with the presence of more potassium ions concentrating inside the cell (~150mM inside to ~4mM outside).[9] In contrast, the outer side of the membrane has higher potential due to the high concentration of sodium (~140 mM outside to ~5 mM inside) and other cations, such as calcium, creating a higher potential (more positive).[8]

Ion transportation across the membrane or between its cellular compartment is mediated by specialized membrane proteins which are transmembrane proteins composed of multiple membrane- spanning segments (mainly alpha helices). Such transmembrane proteins facilitate the movement of hydrophilic substances, such as ions without being in contact with the hydrophobic part of the membrane. The protein membrane transporter is being classified into three main groups: ATP-powered pumps, ions channels, and transporters.

ATP-powered pumps are ATPases uses the ATP hydrolysis to get the energy to be able to move ions or small molecules either against the concentration gradient or the charge gradient, or both. This process is also known as "active transport". Ion Channels transfer ions down their concentration gradient without energy consumption and this also is known as "passive transport", facilitative transport, or non-gating". However, most ion channels are controlled by specific chemical or electrical signal and are referred to as "gated channels". In fact, like all other transporter proteins, ion channels are selective to the type of molecule they transport.[8]

The third type of protein transporters, are also called "carriers", moving a wide variety of ions and molecules but in lower rate compared to ion channels. It is further classified into three main types: Uniporter (facilitated transporter), antiporter, and symporters. Uniporter transfer a

single type of molecule down its concentration gradient. Glucose and amino acids are transported with the aid of uniporter. On the contrary, antiporters and symporters facilitate the movement of one type of ions against concentration gradient with the movement of another ion down its concentration gradient either in the same direction (symporters) or in the opposite direction (antiporters). Both types can also be referred as "cotransporters" due to their ability to transport two or more molecules at the same time.[8]

2.2 Normal vs Cancer Cell Metabolism

2.2.1 Normal cell metabolism

In multicellular organisms, such as human body, cells are surrounded by blood vessels carrying a constant nutrient supply. Proliferation regulation is crucial to the human body survival especially when the nutrient level exceeds the need for cell division. Therefore, uncontrolled cell division is prevented by inhibiting taking up nutrient unless stimulated by stimulator, such as growth factor. However, cancer cells overcome this regulation by altering receptor-initiated growth factor. Studies have shown growing evidence that some of the cellular pathways have constantly been activated the nutrient uptake promoting cell survival and growth.[10, 11]

In mammalian cells, glucose is the primary source of energy and play an essential role in cell metabolism. Under normal conditions, one mole of glucose will undergo glycolysis and will end up with two molecules of pyruvate, ATP, and NADH. In the mitochondria, pyruvate will be utilized in Krebs cycle generating more NADH, the oxidative phosphorylation electron donor, generating 18-folds of ATP than in glycolysis.

Normally, most mammalian cells in culture depend on glucose and glutamine as the main supply for most of the carbon, nitrogen, and free energy. Due to this fact, cells tend to alter the glucose utilization of differentiated cell to meet the cell proliferation needs. For example,

glucose will be converted to precursors such as Acetyl-CoA for fatty acid, non-essential amino acids, and ribose for nucleotides.

2.2.2 Warburg effect and cancer cell metabolic symbiosis

In the 1920s, Otto Warburg reported that the tumor ascites had a high glucose consumption and high lactate production under normal oxygen levels. This observation named as the Warburg effect or aerobic glycolysis and considered a landmark of aggressive tumors.[12, 13] The phenomena appeared to be associated with an increase in the glycolysis been supported by molecular and functional data.[14] Microarray data collected from different studies have shown consistently an upregulation in genes related to glucose transportation and glycolysis in a wide range of tumors.[15-17] Glucose transporters have been reported by several studies to be overexpressed in breast cancer, hepatocarcinomas, lymphoblastic and others.[18-20]

The metabolic reprogramming changes the metabolic activity by enhancing glycolysis and restricting the Krebs cycle to lower the oxygen availability. Several regulatory pathways contribute to the metabolic reprogramming of tumor cells include MYC, HIF-1α, and PI3K/AKT/mTOR.

One of the main regulatory mechanism in aerobic glycolysis is by activating hypoxia-inducible factor (HIF-1). The activation of HIF-1 alters the expression of 450 genes involved in glycolysis, lactate production and lactate proton excretion, iron metabolism, angiogenesis, and metastasis. Also, the genes involved in the upregulation of glycolytic enzymes different than found in normal cells, such as glucose transporter (GLUT1, GLUT3), glycolytic enzymes (HKI, HKII, PFK-1, ALDO-A, ALDO-C, PGK1, ENO-α, PK-M2, PFKFB-3), and enzymes related to the production of lactate and lactate/ proton excretion (LDH-A, MCT4).[21, 22] Hypoxia also upregulates the production of two pyruvate dehydrogenase kinases (PDK1 and PDK2) carrying the phosphorylation and the inactivation of three isoforms of pyruvate dehydrogenase (PDHA1,

PDHA2, and PDHB) that convert pyruvate to acetyl-coA.[23-26] Regulators like HIF-1 and Akt may play an important role in acidosis. HIF-1 also enhance the expression of intracellular pH (pH_i) regulatory systems. These include monocarboxylate transports (MCTs), Na^+/H^+ exchangers (NHEs), proton pumps (V-ATPase), and membrane-associated and cytosolic carbonic anhydrases (Cas). [27] These systems are important to maintain intracellular pH for cell survival.

Tumor cells consume more glucose to secrete massive amount of lactate to toxify healthy cells. However, cancer cells developed a survival mechanism to adapt to acidosis (toxic environment). In addition, CO_2 is another source of acidic extracellular pH (pH_e). In the tumor microenvironment, carbonic anhydrase (CA) hydrate CO_2 producing bicarbonate (HCO^-_3) and H^+.[28] Hypoxia and acidosis are usually associated, however, acidosis can be observed in normoxic conditions because of the Warburg effect (**Figure 2.2**).

Moreover, studies showed developing hypoxia and acidosis in the microenvironment of premalignant epithelial cells. The partial pressure (pO_2) inside the tumor is relatively lower than the surrounding healthy tissue. Hypoxia and acidosis create a selective environment in which cells having metabolic adaptation by uncoupling glycolysis from the respiratory chain and using glycolysis as the main source of ATP production.[29]

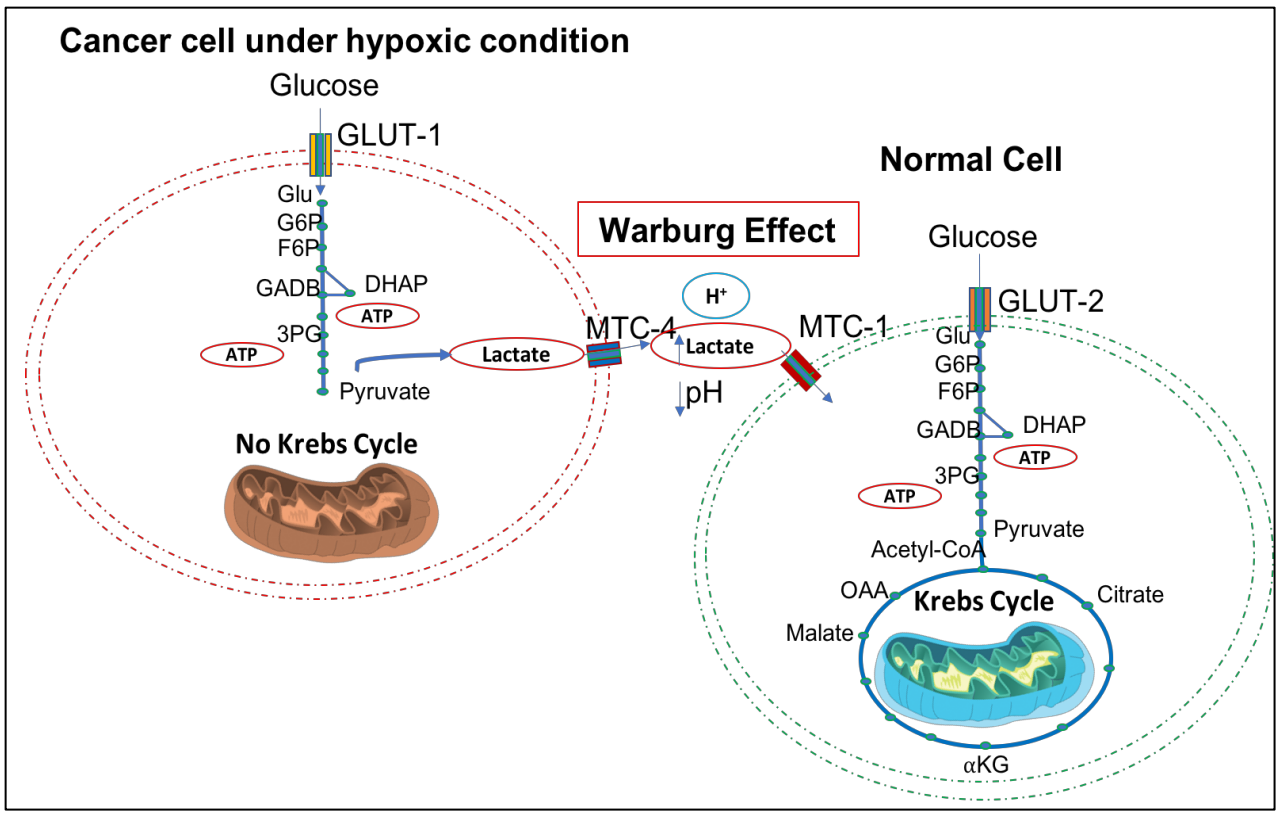

Figure 2.2: Schematic drawing of cancer cell metabolism (Warburg effect).

In tumor cell populations the oxygen level varies generating well-oxygenated regions (aerobic) and poor oxygenated (hypoxic) regions. Some studies revealed the fact that tumor cell can change from hypoxic to normoxic conditions and vice versa in a very short period of time and this can be called "metabolic symbiosis".[30-32] In the hypoxic conditions, cancer cells increase the expression of GLUT-1, which is activated by HIF-1. Increasing the glucose flux, in turn, increases the lactate production that needed to be secreted to prevent intracellular acidification thought the monocarboxylate 4 system (MCT4), a lactate transporter coupled to H^+. On the contrary, cancer cells growing under normal oxygen level will take lactate instead of glucose supporting the metabolic symbiont concept. In aerobic cancer cells, MCT-1 transport lactate into the cell to be converted to pyruvate via lactate dehydrogenase B (LDHB). Krebs cycle and its products will be oxidized through the Krebs cycle (OXPHOS pathway) for energy

production. Inhibiting MTC-1 will make aerobic cancer cells to consume more glucose than lactate, breaking the metabolism symbiosis, leading the apoptosis of anaerobic tumor cells due to glucose deprivation. MCT1 expression found to be exclusively in aerobic regions of human tumor tissue from the head, neck, breast, and colon cancer. The result came along with the expression of LDHB allowing the lactate utilization as a source of energy.[29] The phenomena were observed in murine mice model in which hypoxic tumor death was induced due to the inhibition of MCT1 as a treatment from lung cancer. [29] This observation is critical to treat patients, because blocking MCT1 in cancer cells allows chemotherapy and radiation treatment to be more effective, especially in reaching the hypoxic zone within the tumor region. [33]

To conclude, acidosis promote selective checkpoints of both cell cycle and apoptotic mechanism.[34] After several cell generation, acidosis select the most resistance phenotype for higher invasion and metastasis.[35] Acidosis will also facilitate the extracellular matrix degradation to increase the cancer invasiveness leading to cancer spread (metastasis) through the circulatory system and ultimately patient death.[35] Therefore, diagnosis and treatment are critical to be done before reaching the late stages to overcome bad prognosis.

Chapter 3. Impedance Cell Biosensing Based on Nanomaterial

3.1 Cell Biosensing Using Impedance

Electrochemical Impedance Spectroscopy (EIS) is a well-established and widely used technique in the biosensor's development. EIS is highly a sensitive technology that uses alternative current (AC) for detecting electrochemical phenomena over a wide range of frequencies. This can be used as an electrochemical detection tool that is well known to be simple, free label, real-time, and at low-cost.[36, 37] Since the 1920s many research studies have concluded that malignant breast tumors have a significantly different electrical impedance or electro potential values compared to those of normal tissues and benign lesions, and such properties are used to distinguish different tissues based on distinct electrophysiology characterization of a particular tissue in the frequency domain.[3, 38] Among all conducted studies, the main focus is on studying pathological tissues. [39, 40] The EIS approach offers new cancer detection technique of a variety of cancers in the liver[41], skin[42], and breast[42], and the topic has been discussed extensively in the literature reviews.[36, 43-45]

In 1984, Pethig [46] attempted to review the dielectric properties of tissues and biomolecules. The review included various research studies which have, at a molecular level, tried to analyze the dielectric properties characteristics of malignant breast tissues that may be different in between normal and malignant breast tissue's properties. Some of the characteristics stated include higher water content and sodium concentration of cancerous cells, different electrochemical properties of their cell membranes, and reduced membrane potentials. Normal epithelial cells are electrically polarized by an ionic gradient across the cell membrane, and the charge gradient between the apical and basolateral cell membrane is known as trans- epithelial electro-potential.[47,48] Na+/K+ ATPase pump maintains the electrical gradient across the

membrane. This electrical gradient difference creates a trans-epithelial potential difference of 30 mV (**Fig.3.1**).

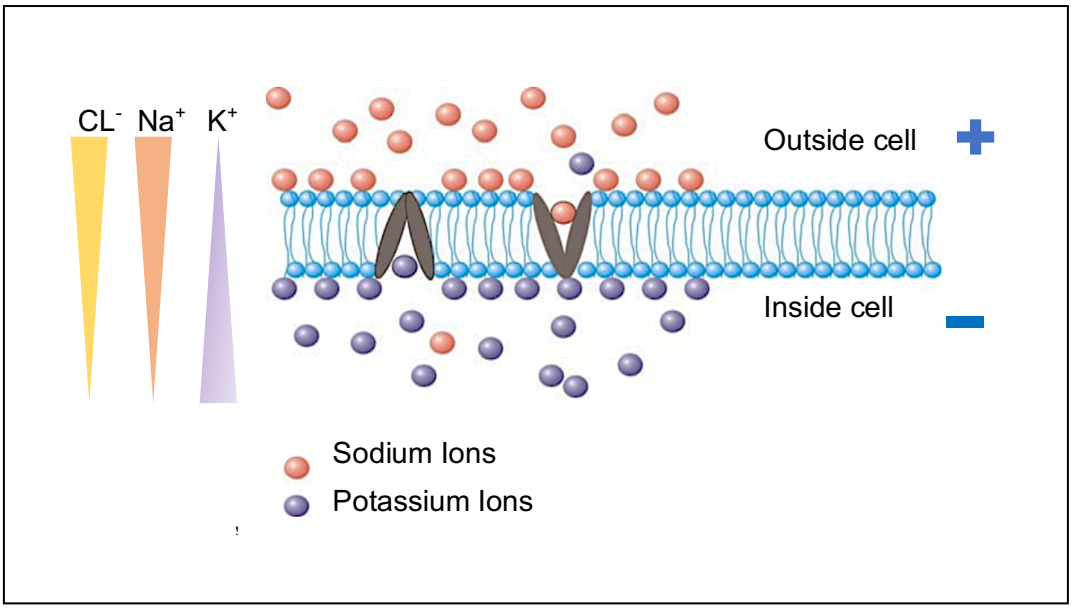

Figure 3.1: Illustration of electrical gradient across the cell membrane.

When epithelial cells divide, the charge is dissipated, creating an electrical depolarization. Therefore, the development of breast cancer will cause the cells to divide even faster resulting in generating pockets of relative depolarization. Further, when the tumor becomes invasive, it starts to destroy the ductal structure, thus increasing the permeability of ions. This differential in electrical potential can be detected at the skin surface and can be used as a diagnostic tool. Other studies [49-52] have used the membrane permeability, cellular water, salt content, packing density, and cell orientation within the malignant tissue to identify cancer lesions. In addition, any studies so far have confirmed that the impedance test can be used as a tissue differentiation tool using specified frequency range.

Similarly, at the cellular level, electrical properties of the cell may vary depending on biochemical changes caused by the disease.[53] Electrical Cell-substrate Impedance Sensing

(ECIS) was first introduced as a noninvasive method by Giaever and Keese to study the properties of cell attachment.[54] The cell contains an intracellular medium surrounded by a semipermeable membrane, which separates the extracellular from the intracellular ionic solutions, and both are resistive in nature. The cell membrane as we discussed earlier is made from a lipid bilayer, proteins, and some polysaccharides. The membrane exhibits capacitive properties due to the presence of the potential difference. The impedance of cell membrane capacitance changes corresponding to the frequency. At low frequency, the cell membrane act as an insulator preventing the current to flow through the membrane, and lead to have a higher impedance level, i.e. highly resistive. When the frequency tends to be higher, the cell membrane act as a capacitor and start to conduct and allow the current to go through the membrane resulting in a lower impedance level.[55]

Since it is clear that the frequency can distinguish tissues pathological stages, scientists, when plotting relative permittivity against the frequency, observed three distinct regions called alpha (f <1000 Hz), beta (1000 Hz < f < 100 MHz) and gamma (f > 1 GHz) regions. [53, 56, 57] Blad *et al*. [40] reported that alpha and beta regions are the best to detect cancerous cell electrical properties that are different from normal cells.

Further, such biochemical changes can be detected through electrical impedance (EI) sensing of cell-substrate interaction.[58, 59] A cell suspension analysis conducted by Han *et al.*[60] using a sophisticated chamber showed that significant differences occur in the phase angle and magnitude of corresponding impedance over the frequency range of 100 Hz to 3 MHz in non-tumorigenic MCF10A, MCF7 (non-invasive cancer cell line), MDA-MB231 and MDA-MB435 (invasive cancer cell line). Also, the membrane capacitance and resistance differences were reported among those cell lines. Yang *et al.*[61] conducted a real-time impedance-based measurements of cellular activities using RT-CES system to distinguish OSCC cell line and the

non-cancerous epithelial esophageal Het-1A cell line. Qiao *et al.*[62] reported differences in the impedance measurements in both suspension of MDA-MB231 and MCF10A breast cells using a platinum needle as an electrode. Nwankire *et al.*[63] created a centrifugal microfluidic system by using a platform on a five-layered disc attached to a gold electrode functionalized with anti-EpCAM to quantify ovarian cancer cells (SKOV3) extracted from a blood sample using EIS. Thus, such studies have shown that impedance spectroscopy (EIS) is a powerful technique for distinguishing cancerous cell electrical properties from normal cell electrical properties.

Furthermore, electric cell-substrate impedance (ECIS) has been used to reflect various cells properties and behavior including attachment [64] and spreading[65-67], motility[68-70], and proliferation.[71] This approach can be also used to monitor cell response to drug treatment and cytotoxicity assessment in real-time.[72-74] Impedance- cell-based biosensors is further applied to identify active molecular targets involved in various diseases.[72] It is also involved in detecting the drug toxicity and efficacy at a cellular level with nanoscale resolution.[75]

Kuo *et al.* studied the invasive properties of human breast cancer cells (MDA-MB 435) into human umbilical vein endothelial cells (HUVEC) [76]. MDA-MB 435 cells were treated with transforming growth factor (TGF)-ß and added to HUVEC monolayer. In one hour, MDA-MB 435 invaded HUVEC resulting in decreasing the resistivity after 4 hours. The study also demonstrated the cellular role of (TGF)-ß in activating mambrane type 1-matrix metalloprotenase (MT1- MMP), which mediates the cleavage of CD44 to the soluble form. CD44, in turn, plays an important role in cancer cell migration.

Recently, Stanica *et al.* used ECIS to evaluate hypoxia-induced bioeffect including pH on the tumor microenviroment using a multiplexing module (8 channels) on human colon cancer HT-29 cell line. [77] The study revealed a dynamic change of cellular responses during hypoxic condition and in response to acetazolamide (AZA), a carbonic anhydrase inhibitor.[28]

In conclusion, biosensors that utilize the electrochemical impedance technique present a unique technology with a great potential to meet the rapid, real-time need for breast cancer detection. It is important to point out that all metal electrodes in these studies are used without any further surface modification, which can improve the detection sensitivity. Surface modifications using different materials is a new direction that our group is being introduced in this study.

3.2 Nanostructured Biomaterials and Biosensors

3.2.1 Development of nanostructured biomaterials

Nanomaterials can be referred as nanostructured materials, which have a size between 1 and 100 nm. These nanomaterials offer new properties compared to their bulk compartments and are being used for developing new applications and devices to improve our daily life. In recent years, a wide range of nanomaterials have been developed such as nanowires (NW), nanotubes (NT), nano roads (NR), nanoparticles (NP), nanoflowers (NF), nanoshell (NS), nanocages (NC). These nanostructured materials have established a new field called “Nanotechnology”. Nanotechnology is defined as the field that studies materials to be synthesized, controlled, and manipulated in nanometer size range. It is a rapidly growing field aiming to develop multifunctional systems targeting, diagnosing, and treating devastating diseases such as cancer. Nano-sized objects are carrying novel properties and functions that open the doors for creative biomaterials to be used in biomedical applications. For example, medicinal and structural chemists have been creating and manipulating nanometer- and sub-nanometer-sized components of drugs for decades and will continue to do so into the foreseeable future. A “Nano bullet for Tumors” is a good example of how research from diverse sources can utilize nanoparticles to

target cancer cells.[78] The field showed promising developmental stages to design and create new nanomaterials and technology to achieve the desired goal.

3.2.2 Nanofibrous bioscaffolds as extracellular matrix analogues

The extra cellular matrix (ECM) is a mesh network composed of both mechanical and functional proteins, being unique tissue-specific assembled architecture. It provides both a mechanical and functional substrate for cell signaling. The dynamic signaling of ECM is a key role in tissue development and homeostasis.[79] The synthetic nanofibrous scaffolds are designed to provide a supportive framework for cell proliferation and survival, mimicking the ECM.[80, 81] The ideal scaffold would promote cell attachment, proliferation, and differentiation. Earlier studies showed the vital role for self-assembled peptide nanofibrous bio-scaffold to connect the natural ECM and promote cell regeneration corresponding to a lesion.[82, 83] To date, fabrication of nanofibrous bioscaffolds can be achieved through mainly four techniques: electro-chemical dip-in lithography, mechanical stretching [84], template-directed electrochemical synthesis, and electrospinning.[4, 85-87] The most well-known technique to produce nanofibers is called electrospinning.[85, 88] This method uses a microfabricated scanned tip, which is dipped in a polymer solution to get a droplet as a source of material. Applying a sufficiently high voltage to the tip generates a Tylor cone and a polymer will be extracted. Moving the tip, acting as a counter-electrode, allows the nanofibers deposition on a substrate surface structure for fabrication. Beside fabrication, electrospinning can also produce oriented polymeric self-assembled nanofibers.[89-91] The diameter of the nanofibers can be controlled using various methods.[92-94] Furthermore, nanofibrous bioscaffolds can be modified and functionalized with bioactive molecules to mimic the architecture of the extracellular matrix and promote cell outgrowth. The designed structure, composition, morphology will ultimately impact the cell

adhesion, proliferation, spreading, migration, differentiation corresponding to biochemical signals.[95, 96] Several studies discussed the mechanical strength and evaluation through theoretical modeling of such nanofibrous assemblies and the challenges upon developing/forwarding the technology toward the clinical settings.[79] The fibrous alignment also showed significant results in enhancing mouse embryonic stem cells (ESCs) differentiation into neural cells and further outgrowth compared to the random nanofibrous alignment.[97] A better understanding of the synthetic scaffold materials in supporting different injury sites will improve their usage and ultimately their clinical outcomes.

It is well known that human cells generate biological electrical field through voltage gradient of 10-90 mv across the cell's membrane. This gradient initiate cell signaling, which alters cell proliferation and differentiation. This phenomenon inspired researches to develop electroactive polymers to generate electrical stimulation for repairing injured tissues. Up to date, a few studies showed a promising electroconductivity capability of the biocompatible scaffold. Researchers have demonstrated the ability of these polymers to trigger cell proliferation and differentiation corresponding to material's electrical conduction.[91, 98] Common electroconductive polymers include polyacetylene (PE), polyaniline (PANI), polypyrrole (PPy), polythiophene (PT) , poly(para-phenylene vinylene) (PPV), and Poly(3,4-ethylene dioxythiophene) (PEDOT) .[99] Piezoelectric polymers include Polyhydroxybutyrate (PHB), Polyvinylidene fluoride (PVDF), and Poly(L-lactic acid) (PLLA), as well as polyelectrolyte gels. Bangar *et al.* used dielectrophoretically aligned Polypyrrole (PPy) nanowires across a pair of gold electrode, separated by 3 μm gap, for detecting cancer antigen 125 (CA 125) by corresponding antibody. [100] The immunosensor showed good sensitivity in low concertation (1 U/mL) as well as in higher concentration (1000 U/mL). Although Ppy showed high sensitivity, it would be critical to know the chemical stability of the polymer after several uses.

Electroconductive polymers are also used to trigger neural, muscular, skeletal, and cartilage cells differentiation and proliferation.[91] However, the valid range of electrical stimulation is not well defined. Therefore, more fundamental *in vitro* and *in vivo* studies are highly needed to determine how different tissues respond to electrical stimulation. Another challenge is how to promote a multi-tissue regeneration using such synthetic electroactive scaffold *in vivo* with large animal models. Further studies should focus on investigating the combination of both chemical recognition and conductive material, through ion-exchange or electron transfer, which can be further applied in real-time for cell electrochemical sensing.[99]

3.3 TiO_2-Based Nanostructured Bioceramics

3.3.1 Syntheses of TiO2 –based nanostructures

TiO_2-nanostructured material has been synthesized through several methods: template synthesis[101], nano-seeding[102], nanocoating[103], electrospinning[104], and hydrothermal synthesis[5, 105] (**Fig. 3.2**). The template synthesis includes sol-gel template, sol-gel coating, polymer mold, direct deposition, and super-molecular assembled process, in which a well-controlled length and diameter TiO_2 nanowire is aligned on a substrate.[106-108] The electrochemical nano-seeding include direct anodization of Ti foil in an H_2O-HF electrolyte at room temperature or seeding Ti substrate with the TiO_2 nanoparticle.[109, 110] The nanocoating synthesis Ti substrate is performed by the Galvano dynamic anodizations.[111] Alkaline hydrothermal synthesis was reported by Dong *et al*, where Ti metal oxidation (corrosion) occur in a large-scale solution fabrication (NaOH or KOH) at relatively low temperature. The nanowire root inside the Ti substrate was attached firmly by an unusual downward growth, while the nanowire tip grows upward to self-assemble to form the scaffold.[112] The scaffold, reported by Dong *et al*, is composed of macropores of 2-10 μm in diameter promoting cell adhesion and proliferation, controlled drug release, photocatalytic

sterilization, and electrochemical detection, which was an ideal multifunctional Titanium-based implant.[5]

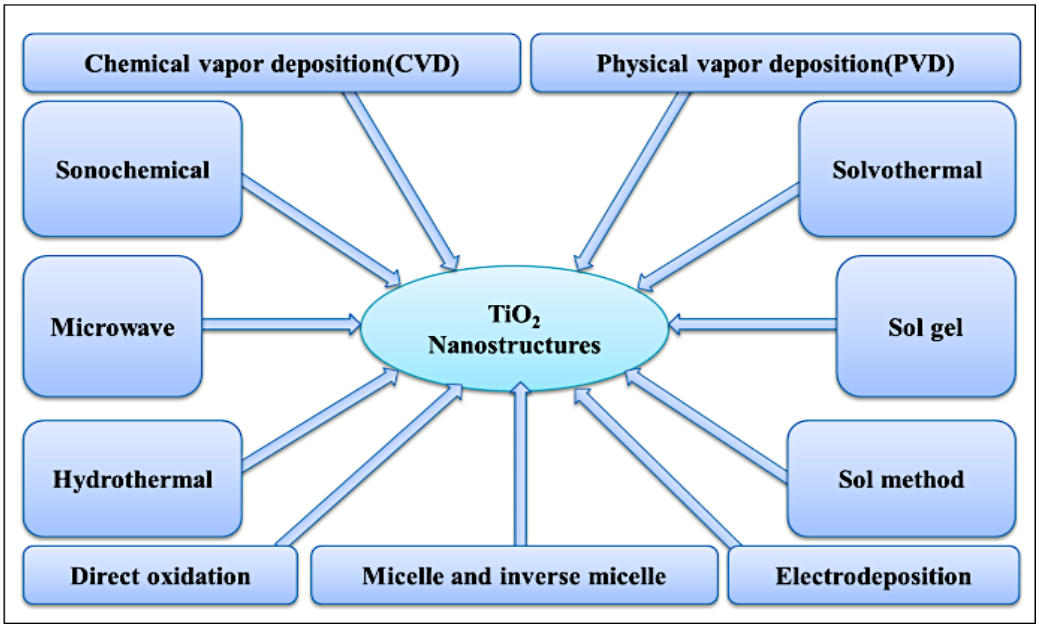

Fig. 3.2: Schematic for common synthesis methods of nanostructured TiO_2.

3.3.2 Commonly seen nanostructures and dimensions of TiO2- based bioceramics

Many studies showed that titanate can be formed in different shapes and dimensions. **Fig.3.3** shows a summary of different TiO2 nanostructure morphology and dimensions: zero-dimension, one-dimension, two-dimension, and three dimensions. Nanoparticles considered an example of zero-dimension. Nanorods, fibers, tube, and belts are examples of one-dimension. Nanoplates and sheets are a two-dimension structure. Due to the flexibility and diversity of titanate structure, it considered as an excellent platform to incorporate other materials such as metal oxides or transition metals[113, 114], noble metals[115, 116], and carbon-based material[117, 118]. The surface properties of these composite are entirely different from the bulk material, due to the quantum size effect.[119]

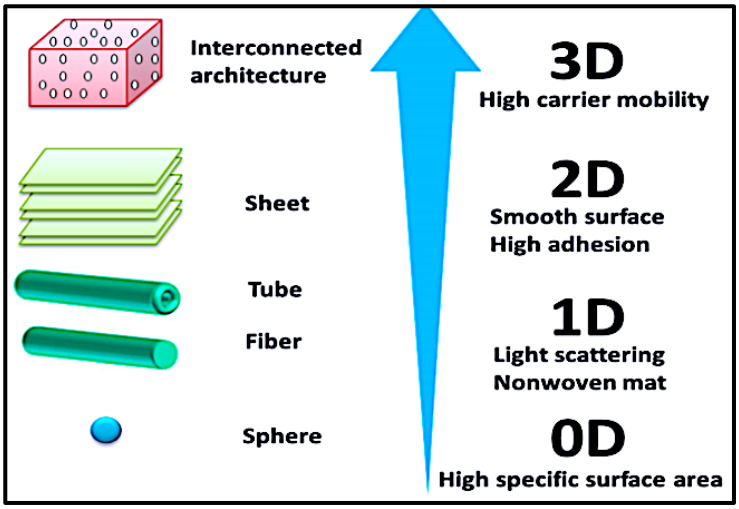

Fig. 3.3: Schematic diagram of TiO_2 of different dimensional structure.

3.3.3 Properties and applications of TiO2–based nanobioceramics

Alkali TiO_2 is the most common form of TiO_2 with the formula $A_2Ti_nO_{2n+1}$ (A= Li, K, Na). They are characterized by a large surface area with unique layers and tunnel crystalline structures.[120-122] It has been used for a long time as a white pigment in paint. After the discovery of its photolytic activity on water under the UV light in the late 1970s [123], the field of TiO2-based nanomaterial was established.[124] The TiO_2 structure known as "Zwitterionic", meaning that it consists of multilayers with negative charges and positive charge interlayers while maintaining a zero-net charge for the overall structure (**Fig.3.4**).

The titanate has (TiO_6) octahedron as the main building block.[125-127] The edge shared (TiO_6) structure will for a negatively charged nanolayer structure. The cations (e.g. Na^+) will fill the adjacent layered spaces. The distance between the layers will depend on the type of cation (size) and the hydration degree of the cation, which results in the flexibility characteristics of the long nanofiber. Sodium titanate (Na_4O_4Ti) has been used in various fields including environmental, medical, food, cosmetics, space, and energy (**Fig.3.5**).

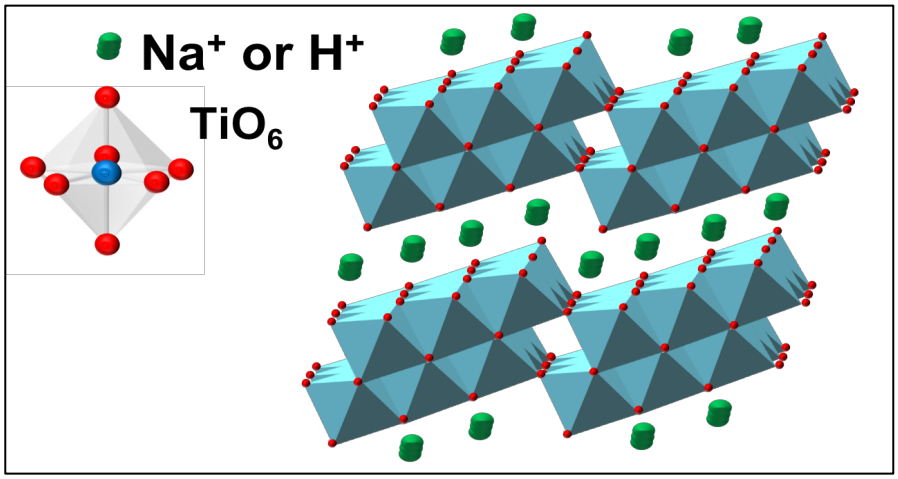

Figure 3.4: Illustration of layered TiO_2 crystal structure

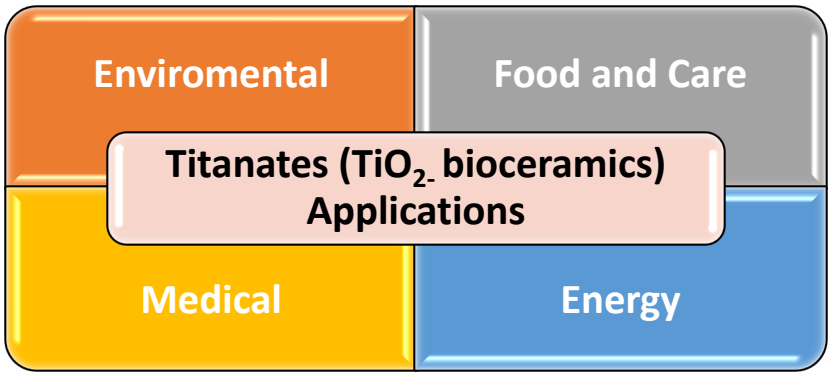

Figure 3.5: Schematic diagram of TiO_2 applications.

The ability of TiO_2- based material to merge into various field came from its unique chemical and physical properties. These properties include low toxicity, biocompatibility, thermal/chemical/photochemical stability, optical transparency, and large surface area. Moreover, the layered titanate nanomaterial is capable of cation intercalation. Meaning that the material allows the process of ion exchange, which has been studied using alkali metals[75] cations and transition-metal-ions[76]. The interlayered distance remained the same after intercalating with alkali metal cations (Na, K, Li, Rb, Cs) in aqueous solution.[75] Magnetic and optical properties

can be further tuned using different transition-metal cations (Ag^{+}, Cu^{2+}, Co^{2+}, Ni^{2+}, Zn^{2+}, Cd^{2+}) by stirring the material in different transition-metal solutions. [76] Based on this, titanites could be potentially a good candidate as an electrode material for a number of reasons including (i) easy charge diffusion in to a short distance to reach inter-layer position, (ii) alkali ions in between the titanate layers can be exchanged with other cations as described earlier, and (iii) cyclic stability can be boosted by the intercalation process of ions to modify the layered structure and enhance detection sensitivity.

3.4 Biosensors Based on Nanowires

A biosensor is an analytic device used for biological sample analysis. Its main role is to convert response, either chemical, biological, or biochemical, into an electrical signal proportional to the analyte concentration in the reaction.[128, 129] Biosensor application are for pollutants, pathogenic microorganism, disease-causing biomarkers detection, or drug monitoring. A typical biosensor system (**Fig 3.6**) is composed of the following:

- Analyte: The molecule or the complex compound being detected in the sample. For example, glucose is a simple molecule to be detected in glucose sensor form body fluids (blood, urine, saliva). Hormones, cells, and pathogenic bacteria are also examples of complexed subjects that can be detected by biosensors.
- Recognizer: The part of biosensor that recognizes the interested analyte is also known as bioreceptor. Enzymes and antibodies are a good example for bioreceptors. Upon the interaction, a signal will be generated (inform of pH change, heat, light, charge or mass transfer), and this is known as bio-recognition.

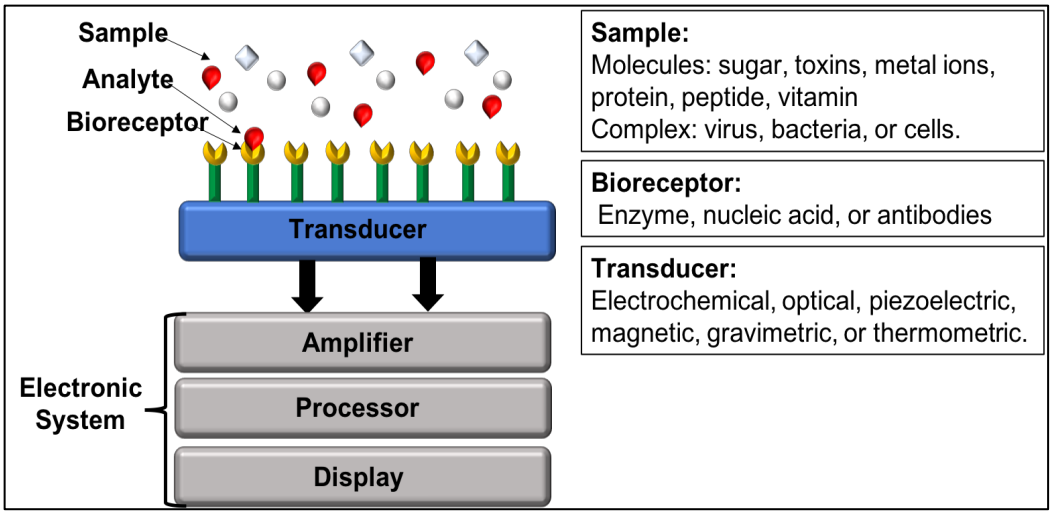

Figure 3.6: Schematic illustration of a typical biosensor**.**

- Transducer: Is the equipment that converts the signal from one form to another. In biosensor, the signal can be converted from chemical to electrical or optical signal and this is known as signalization. The amount of signal is proportional to the amount of analyte in the sample
- Converter: It consists of complex electronic circuitry and responsible for converting the signals from analogs to digital form preparing it to be quantified.
- Display: The part responsible for generating the results in an understandable and user-friendly manner. The results will be shown as numbers or graphs on a computer screen.

The following criteria must be implemented to construct a successful biosensor:[130]

- Selectivity: it is reflected by the ability of the biosensor to detect a specific analyte in a sample containing a mixture of other analytes or contaminants. Antibody-antigen interaction is the best example of high selectivity. Usually, the antibody will be immobilized on the surface of the transducer and the antigen will be present in the sample and will interact with its specific antibody to generate the signal.

- Sensitivity: It is also known as the limit of detection (LOD), which is the minimum amount of analyte can be detected by the system. In case of simple molecule analyses, the detection range should reach as low as ng/mL or fg/mL. For example, prostate-specific antigen (PSA) will be present at low concentration in the blood (4pg/mL) as a characteristic of prostate cancer. Therefore, sensitivity is crucial for an effective biosensor.
- Stability (shelf-life): Is the degree of consistency and the ability to avoid any destruction in and around the biosensor. Any disturbance can cause an error and a shift in the signal being measured. The interaction between the analyte and the bioreceptor should be a strong electrostatic bounding or a covalent linkage to ensure the stability of the system.
- Reproducibility: The ability of the biosensor to generate similar up to identical responses in repeated measurements. This reflects the high reliability and robustness to the response generated from the biosensor. It is an important characteristic of a precise transducer and electronic system in the biosensor.
- Linearity: It reflects the accuracy of analyte measurement. For example, measuring the different concentration of analyte reflects a linear relationship, which can be mathematically represented by $O= sc$, Where O is the output signal, c is the concentration of an analyte, and s is the sensitivity of the biosensor. The concentration range of analyte that generate a linear biosensor response is called linear range. Linearity is also associated with the resolution of the biosensor, which is the smallest change in analyte concentration to generates a response in the biosensor.
- User-friendly and mass-producibility: simple, low-cost, small, minimal sample size and pre-treatment, rapid measurement, and real-time analysis.

Recently, researchers aimed to reduce the size of biosensors for many reasons. For instance, reducing the biosensor size to the micro- or nano-scale showed advantages such as increase the surface to volume ratio, improve the sensitivity and efficiency of detection, reduce the signal-to-noise ratio, lower sample size, and lowering the cost.[131]

Interestingly, the nanoscale electrochemical systems have lower double layer capacitor due to the decrease in the electrode area. Thus, the system has low solution resistance R_s and double layer capacitance C_{dl} allowing ultra-fast electron transfer kinetics for detecting short-life species in short time, which can reach up to the nanosecond scale.[130] It is also applicable to keep both R_s and C_{dl} constant to perform the detection without the need of supporting electrolyte.[132]

In terms of nanomaterials, the discovery of graphene sheets and metal oxides in different shapes are being reported in the literature, especially in electrode fabrication. Biosensors with further nanoscale fabrication can lower the detection limit more than previously reported and potentially improve future single-molecule detection.

3.4.1 Silicon nanowires for biosensing—the state-of-art at present

Cancer biomarkers are used to predict the tumor prognosis. Since they are present in the tissue or blood in extremely low concentration, a highly sensitive detection method is needed. Several studies have used silicon nanowires as a biosensor for medical diagnosis. [133]
For example, prostate-specific antigen (PSA) normally excreted by prostate cells in very low concentration, while higher concentration is related to prostate cancer existence. The field of nano-sensing started with using silicon nanowires (SiNW), which was first reported by Liber's group. *n-type* and *p-type* silicon nanowires were functionalized by monoclonal antibodies (m-Ab) for three cancer markers: free protein-specific antigen (f-PSA), carcinoembryonic antigen (CEA), and mucin-1 showing high selectivity and sensitivity.[134] Further, Kim *et al.* developed an ultrasensitive (n-type) SiNW- field effect transistor (FET) biosensor fabricated by a top-down

approach for detecting PSA. The detection sensitivity also increases to reach below fg/mL by decreasing the nanowire dimension because the n-channel with low density can be easily depleted by negatively charged molecules.[135]

MicroRNAs are another example of biomarkers, consisting of 20-24 nucleotides-long noncoding RNA molecules, involved in gene post-transcriptional regulations and affecting both the stability and translation of mRNAs in eukaryotic species. Existing methods are depending on indirect methods through hyperdilation to a complementary probe molecule or a labeled target miRNA. Thus, it is important to develop a direct detection method being simple with high selectivity and sensitivity. Zhang *et al.* [136] developed a free-label direct detection to miRNA (let-7b) using immobilized peptide nucleic acid (PNAs) on the surface of SiNW. PNA is neutral and doesn't have anionic phosphate backbone. This results in increasing the melting temperature and enhancing the RNA-PNA hybridization efficiency. Further, the detection of let-7b showed an increase in the resistivity corresponding to the increase in concentration from 1fM to 1nM. The essay was further tested by extracting let-7b from Hela-cells. The let-7b was diluted with buffer solution and detectable concentration was $2.15 \pm 0.25 \times 10^7$ copies/ μg RNA being acceptable when compared with previously published work using array-based Klenow enzyme (RAKE) assay. [137]

Recently, only two groups applied SiNW for cell sensing application. Abdolahad *et al.*[138] fabricated a circular shaped sensing electrode with SiNW using thermal oxidation and being doped with c-phosphorus. The free label sensing electrode was used against another SiNW counter electrode forming a bioelectronic device to detect invasive colon cancer cells (SW48) in a mixed sample with another benign colon cancer cell line (HT29) in different ratios. Results showed different membrane dielectric properties reflecting the pathological condition of the cell before and after metastasis. Shashaani *et al.*[139] used a similar electrodes configuration to test

Mebendazole (MBZ, 2nM) drug effect on MCF7 by releasing Cytochrome C to its cytoplasm, which ultimetly changed the cells electrical activity (anodic/cathodic peaks). The changes were detected using cyclic voltammertry (CV) and differential pulse voltammograms (DPV). Alikhani *et al.*[140] investigated the relation between acidosis (decrease pH) and electrical resistivity among breast cancer cells. The study reported that the most aggressive cell line (MDA-MB468) recorded higher electrical resistivity in acidic medium (pH 6.5) compared to moderate (MCF7) and sharp (MCF10) decrease in their resistance.[140]

Although silicon nanowires appear to be promising materials, they form a silicon dioxide (SiO_2) layer (silica) when being exposed to oxidizing agents (e.g. air or water). This can affect electrical conductivity because SiO_2 is an electrically insulating material and will ultimately affect the semiconducting properties that silicon nanowires might have.[141]

3.4.2 Titanate nanowires for biosensing—the game changer

Various forms of TiO_2 based materials such as nanotubes[142, 143], nanoparticles[144], nanosheets[145], sol-gel macromatrics[146], and 3D microporous material[147] have been used extensively to develop biosensors for medical diagnosis.[148]

As mentioned earlier, the unique chemical and physical properties have attracted researchers to use titanate in different applications in the life science and medicine. Recently, titanate nanowire material has attracted attention to be used in bio-sensing technology. This is due to their unique properties of being semiconducting with high sensitivity to detect even a single molecule.[4] Titanate based semiconductor nanowires can be grown on top of Titanium metal and in turn it can be used as an electrode to sense cancer cells. These titanate nanowires can have their band gap varied between 1.8 and 4.1 eV, making it unique from other nanowires in giving the best sensitivity ranges. In addition, the titanate nanowires are easy to fabricate, hold

high biocompatibility and chemical stability.[5] These properties make TiO_2 nanowires an ideal material for biosensing applications.

So far, only a few studies have shown a promising use of TiO_2 nanowires as biosensors. Wang and his coworkers have implemented TiO_2 nanowire (TNW) microelectrode for detecting Listeria monocytogenes.[149] A specific monoclonal antibody for Listeria monocytogenes was covalently attached on the TNW surface and placed in between two gold microelectrodes blocked with 2-methyl-2-propanethiol ($SH\text{-}(CH_2)_3\text{-}CH_3$). The detection limit could detect as low as 10^2 CFU/mL of Listeria. Luo *et al.* demonstrated that TiO_2 nanowires can be conjugated with cytochrome c and applied to detect H_2O_2 being secreted from liver cancer cells (Hep G2).[150] H_2O_2 is considered a metabolic biomarker for cancer cell characterization. The study showed linear amperometric responses for H_2O_2 over a broad range and low detection limit (2-100 mM). Recently, another group used TNW to immobilize Horseradish peroxidase (HRP) as a H_2O_2 sensor.[151] The detection limit reported is lower than the previous study to reach 1.2 $\mu M/mL$ with 30-days stability, retaining 91% of its activity and showing fast and sensitive response compared with other biosensors made from different nanomaterials.

To conclude, the TiO_2-nanowire is a promising nanomaterial that showed promising biosensor capabilities. Few studies were done using TNW materials. Up this point, the usage of TiO_2-nanowires to characterize and study the cell behavior under different pathological stages, stimulators, or pharmaceutical effects have not been reported. Thus, the purpose of this study is to introduce the TiO_2-nanowires ability in recognizing the electrochemical properties of cancer cells and apply them to help in developing a prognostic tool for future diagnostic technology. This new method also can be potentially used in various important applications in cancer screening and monitoring, which are doable in vitro at ultra-low-cost and in real-time.

Chapter 4. Major Methods for The Characterization

4.1 Power X-Ray Diffraction (PXRD)

X-ray diffraction (XRD) is long-used as a reliable method for characterizing a crystal phase. It tells the atomic and the molecular structures in a three-dimension (3D) crystal lattice. The XRD instrument consists of three main parts: X-ray tube, substrate, and the detector. When the monochromic X-ray striking on the sample, the scattering X-rays from crystallized atoms can interfere and diffract into a unique XRD pattern, as characteristics of the crystal lattice, that can be detected by the XRD detector. The PXRD is commonly used to identify the crystal phase, orientation, size and perfection of nanomaterials, based on the Bragg's law:

$$2d\sin\theta = n\lambda, \quad (1)$$

where the *(d)* is the spacing between two parallel and identical lattice-planes, *(θ)* is the XRD angle between the incident beam and the atomic plan in the 0-180° arrangement, *(n)* is an integer (order of the XRD), and *(λ)* is the wavelength of the incident X-Ray beam. Since the angle *(θ)* collected form diffracted beam and the wavelength are known, the lattice parameter *(d)* can be calculated from Bragg's law, a. s explained in detail in the **Fig. 4.1**. Standards in Joint Committee on Power Diffraction Standers (JCPDS) or International Center for Diffraction Data (ICDF) can be used to identify the crystal structure of a new nanomaterial, which is a common practice in the nanomaterial's chemistry.

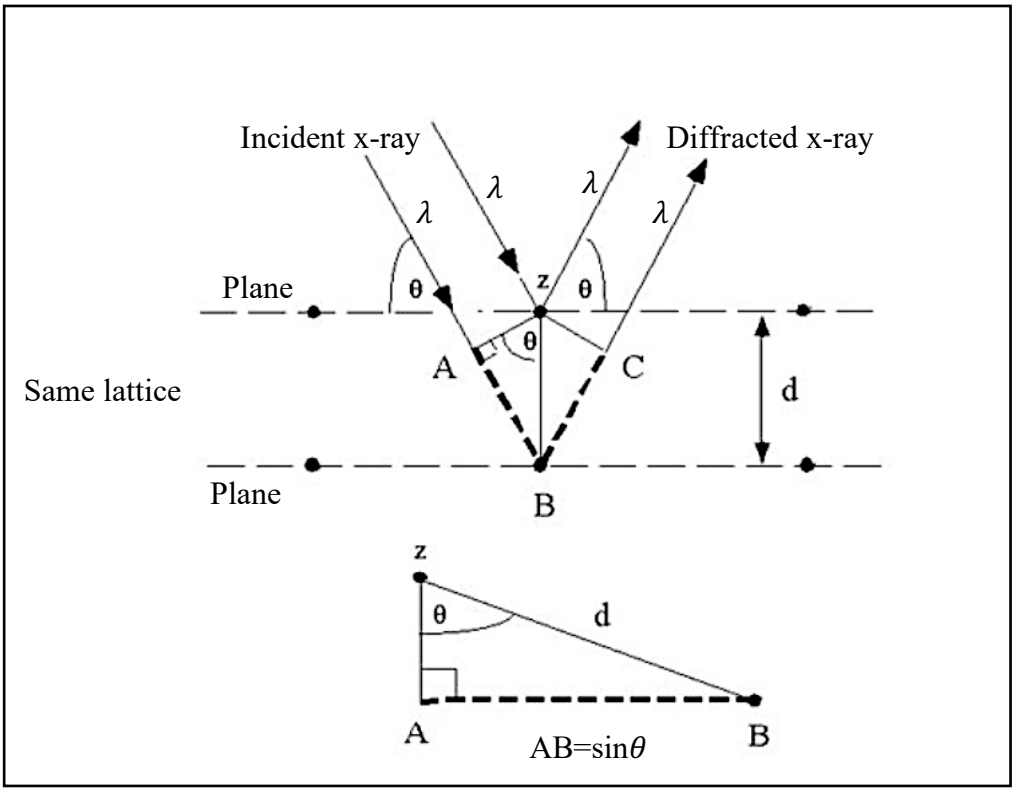

Figure 4.1: Bragg's Law illustration.

4.2 Scanning Electron Microscopy (SEM)

Compared to regular optical microscope, the SEM provides a higher magnification (10,000 times more), higher resolution, and much clearer three-dimensional (3D) image with a much greater focal depth. Therefore, SEM is used commonly to characterize the topography and the morphology of the material of interest. The topography reflects the relationship between material's surface feature and the properties of that material. On the other hand, the morphology reflects the nanomaterial's shape, size and spatial organization that are all crucial to widely vary the nanomaterial's properties and applications.

An SEM is basically structured as shown in the **Fig 4.2**. The electron gun generates a focused beam of electrons from, commonly, a tungsten filament with a sharp loop-tip that emits a

narrow stream of electrons upon being heated by an electrical current. The anode (accelerator) is located under the electron gun, using its negatively charged surface to repel negatively charged electrons thus focusing and accelerating them. The magnetic lenses are to focus the electrons on to the sample i.e. narrowing the beam of electrons to hit the sample.

In the SEM sample preparation, the sample surface is coated with gold usually in a plasma sputtering coater under a vacuum form a mechanical pump. The surface gold coating provides an electric grounding path to prevent the electron-accumulation (charging) problem thus-getting a clear micrograph, on the SEM detector, of the sample surface topography.

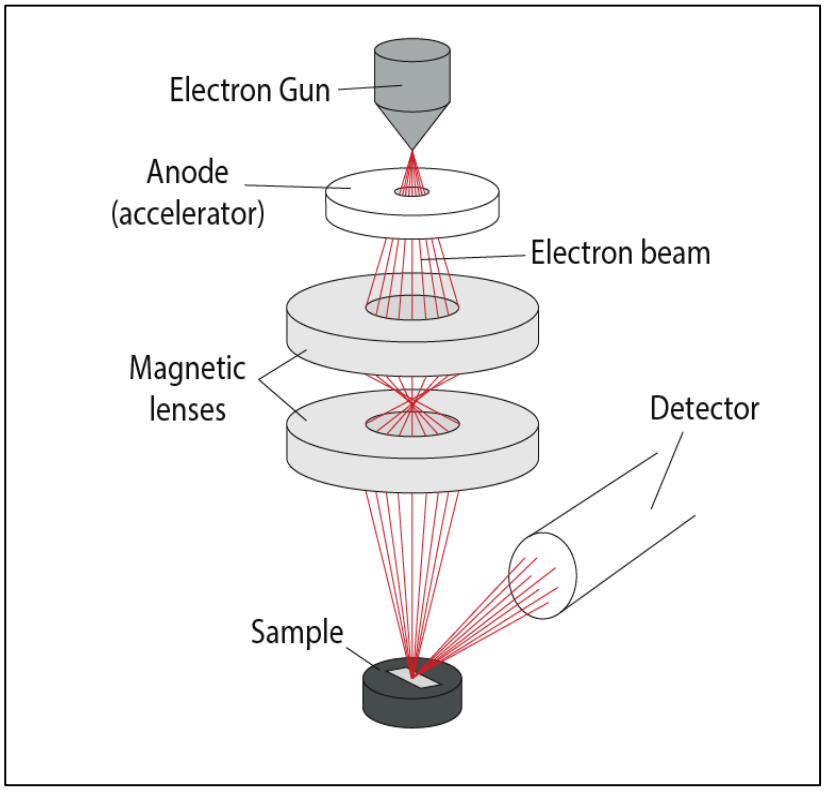

Figure 4.2. Schematic representation of the basic SEM components.

4.3 Electrochemical Impedance Spectroscopy (EIS)

Electrochemical Impedance Spectroscopy (EIS) is a well-established method widely used in biosensing, using an alternative current (AC) to detect electrochemical impedance. The impedance is defined as the ability of circuit to resist the flow of electrical current in a complex system, for measuring over a wide range of AC frequencies the dielectical properties of a material. EIS has been used in this work to develop a label free biosensor that hopefully can distinguish multiple electrochemical changes occurring at the same time. For example, it may identify the diffusion-limit of a passive film and the electron transfer rate of a reaction, the capacitive behavior of the system, etc.

In the impedance sensing experiment, an AC voltage signal ($V_{(\omega)}$, usually sinusoidal) is applied as a frequency-dependent excitation. Then, a response ($I_{(\omega)}$) is measured (**Fig. 4.3**).[43]

$Z_\omega = E_\omega / I_\omega$, Z_ω= Frequency-dependent impedance, SI unit ohm (Ω)

E_ω = Frequency-dependent potential (voltage), mV

I_ω = Frequency-dependent current, A

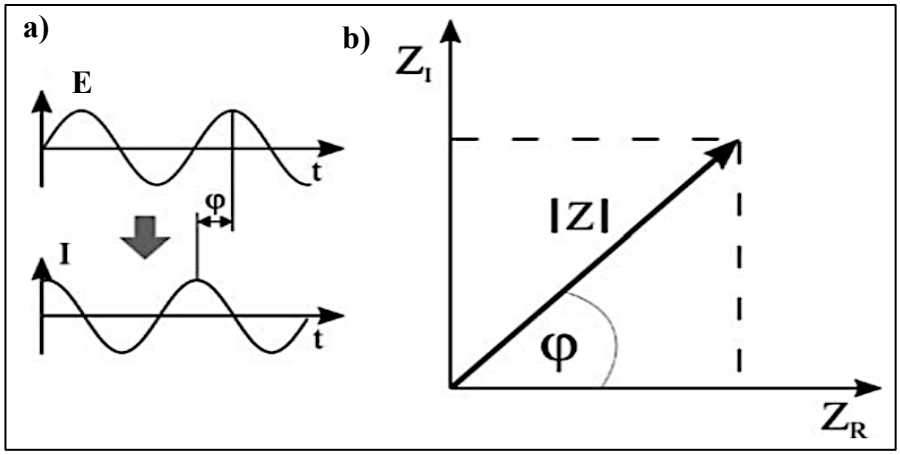

Figure 4.3. a) The phase shift between the voltage and current. b) The phase shift as an angle between the real (Z_{RE}) and imaginary (Z_{IM}) parts of the complex impedance.

Phase shift between voltage and current can be expressed by (Fig 4.3 (a)):

- **excitation as f(t)** $E_t = E_o \sin(\omega t)$

  Where:

  E_t- potential at time t

  E_0- amplitude

  ω- radial frequency = $2\pi f$

  f - frequency

- **response signal** $I_t = Io \sin(\omega t + \phi)$

  Where:

  I_t - response at time t

  I_0 - amplitude

  ϕ - phase

The real (Z_{RE}) and imaginary (Z_{IM}) parts of the complex impedance are called resistance and reactance (**Fig 4.3 (b)**).

4.4 Randal's Equivalent Circuit

The electrochemical cell can be modeled by electrical circuit elements that be determined by EIS (**Fig. 4.4**), in which,


Resistor, Z = R (Ohms), 0° Phase Shift

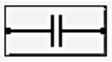
Capacitor, Z = -j/ωC (Farads), -90° Phase Shift


Inductor, Z = jωL (Henrys), 90° Phase Shift

$j = \sqrt{-1}$

$\omega = 2\pi f$, radians/s, f = frequency (Hz or cycles/s)

A real response is in-phase (0°) with the excitation. An imaginary response is ±90° out-of-phase.

 Warburg Impedance: It represents the resistance to mass transfer (diffusion control), and typically exhibits a 45° phase shift. **Equations of equivalent circuit:**

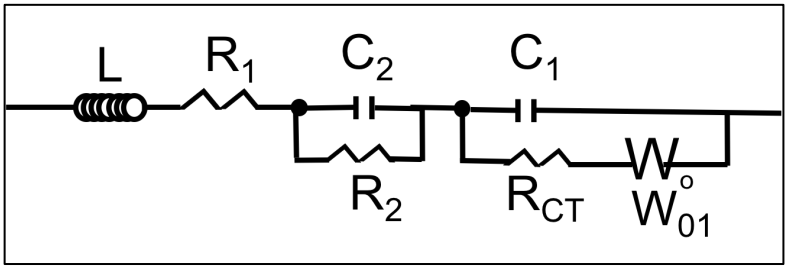

Figure 4.4: The equivalent circuit, with the nanowire induction (L), nanowire resistance (R_1), cell membrane capacitance (C_2), cell membrane resistance (R_2), intracellular matrix capacitance (C_1), intracellular matrix resistance (R_{CT}), and Warburg diffusion impedance (W_{01}).

Table 4.1: Equivalent Circuitry Parameters.

Equivalent Circuitry Parameters Determined Empirically in the Work	**Values**
L	**$1x10^{-7}$**
R1	**50 (Ω)**
R2	**10 (Ω)**
C1	**$1x10^{-6}$ (F)**
C2	**$2x10^{-6}$ (F)**
R_{CT}	**3 (Ω)**
Sigma (σ)	**0.0005**

The overall impedance of the circuit in (Fig 4.4) is given by:

$$Z = j\,\omega\,L + R_1 + \frac{R2\,\frac{1}{j\omega C2}}{R2+\frac{1}{j\omega C2}} + \frac{(RcT+Zw)(\frac{1}{j\omega C1})}{RcT+Zw+\frac{1}{j\omega C1}}$$

The Warburg impedance diffusion is described by

$$Z_w = \frac{\sigma}{\omega^{1/2}} - \frac{j}{\sigma\,\omega^{1/2}}$$

Where σ is related to the diffusion coefficient of species in the cell (see Bard)[152]

When separated in the real and imaginary components

$$\mathbf{Z_w = R_e + j\ I_m}$$

$$\mathbf{R_e} = R1 + \frac{R2}{A} + \frac{\mathrm{RcT} + \frac{\sigma}{\omega^{1/2}}}{\mathrm{B}^{2} + \mathrm{C}^{2}}\text{, And}$$

$$\mathbf{I_m} = \frac{\omega \mathrm{L} - w\mathrm{C2R2}\,(1-\omega^2\,LC2)}{\boldsymbol{A}} - \frac{\left(\frac{1}{\sigma\,\omega^{1/2}}\right)\mathrm{B} + \omega C1\left(RcT + \frac{\sigma}{\omega^{1/2}}\right)}{\mathbf{B}^{2}+\mathbf{C}^{2}}$$

Where:

$\mathbf{A} = 1 + (\omega\ C_2 R_2)^2$

$$\mathbf{B} = 1 + \frac{C1\ \omega^2}{\sigma}$$

$\mathbf{C} = \omega\ C_1 \left(R_{cT} + \frac{\sigma}{\omega^{1/2}}\right)$, $\omega = 2\pi f$, f = frequency of interrogating signal

Part II

Chapter 5. Materials, Chemicals and Experimental

5.1 Materials and Chemicals

Titanium substrates (foil,0.25mm (0.01inc) thick, 99.99% metal base) was acquired from the Alfa Aesar, USA. Sodium Hydroxide (NaOH) pellets from Avantor performance martials, Sweden. Glucose was obtained from Sigma-Aldrich, Inc., USA.

Phosphate Buffer Saline (PBS) was prepared following the table:

Table 5.1: Regents for preparing PBS (pH7.40, 1L)

Chemical	**Maas (g)**
Sodium chloride (NaCl)	8 g
Potassium Chloride (KCl)	0.2 g
Sodium phosphate dibasic Na_2HPO_4	1.44 g
Potassium phosphate dibasic KH_2PO_4	0.24 g

An 800 ml of deionized distilled (DDI) water was charged in an a one-liter polyethylene bottle and stirred with a magnetic stirrer while adding the chemicals in the order (**Table 5.1**). The pH was adjusted to 7.4 by titrating with a 1M HCl solution, the volume was adjusted to one litter, and the bottle was stored in a refrigerator at 4°C.

Four cancer cell lines, MCF-10A, MCF7, MDA-MB 231, and HCT 116 (all from the ATCC, USA) were obtained from Dr. Du's and Dr. Shi's labs (the first three) and Dr. Muldoon's lab (the HCT116) on campus through collaborations. The MCF 10A is a normal human epithelial

cell line, MCF7 is a human non- invasive epithelial breast cancer cell line, MDA-MB231 is a human invasive epithelial breast cancer cell line. The HCT 116 is a colon cancer cell line.

5.2 Experimental

5.2.1 TiO2- nanowire hydrothermal synthesis

A titanium sheet (from Alfa Aesar) of 1.5 cm × 2.0 cm in size was sonicated in 10 mL of acetone in a vessel for 15 min at room temperature (25ºC), then taken out and rinsed with DDI water (**Fig 5.1**). Next, the Ti-sheet was placed in 10 mL of 1.0 (M) NaOH solution in a Teflon-lined vessel (Parr Instruments, **Figure 5.2**) that was sealed and hydrothermally heated in an oven at 160-250 ºC for 4−8 hrs, then cooled in air outside of oven for 4− 24 hours. Thus-treated sample now, surfaced fully with the titanate nanowires-entangled scaffolds, was rinsed with DDI water until the surface reached pH ≈ 7, and dried in air.[5] Lastly, each sheet was scratched atop to expose metal for connecting the electrode, and epoxy-glued on rest edges and back, leaving a small front area sensing cells.

5.2.2 The nanowire characterization

5.2.2.1 X-ray Diffraction (XRD)

The phase purity and crystalline structure of the nanowires were characterized by X-ray diffraction (XRD) using Rigaku Miniflex X-ray diffractometer with a Cu Kα (λ=1.5405Å) radiation source, scanning from angle 20 to 70 (2θ) with a 0.02˚step and a step time of 1.25 s.

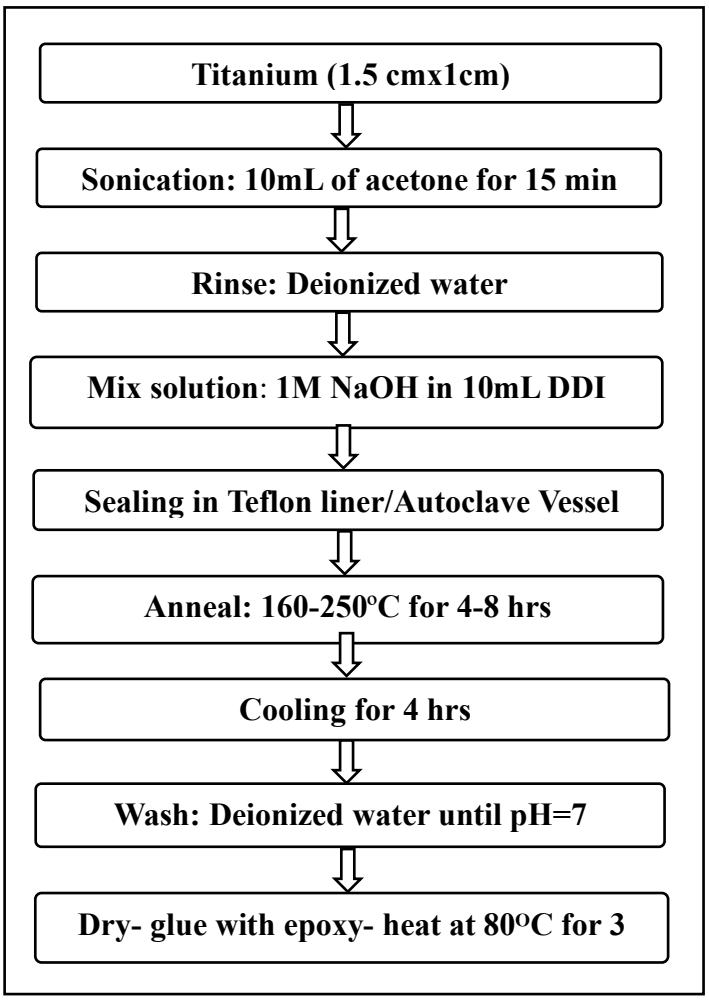

Figure 5.1: Schematic illustration for TiO_2-Based nanowire hydrothermal synthesis process.

Figure 5.2: The autoclave chamber (left) and the Teflon liner (23mL) (right).

5.2.2.2 Scanning electron microscope SEM

The morphology of the nanowire scaffolds was examined under a scanning electron microscope (SEM, Tescan SEM VEGAII SBH) performed at 30kV. Both top and cross sections of TiO_2-based nanowire.

5.2.2.3. Point-of-Zero-Change (PZC) of H-Titanate nanowires

To estimate the PZC of the TiO_2-nanowire, a range of different pH from 2 to 12 were prepared by using 0.1 M of hydrochloric acid (HCL) and 0.1 M of sodium hydroxide (NaOH) in the DDI water. The pH was checked by the pH meter. The aqueous solutions containing the sample were rotating overnight at room tempreture. The rotating will allow the nanowire to be exposed to the different pH solution. The clear solution will be used to measure the final pH using the pH meter and the result of initial and final pH will be used to determine the Point-of-Zero-Change (PZC).[153]

5.2.2.4 Impedance characterization of the nanowires

The platinum (Pt) was the counter electrode. The titanate scaffold sheet in a similar initial impedance curve was used as background. The impedance was tested by means of a Gamry Potentiostat (Reference 600, Gamry Instrument, USA), with the parameters of 5mV AC and frequency range 0Hz-1MHz (**Fig. 5.3**).

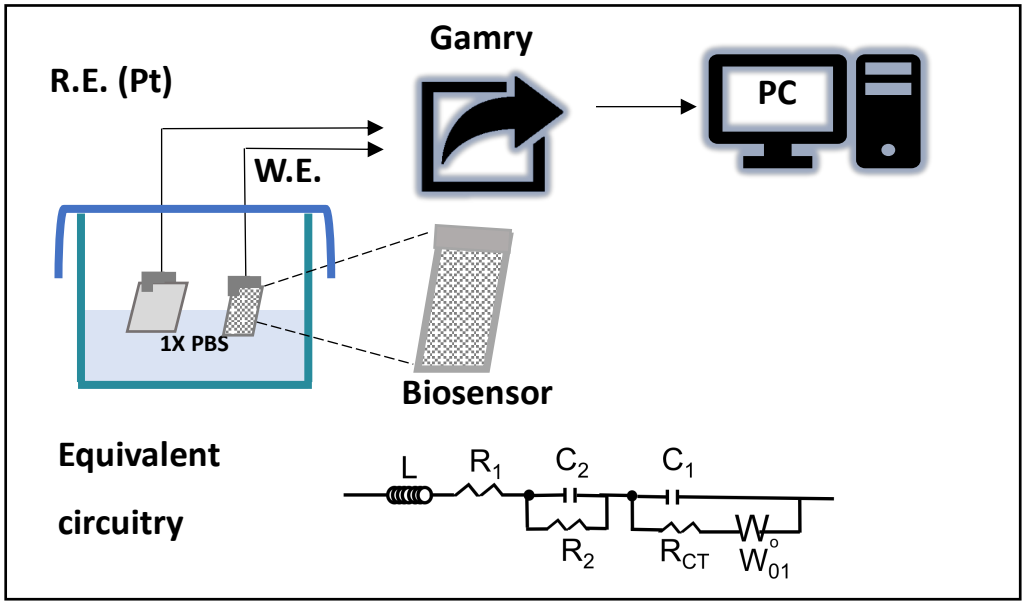

Figure 5.3: Schematic illustration for the set-up and corresponding equivalent circuitry.

5.2.3 Bioimpedance cell sensing on the titanate nanowires

5.2.3.1 Impedance test for breast cancer cell lines

This test was carried out to determine if the biosensor can distinguish the cancer cells pathological malignance. The frequency was swept to determine range giving the a clear impedance difference (separation) between the cancer and normal cell line. At least three such biosensors having similar initial impedance curve were incubated in a 10ml (1×PBS) solution containing one million (10^6) cells/ml for 35 minutes at room temperature (25℃), with each of the three breast cells lines (MCF10A, MCF7, and MDA-MB 231) and one colon cancer cell line (HCT116), respectively.

5.2.3.2 Impedance test for breast cancer cell lines at various incubation frame

Cells where incubated in different time intervals (25, 35, and 45 minutes). The impedance was recorded for the three cell lines (MCF10A, MCF7, and MDA-MB 231) to determine the best incubation time to do the impedance test as described earlier. The parameters setup was by changing the frequency starting from 30 kHz till 1MHz.

5.2.3.3 Impedance test for normal and breast cancer cell lines in mixed sample

This test aims to determine if the biosensor can detect the presence of abnormal cells within the normal population and can distinguish the pathological stage of cancer cell. Both cancer cells lines (MCF7 and MDA 231) where mixed with normal cell line (MCF10A) in different (cancer cell: normal cell) ratios (1:100, 1:50, 1:25, 1: 10, 1:5). The parameters setup was by changing the frequency starting from 30 kHz till 1MHz.

5.2.3.4 Impedance test for breast cancer cell lines at 37℃

This test was conducted to determine if the tempreture affect the different cell impedance. The cancer cell lines and the biosensor (TiO_2) where incubated for 35 minutes. Impedance test was done as described previously under two different tempreture, 25 and 37℃. The parameters setup was by changing the frequency starting from 30 kHz till 1MHz.

5.2.3.5 New impedance test for glucose effect on the breast cancer cell lines

This test was done to investigate the effect of glucose on the cancer cell behaviors and in turn the impedance readings. The four cell-lines (MCF10A, MCF7, MDA-MB231, and HCT116) were suspended in a 10mL 1×PBS containing 5.5 (mM) of glucose. The impedance test was done

as described in the above. The parameters setup was by changing the frequency starting from 40 kHz till 1MHz.

5.2.3.6 New impedance test for Doxorubicin effect on the breast cancer cell lines.

This test was performed to investigate the effect of a well-known chemotherapy drug Doxorubicin on two different cancer cell lines. MCF7 is known to be more resistive to DOX than MDA-MB231.[154] To investigate the cell impedance change due to the DOX, the two cell lines were first cultured to reach 90% confluence and then the DOX (2μM) was added over two time-intervals, 24 hours and 48 hours. The cells were then harvested using trypsin and counted using the hemocytometer and trypan blue stain to control the cell number. The cells were then suspended in 10mL of 1× PBS with the TiO_2-nanowires sensor for 35 minutes, and the impedance was tested likewise from 40 kHz to 1MHz.

The second set of experiment was done as in the first step, with glucose (5.5 mM) in the cell suspensions to investigate the cell impedance correspondence to glucose effect after being treated with DOX. The biosensors were done after 35 minutes in the cell suspension, with the impedance parameters same as described previously.

5.2.4 Microscopic visualization using Fluoresce staining

After the data collection, the three scaffolds were dyed with SYTO®24 Green-Fluorescent Nucleic Acid stain (from Life Technology) with 490 absorptions and 515 emission wavelengths to visualize the attached cells. After fluorescence images were taken by Olympus BX41 microscope, cells were detached with trypsin and washed until no significant fluorescence could be seen. The test confirms the attachment of cells to the TiO2- nanowire surface and confirming that the change in nanowire resistivity is coming from cell attachment.

5.2.5 Error analysis

All experiments were repeated three times using the same TiO_2-nanwire scaffold. All cell suspension contains the same cell number/ml. All data are expressed as mean $\pm$ standard deviation for at least three repeats.

Chapter 6. Results and Discussions

In **Fig. 6.1,** the intermediate sample (4hrs reaction) looks dark grey, and the final product of the nanowire-covered surface seems grayish, both far from the Ti-metal that looks like the stainless steel. This implies that even the Ti-metal and nanowire should show different PXRD patterns.

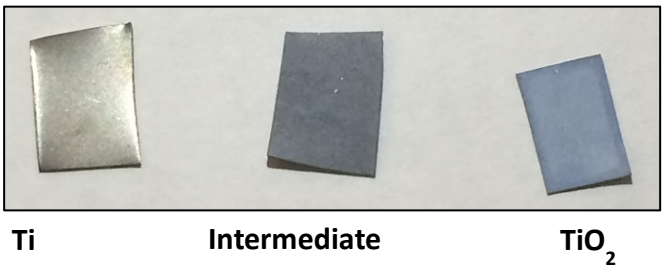

Figure 6.1: The physical morphology of titanate after the hydrothermal treatment.

6.1 Nanowire Characterization

6.1.1 Powered X-ray diffraction (PXRD)

The PXRD study was conducted to characterize the crystallinity and structure of the nanowires grown directly on the Ti-metal surface. The **Fig. 6.2** shows the PXRD pattern of a typical sample with the nanowires grown in situ on the Ti-metal. Comparing with the data reported by others including those from our same lab in literature [5], the five peaks at the 2-theta values of 32, 34, 36, 38.5, 40 ,53, 70, and 78 belong to the Ti-metal under the nanowires, while the rest peaks at the 2-theta values of 10, 24, 28, 48, 50 match the clay-like layered structure of sodium titanate ($Na_2Ti_3O_4$).

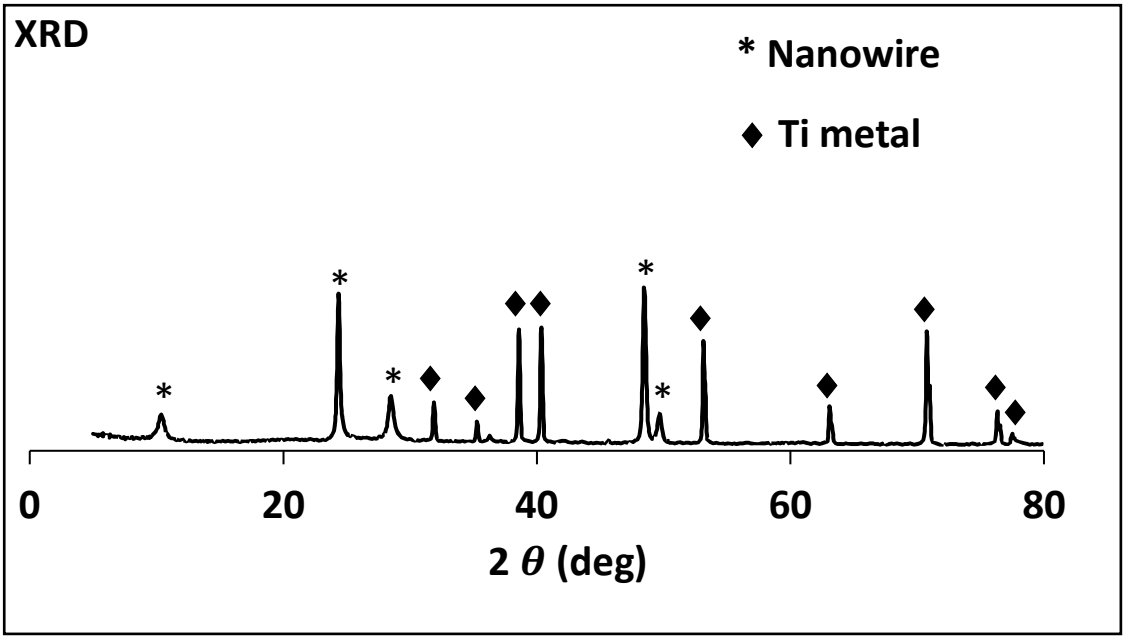

Figure 6.2: PXRD pattern for titanate nanowire pattern of a typical sample with the titanate nanowires on the Ti-metal after 24 hours of the hydrothermal treatment (see the discussion on the time-study below).

6.1.2 Scanning electron microscope SEM

As schematically illustrated in the **Fig. 6.3**, the SEM micrographs illustrated the growth and entanglement of the nanowires in the hydrothermal reaction on the Ti-metal. After the hydrothermal treatment for 4, 8, and 12 hours, the nanowires grew long enough over time to start to naturally entangle atop, self-assembling into the bioscaffolds with "bird-nest" like concaves (i.e. cell-nest) on the sample surface, as depicted in the cross-section images in the **Fig. 6.4**. Further prolonging the reaction time to 7, 18, and 24 hours, respectively resulted in slightly better developed and organized cell-nests (**Fig.6.5**). On this basis, the samples from 8-hours of the hydrothermal growth with enough well-developed "cell nests" were chosen to support the low-cost, quantitative, label-free, and real-time detections and differentiations of cancer cells for the first time on a smart bioscaffold.

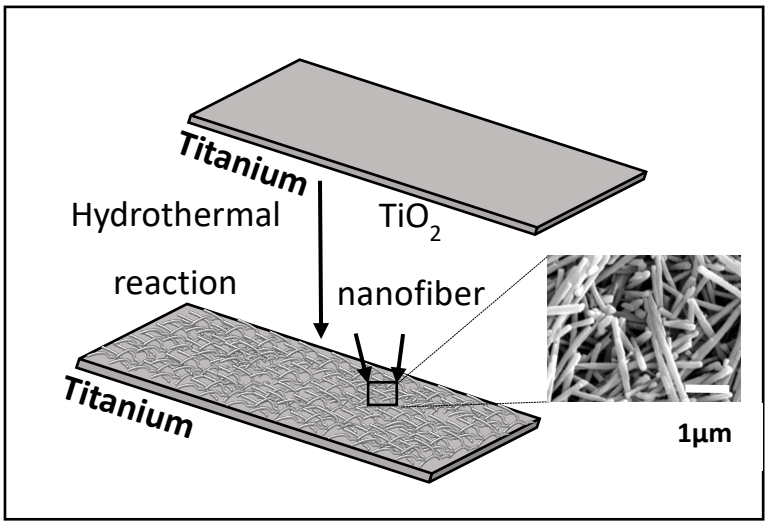

Figure 6.3: A schematics for illustrating the change on the Ti-metal surface after the hydrothermal reaction, as supported by the SEM micrograph.

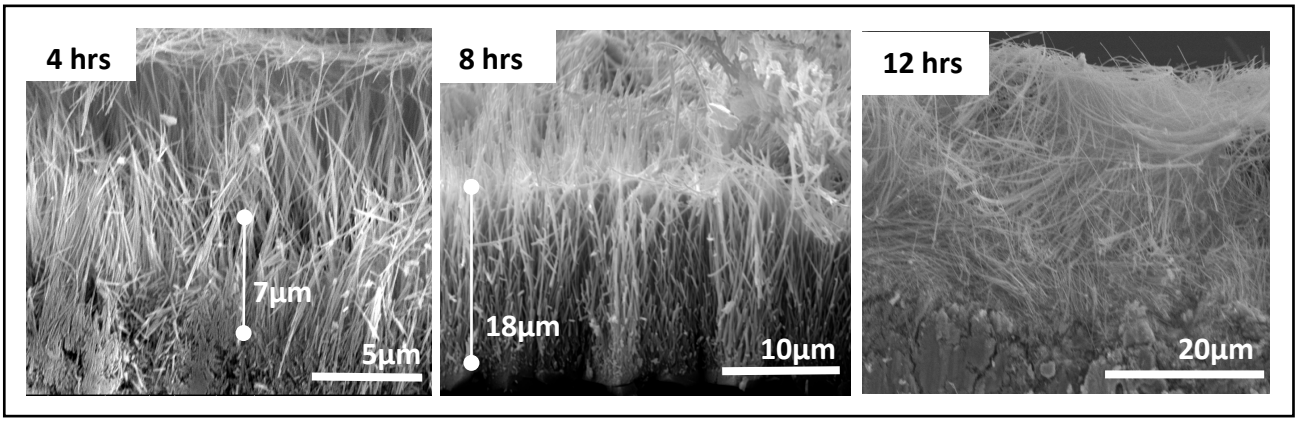

Figure 6.4: The SEM study on the nanowires from the growths over the 4, 8, and 12 hours.

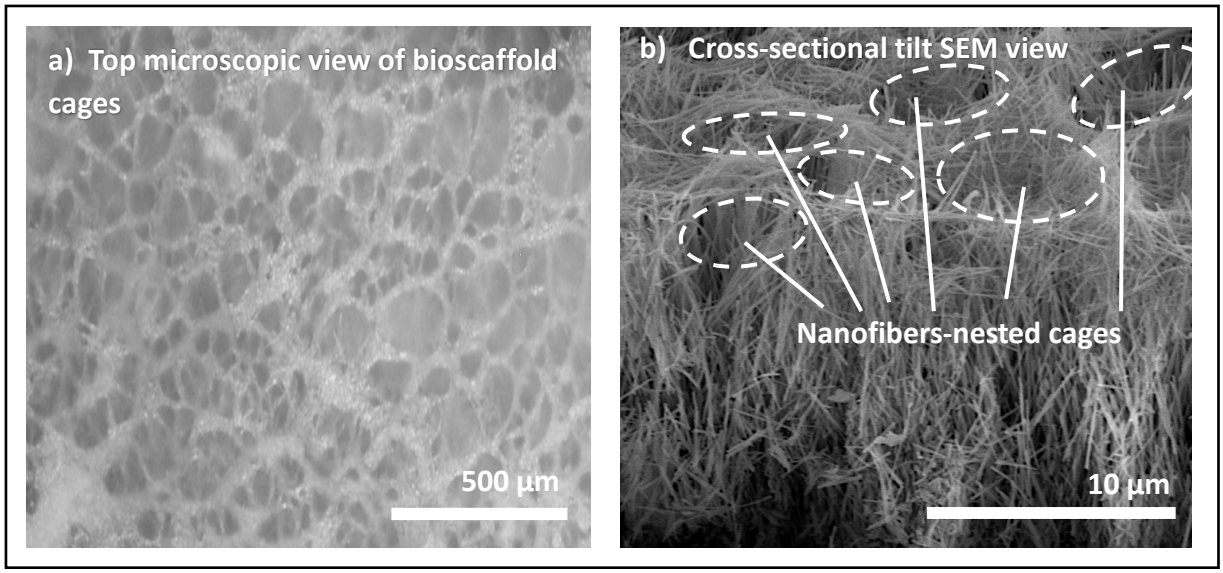

Figure 6.5: The SEM characterization of the bioscaffolds on the typical sample from 8-hour hydrothermal synthesis. (a). The face-on view on the sample-top; (b). The tilt view.

6.1.3 Point-of-Zero-Change (PZC) on H(Na)-Titanate

To understand the surface cation exchange of titanate nanowire, a simple pH-titration was conducted to estimate, on the nanowire surface, the point of zero charge (PZC) value from the equilibrium between the H^+ on the nanowire surface and that in the solution. In the plot of the initial vs. final pH values (**Fig. 6.6**), the flat region's pH is often regarded as the PZC.[153]

Accordingly, the nanowire's surface ion-exchanged protons (H^+) (i.e. Lewis acid) and surface hydroxide (OH^-) (i.e. Lewis base) groups can co-affect the average surface acidity/basicity at the nanowire-water interface. This further suggests (i) the continuous $H^+ \leftrightarrow Na^+$ ion-exchange can make the nanowire surface to buffer between pH 4 (of the hydrogen titanate) and pH 10 (of the sodium titanate),[155] (ii) the capacity and kinetics of nano-buffering may reflect the completeness of intercalation of the Na^+ with the H^+ on the titanate nanowire, (iii) the negative framework made of $(Ti_3O_7)^{-2}$ tend to be a multi-deck Lewis base host, as H^+ is a strong but Na^+ is a week Lewis-acid guest. This new insight of the surface dynamics in the solution surface nanochemistry and "conjugated acid-base" nanochemistry supports that a controlled time (i.e.

degree) of the DDI washing (i.e. H^+ exchange) can convert the nests of as-made Na-titanate nanowires to that of a H(Na)--titanate nanowire with a PZC at/around the pH 7 for doing the cell-biosensing.

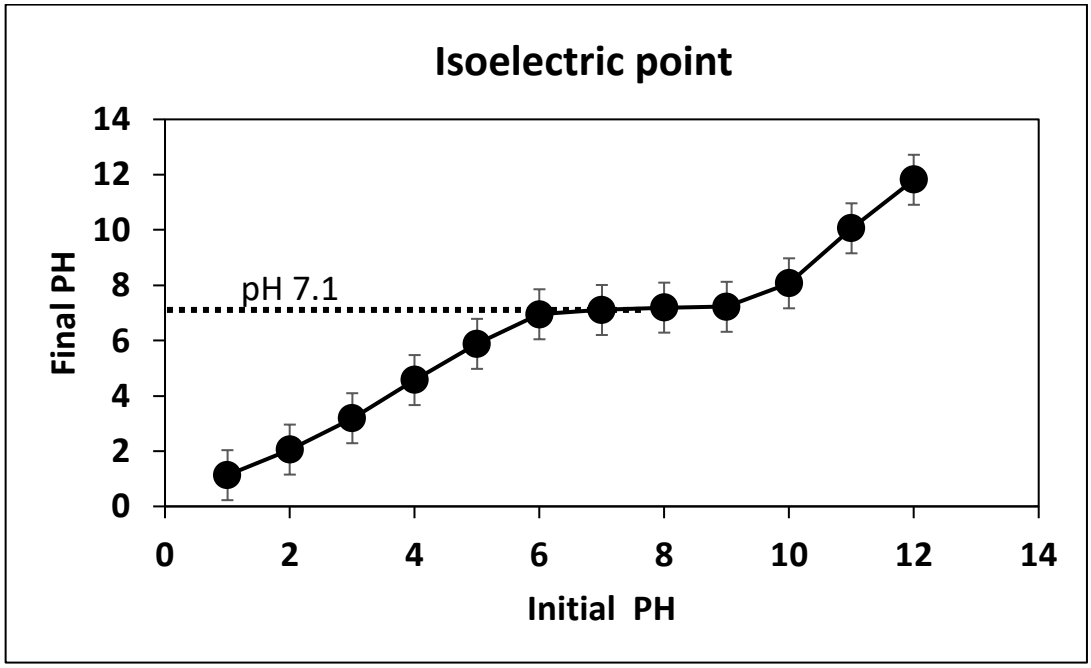

Figure 6.6: Point of zero charge (or isoelectric point) of the DDI-washed titanate nanowires from the titration between pH 1 and pH 12.

6.1.4 Impedance characterization for the titanate nanowires-entangled cell-nests

A series of (1×) PBS solutions between pH 4 and pH 8 were used to quantify the effect of pH on the impedance of the titanate nanowires-entangled cell-nest (**Fig. 6.5**). The result shows a clear correlation between the impedance and solution pH, in which the impedance increases generally with the pH. This correlation can be explained again with the Lewis acid/base theory. In the aqueous solution, the hydroxyl group on the nanowire surface was deprotonated and negatively charged when the pH ~ 7 (i.e. above the PZC point). On the contrary, the surface -OH groups being protonated (gain H^+) will be positively charged at the pH < PZC point.[153] This is in line with such a fact that an oxide in an aqueous solution above (or below) its PZC the surface pH decreases (or increases) as the surface be deprotonated (or protonated). At equilibrium, no net

proton transfer thus no further change to the PZC point. Thus, the electrical impedance of the nanowires (with the poor electrical conductivity) is commonly used to quantify such surface-PZC point shifting corresponding to the mass transfer of ions of any type in a confined area. Equivalently, when the solution pH decreases, the nanowire surface is more protonated, gaining more positive charges on the nanowire surface to facilitate a faster charge-transfer along the nanowire surface and to reduce the impedance. This supports **Fig. 6.7** and in turn how crucial the water-washing step in controlling the nanowire surface PZC point.

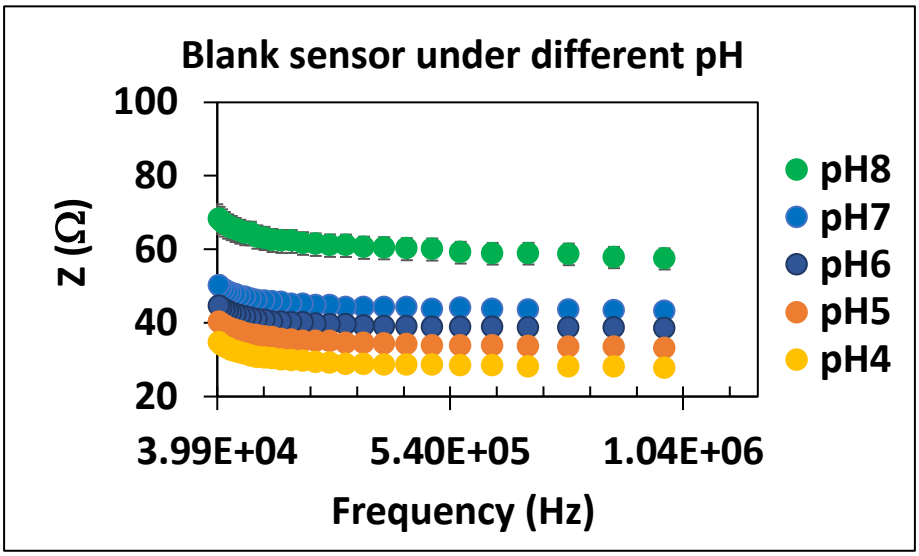

Figure 6.7: The impedance measurements of titanate surface corresponding to pH titration.

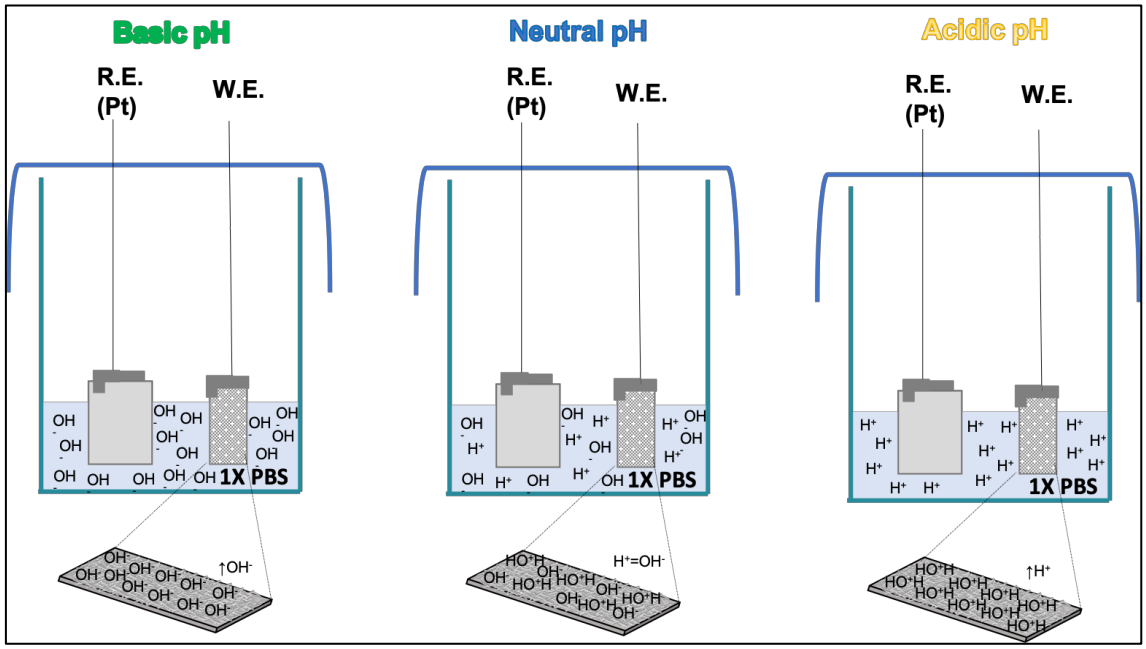

Figure 6.8: Illustration of surface deprotonation and protonation corresponding to the aqueous solution pH change.

6.2 Impedance Sensing of Live Cell on the TiO_2-Nanowires.

Characterizing individual cancerous cells from the blood stream i.e. the circulating tumor cells (CTC) tumors using a simple and quick impedance test is of importance to support both qualitative and quantitative cancer pathology beyond the current practices using either staining or optical imaging that are slow, labor-intensive and expensive. When cancer cells of the malignant and benign subtypes look similar from one another using the staining and optical imaging. However, the subtypes difference in metabolism should enable us to develop an alternative diagnostic tool with negligible false-negative and false-positive problems, which has been underexploited. Such new method should rely on the cancer cells' metabolic wastes among which the ionic spices can change our nanowire-bioscaffold surface's charge-transfer pattern, thus-affording the new cell-sensing method.

6.2.1 Impedance test for breast cancer cell lines over the sensing time

Cells contain an intracellular medium surrounded by a semipermeable membrane, which separates the extracellular from the intracellular ionic solutions using the cell membrane made from a lipid bilayer, proteins, and some poly-saccharides. The membrane exhibits capacitive properties due to the electrical potential difference between the membrane's two sides, and the impedance of cell membrane's capacitance changes with the frequency. At low frequency, the cell membrane is more like an insulator, resulting a higher impedance (i.e. highly resistivity) that allows current in the extracellular medium. When the frequency is high, the cell membrane is like a capacitor and starts to conduct charges and allow the current to go through the membrane, thus-reducing the impedance signal.

In our experiment, more cells were attached onto the nesting nanowires over long time after the bioscaffold-sensor was inserted in the PBS solution containing the cells. Different cells upon attaching onto the nanowire-nest surface can instantly change the nanowires' impedance differently. After the attaching for about 35 minutes, normal breast cells (MCF10A) shift the impedance by 40−50 ohms at the high frequency range (1MHz) (**Fig. 6.9**), while the benign breast cancer cells (MCF7) shift that to about 60 ohms (**Fig. 6.10**), and the malignant breast cancer cells (MAD 253) can do so by 80 ohms (**Fig. 6.11**). The **Figs. 6-11** suggest that the net surface charge for the three cell lines are different, therefore, they change the nanowires surface charge differently, which can be better seen in thus-combined **Fig. 6.12**.

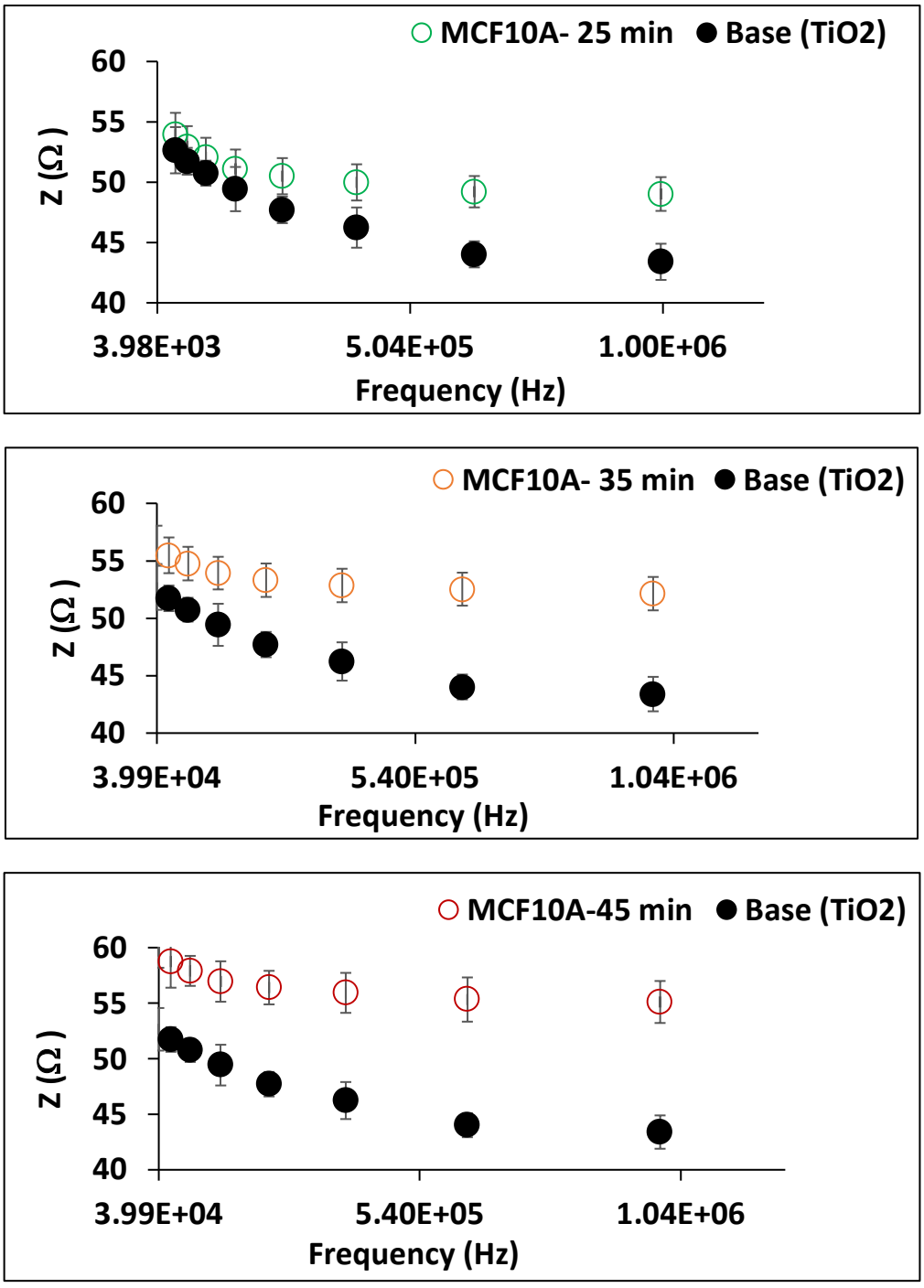

Figure 6.9: Impedance vs Frequency for normal cells (MCF10A) in three-time frames (25,35, and 45 minutes). The error bar reflects three repeats.

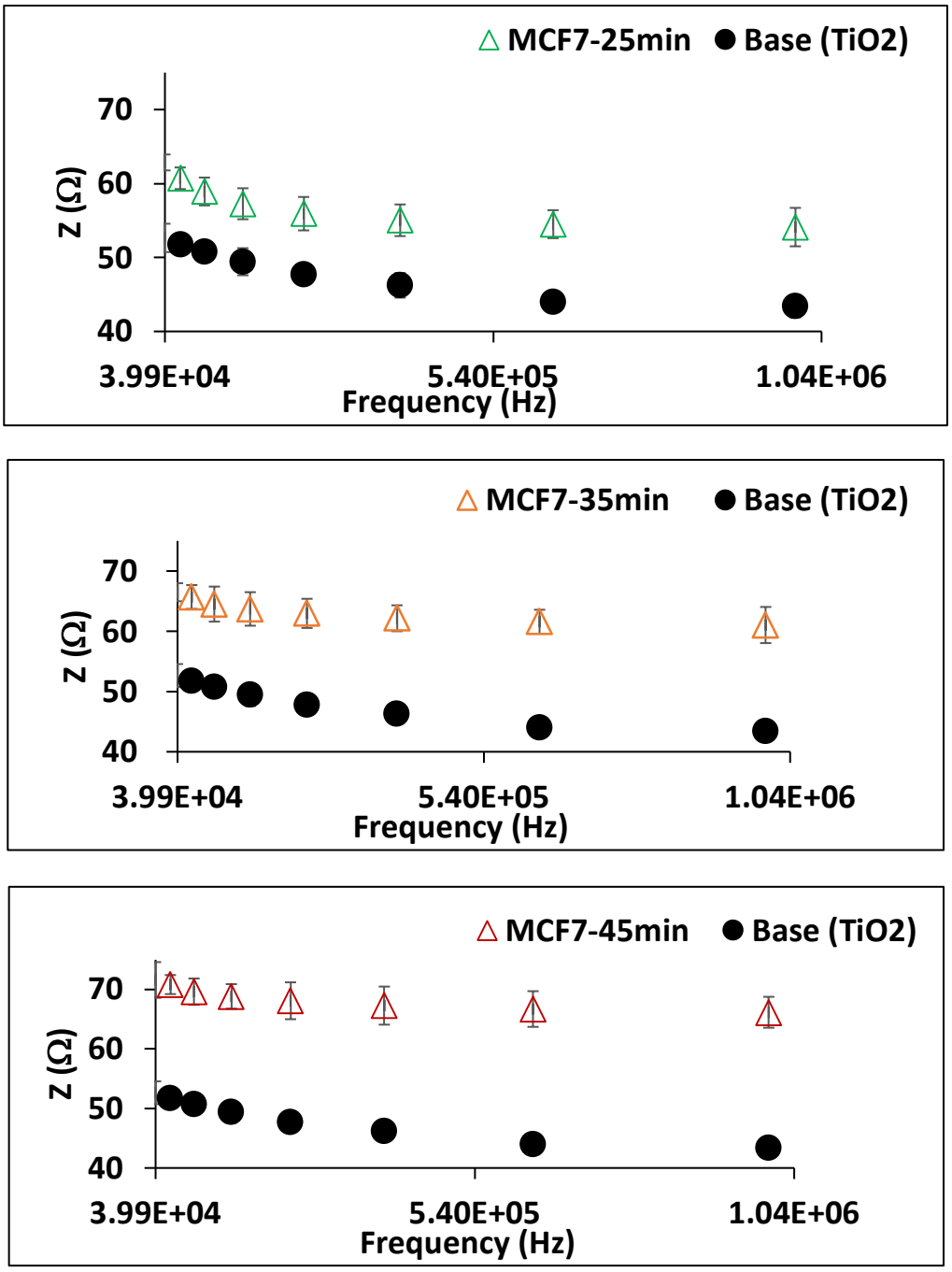

Figure 6.10: Impedance vs Frequency for benign cancer cells (MCF7) in three-time duration (25,35, and 45 minutes). The error bar reflects three repeats.

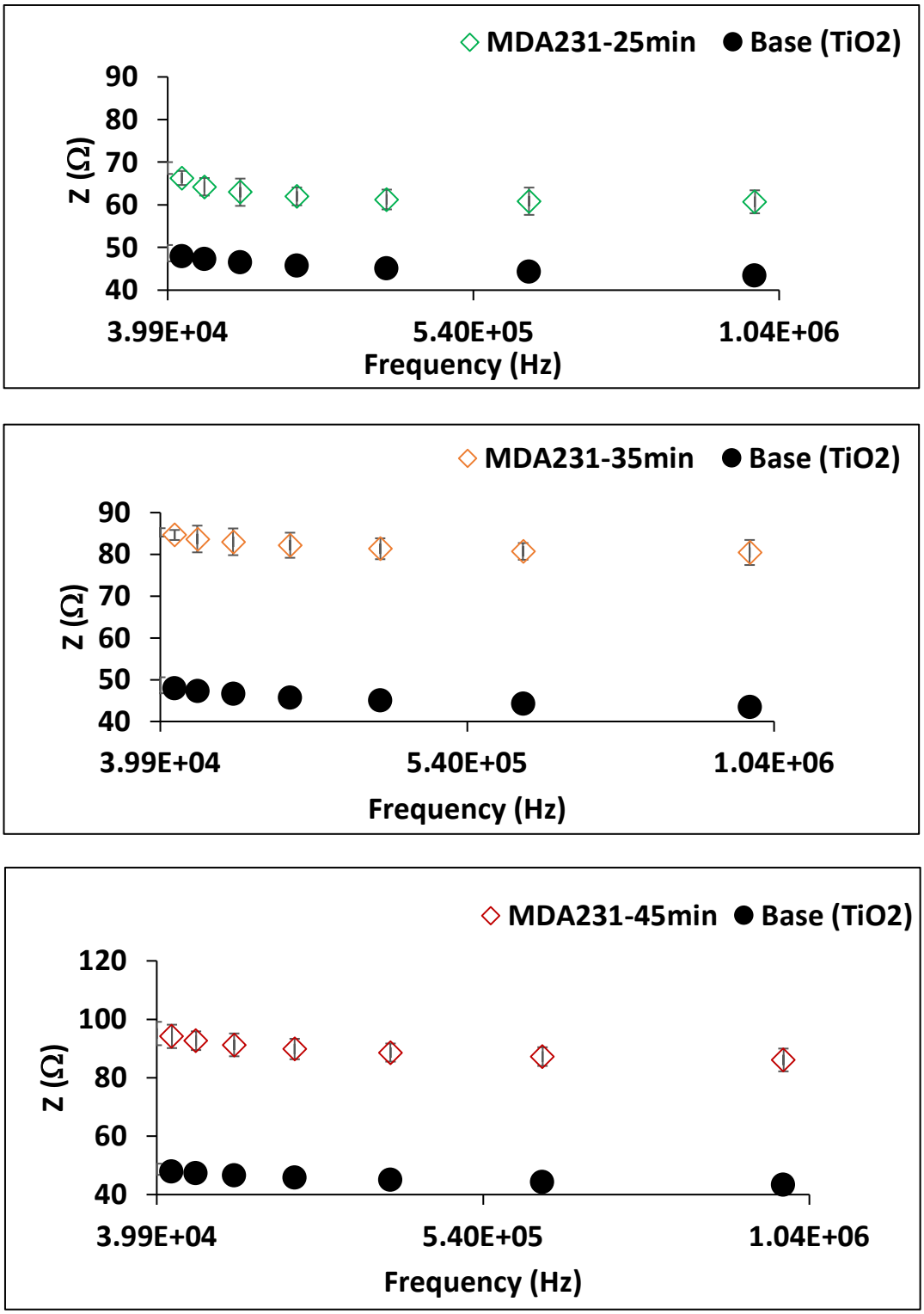

Figure 6.11: Impedance vs Frequency for malignant breast cancer cells (MDA-MB231) in three-time durations (25,35, and 45 minutes). The error bar reflects the three repeats.

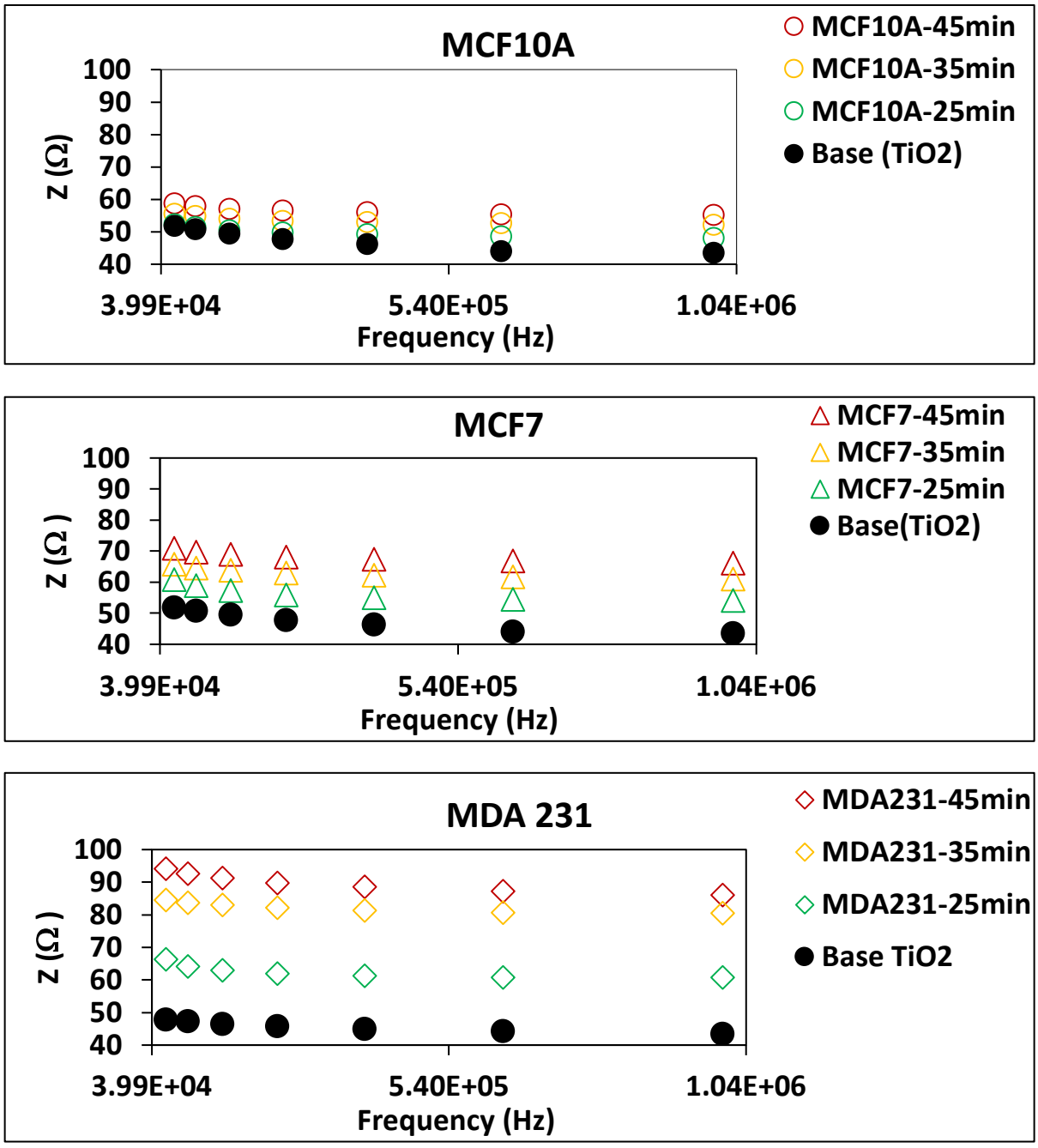

Figure 6.12: Impedance vs Frequency for three breast cancer cells (MCF10A, MCF7, MDA-MB231) in three-time duration (25,35, and 45 minutes).

Dobrzynska[156] and coworkers did the electrophoresis to study the changes of surface electrical properties as a function of pH for the same cell lines, on a four-component equilibrium model with a negligible variation between the experimental and theoretical charge in the pH range of 2.5−9.0. In studying the mammalian cells, the pH was kept narrowly between 6 and 8, which the cell membrane proteins can be maintained during the electrophoresis. The results revealed that at a lower pH the charge density on the cancer cells surface gets more positive, meaning more protonated. Their findings concluded that this increase is related to the acidic (C_{TA}) and basic (C_{TB}) functional groups' *average association constant for hydroxyl ions* (K_{OH}) in the breast cancer cell membrane, especially in MDA 231, which is higher than that in normal cell (i.e. MCF10A) membrane.

From the plasma membrane proteomics,[157] the cell membrane proteins are elevated in MDA 231, comparing with the MCF7 and normal (MCF10A) cells, and the keratin type I Cytoskeletal 17 (KRT17) is present only in the normal cell. As the cell turns malignant, this cytoskeletal filament disappears i.e. being replaced by Keratin type I Cytoskeletal 19 (KRT19) that was found to be higher in the MCF7 cell-membrane. Vimentin (VIM), a cytoskeletal filament mostly expressed in mesenchymal stem cells, is highly expressed in the aggressive cancer cell (MDA-MB231). Microtubule-interacting protein 1B (MAP1B) was only found in MDA-MB231, while the subtype (MAP4) was found in both MCF7 and MCF10A. Myosin regulatory light chain 12B (MYL12B), important in maintaining the cell structure, was found only in MDA-MB231. Further, the MDA-MB231 have more cytoskeletal filaments and some are abnormally expressed. These are important to cause the resistivity changes by e.g. lowering the water content in the cell. These variations can be measured using the impedance to quantify the mass-transfer outside the cells at low frequency and that across the cell membrane (e.g. into the cytoplasm) at high frequency.

Further, the lipid bilayer was investigated to show the cancer cell membrane with fewer fatty acids and phospholipid types.[158] Interestingly, that study found that cancer cells produce more positively charged phospholipids, e.g. (PE 36:2) in MCF7 and (PC 32:0, PC 36:2, PI 36:1) in MDA-MB231. Among the fatty acids, mostly are the oleic acid (C18:1) and palmitoleic acid (C16:0) in MCF7, and the oleic acid (C18:0) and docosahexaenoic acid (C22:6) in MDA-MB231. The presence of such unsaturated fatty acids within the cell-membrane bilayer increases the cell membrane's fluidity, flexibility, and permeability along with the pathological malignancy of the cancer cell. Other studies reported an elevated phospholipid production in the same cell-lines.[156, 159, 160] This overproduction is often correlated to a tumorigenic transformation. This is because in the tumor's external microenvironment, the pH is more acidic (pH 6.5) hence the cancer cell surface net-charge is more positive, as the surface carboxyl, amino and phosphate groups are protonated. Therefore, increasing the number of cell surface phospholipids lead to a more negative surface charge density at high pH but a more positive charge density at low pH.

In breast tumor, the sialic acid was lately found to be upregulated which affects the cell membrane charge, and in turn the acid and basic groups on the cell membrane[160]. Thus, a knock out to an important gene in the sialic acid metabolism disabled the production of the active form of sialic acid and helped lower the lung cancer metastasis rate *in vivo*.[161]

In addition, the reactive oxygen species (ROS) can affect membrane lipids and proteins in the acidic environment, via triggering a lipid peroxidation process. Consequently, phospholipids in the inner lipid layer such as phosphatidylserine (PS) expose to the outside, thus-increasing both the acid group's content on the cell surface[156], and the level of K_{BOH} comparing with the original cell-membrane.

All these reports in the literature consistently support that the transformation in cell membrane structural lipid and protein composition can cause the increase in resistivity due to

exposure of negatively charged groups. In turn, the higher resistivity can lower the cell's outer layer potential, which further increases the resistivity of the cancer cell membrane and supports the selective quantitative cell-sensing and cell-type characterization.

6.2.2 1st impedance test for distinguishing breast cancer cells from colon cancer cells

An important question to be answered in this project is whether there is a difference in the surface charge density of cancer cells developed in different part of the body, e.g. colon cancer cells vs. breast cancer cells (**Fig. 6.13**). The breast cancer cells showed an increase in the impedance level corresponding to the cell's pathological malignancy. However, an opposite response was observed from the same sensing of an aggressive colon cancer cell (HCT 116) on the same set of the biosensors. This HCT 116 cell line has turned the nanowire-surface to be more conducting from apparently a lower impedance level. With little being reported in literature based on our thorough literature survey, the impedance data can guide future cell-biology study on the proteins and lipids in the HCT116 cell's membrane that are different than that in the breast cancer cells'. Further, modifying the breast cancer cell line membrane's protein and lipid constitution may help tell what opposite charge density is in the HCT116 cell with, probably, more amino groups on its surface at the experimental pH 7.4 being protonated to hold a positive net surface charge thus-making the bioscaffold-nanowire to be more conducting. Since the breast tissue (neutral) have different pH in nature than the colon (basic), the colon cancer cells should easily adapt to the acidic environment generated by the tumor tissue.

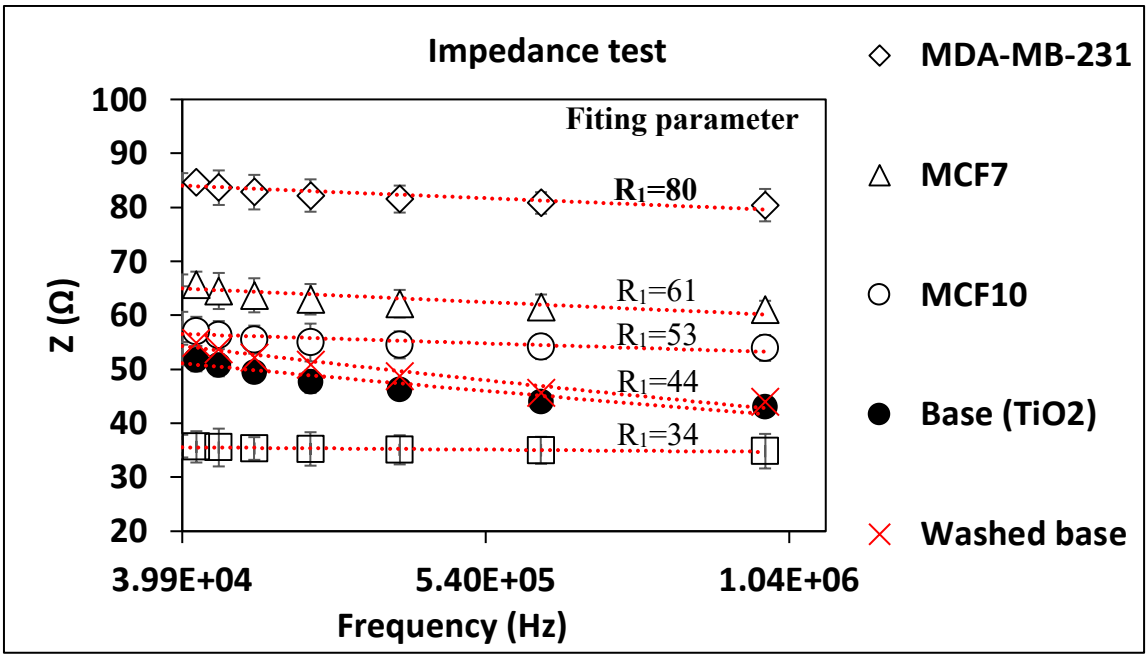

Figure 6.13: Impedance test for normal cell and different cancer cell types.

In the Nyquist plot (**Fig. 6.14**) with the real (Z_{RE}) and imaginary (Z_{IM}) parts of the complex impedance, each cell-line has a characteristic impedance level. Unusually, an induction effect exhibits clearly on every thus-made bioscaffold, due apparently to the nesting nanowires circularly self-assembling into each nest. In other words, the current moves on each nanowire surface from the bottom to the top of the nanowire in a circular manner for spirally electric field reaching the surface of each nest, thus-creating an inductive electromagnetic field for the nano-induction effect. This effect was not observed in pure Ti-metal working electrode, which means that the induction is not generated from the leads (**Fig. 6.15**).

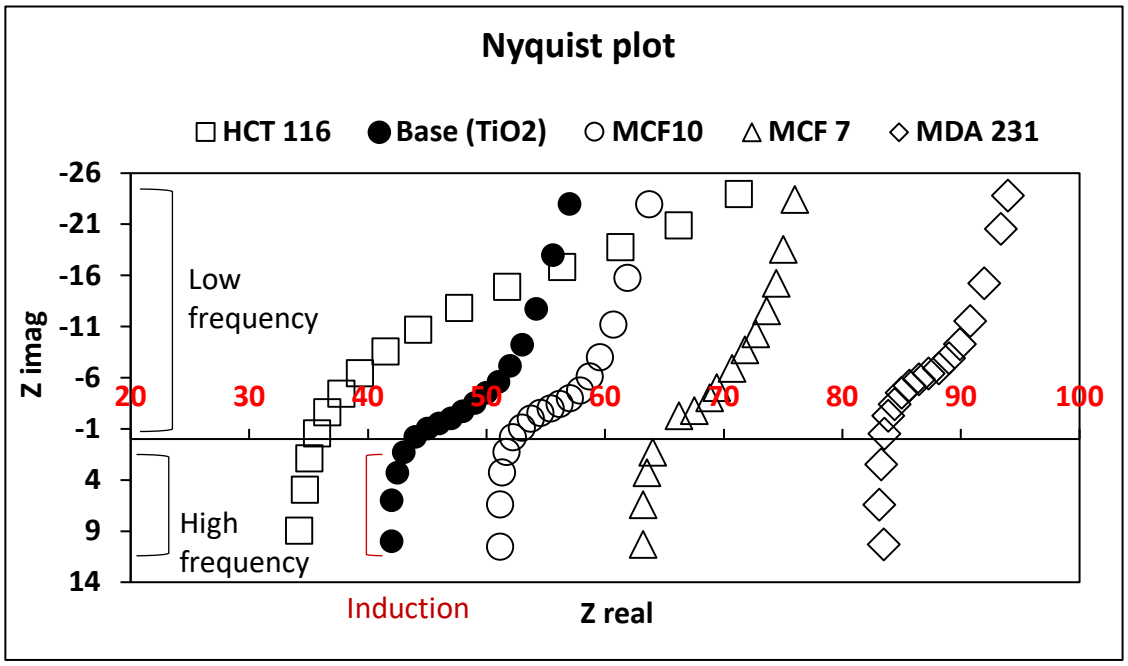

Figure 6.14: Nyquist plot for TiO_2, normal (MCF10A), and three different cancer cell lines.

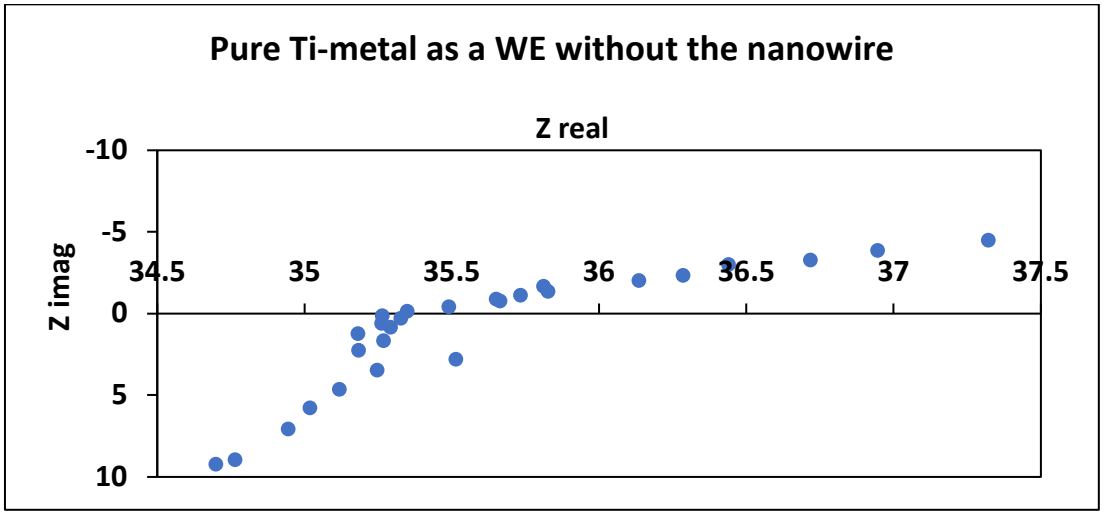

Figure 6.15: Nyquist plot for Titanium metal.

6.2.3 Impedance test for breast cancer cell and normal cell lines in different mixing ratios

This work aims to study how the impedance signal would change when the breast cancer cells and normal cells be mixed together. In this experiment, the MCF10A normal cells were mixed with the MCF7 and MDA 231 cancer cells, respectively, each across a wide range of mixing ratios, from 1:1,00 to 1:5 (**Fig. 6.16**). In the Fig. **6.16**, a linear correlation between the lower mixing ratio and the higher corresponding impedance can help quantify how many cancer cells being mixed in the normal cells. This method, if combined with a simple cytofluorometry (for knowing the total number of cells), can be useful to detect the CTCs in a mixture with other cells, because other lab reported a 5% increase of the impedance from one cancer cell in 100 normal cells.[58]

In literature, a study on these three cell-lines correlated a lower capacity with a higher malignance, due to the increase in the cell permeability for the pathologically more aggressive cancer cell.[60] An electrophoresis study on the same three cell-lines showed significant differences in the cell membrane net-charge, showing cancer cells' more negative electric properties towards negativity more than observed in normal cells.[156] These reports match our study, co-suggesting that our label-free nano-EIS sensor can distinguish normal from cancer cells, and differentiate the pathological malignance stages from early to late cancer progression.

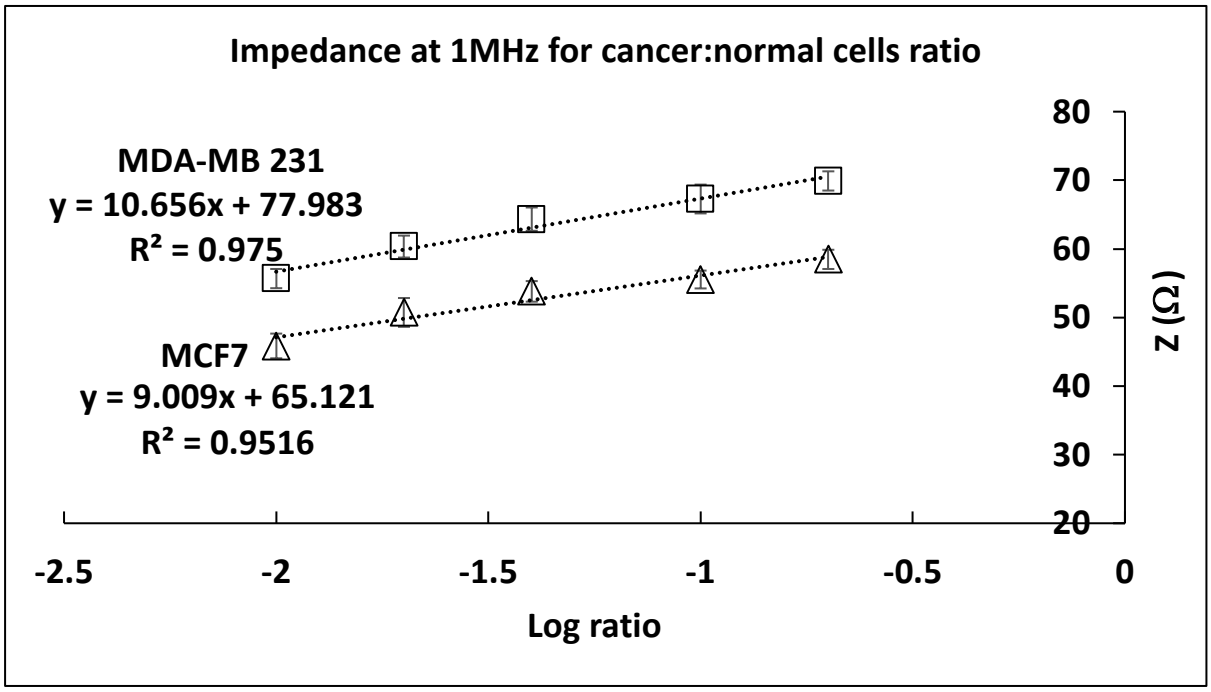

Figure 6.16: Impedance at 1 MHz for mixed sample.

6.2.4 1st impedance test for the Warburg effect on breast cancer and colon cancer cell-lines

The aim of this experiment is to quantify the effect of an electrically neutral metabolic fuel on the cancer cells, which is underexploited so far on an electrochemical nanosensor, but useful for quantifying and even characterizing cancer metabolic wastes, which is important in the basic cancer biology. In **Fig. 6.17**, the cancer cells shifted their impedance level from above to below the base line differently from the normal cells, indicating that the normal and cancer cells secret different metabolic wastes each in a unique charge density to affect the nanowire-surface charge uniquely.

As discussed in the **Chapter 2**, cancer cells consume glucose and secrete lactic acid as a metabolic waste (i.e. Warburg effect), with a consistent upregulation of genes for the glucose transport and glycolysis,[15-17] and the glucose transporters overexpress in hepatocarcinomas as

well.[18-20] By consuming more glucose than individual cancer cells, a tumor secretes a massive amount of lactate aiming to toxify the nearby normal cells more intensively, which can potentially result in a much stronger impedance signal on our bioscaffold sensor.

In cancer biology, under the help of overexpressed GLUT-1 that is activated by the HIF-1protein, cancer cells tend to have a higher intake of glucose results in more production and secretion of the negative-charged lactic acids. Thus-increased [H^+] on the nearby nanowire surface and increased in he nanowire-surface conductivity and lowered the impedance level, which is supported by the pH study in the **Fig. 6.7**. The MCF7 and MDA 231 cancer cells each showed a significant shifting (**Fig. 6.17**) in their impedance level (see the red and blue arrows) after allowing the cells to intake the glucose, thus-proving the Warburg effect for quantifying and characterizing the cancer and normal cells directly on our smart bioscaffold-turned nanobiosensor.

In general, different types of cancer cells may secret different metabolic wastes as the biomarkers. For example, the HCT 116 cells metabolism[162] from an increase in the β-oxidation and urea cycle metabolism secrets four main metabolic wastes: N-acetylputrescine, Phenylacetylglycine, Deoxycarnitine or gamma-butyrobetaine (GBB)**,** and Butyrylcarnitine.[162] These four metabolites each has an amide group in the structure. This explains why HCT 116 act differently from other breast cancer cells on the titanate nanowire-bioscaffold. Overall, different cancer cells secrete different metabolite wastes as the cell's biomarker that if showing a charge in water can help quantify and characterize the cells on the titanate-nanowire bioscaffold-nanosensor.

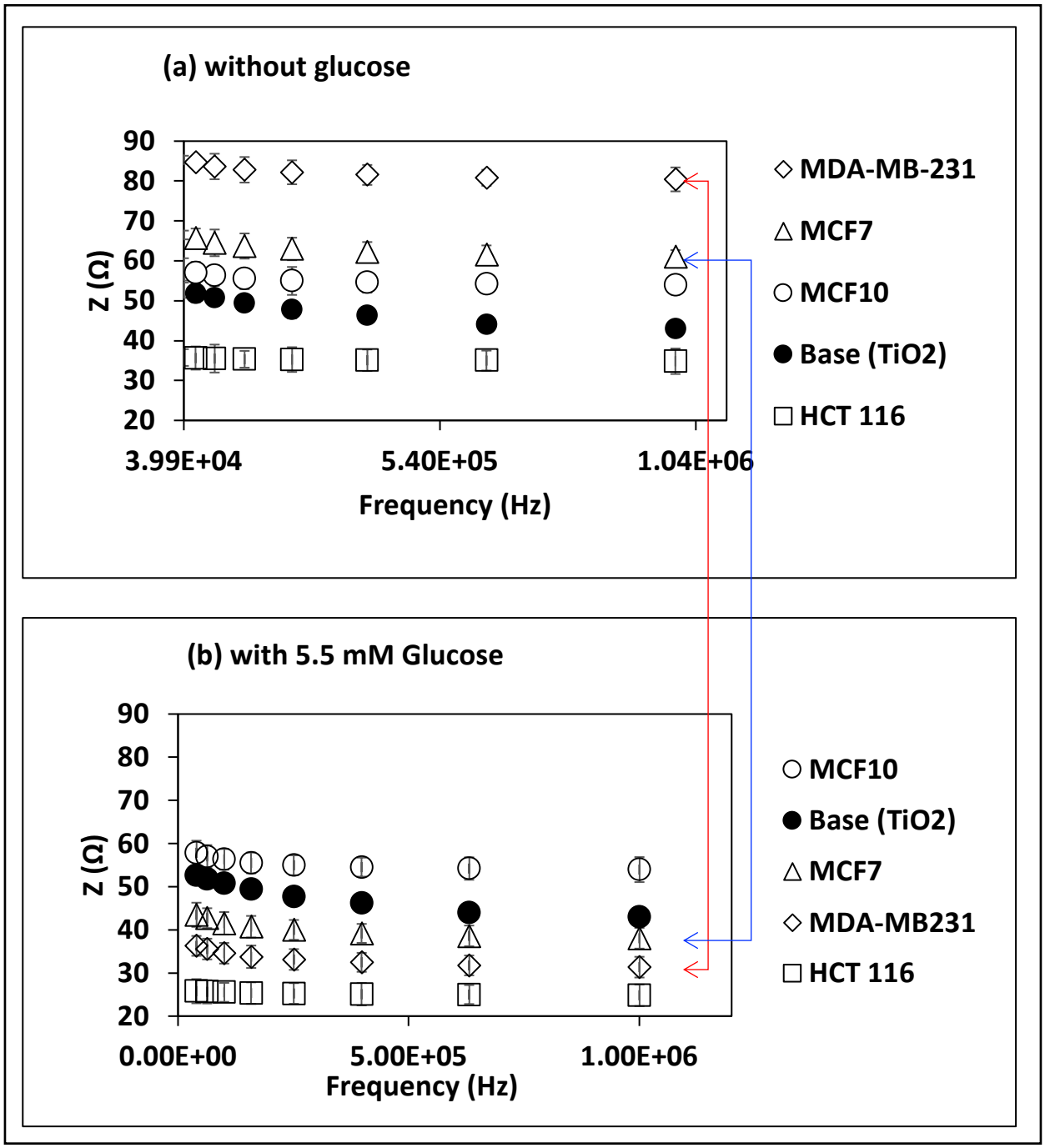

Figure 6.17: (a) Impedance test for different cancer cell lines with no glucose in 1xPBS. **(b)** Impedance test for cancer cells compared to normal cell incubated with 1xPBS+ 5.5mM glucose. *P* value for MCF7 and MDA 231 is $< 10^{-80}$.

6.2.5 Impedance test for the temperature effect on the breast cancer cell lines at 37℃

The abovementioned impedance tests done at room temperature (25℃) have raised a question regarding whether, and if yes how, the temperature that affects the cancer cell metabolism would change the impedance level at human body temperature 37ºC? In this experiment, the MCF7 and MDA 231 cells were attached on the bioscaffold, respectively over 35 minutes at 37ºC , and the impedance tests were done at the same tempreture. The impedance level for MCF7 and MDA 231 breast cell lines show no significant shifting in impedance signal intensity (**Fig 6.18**).

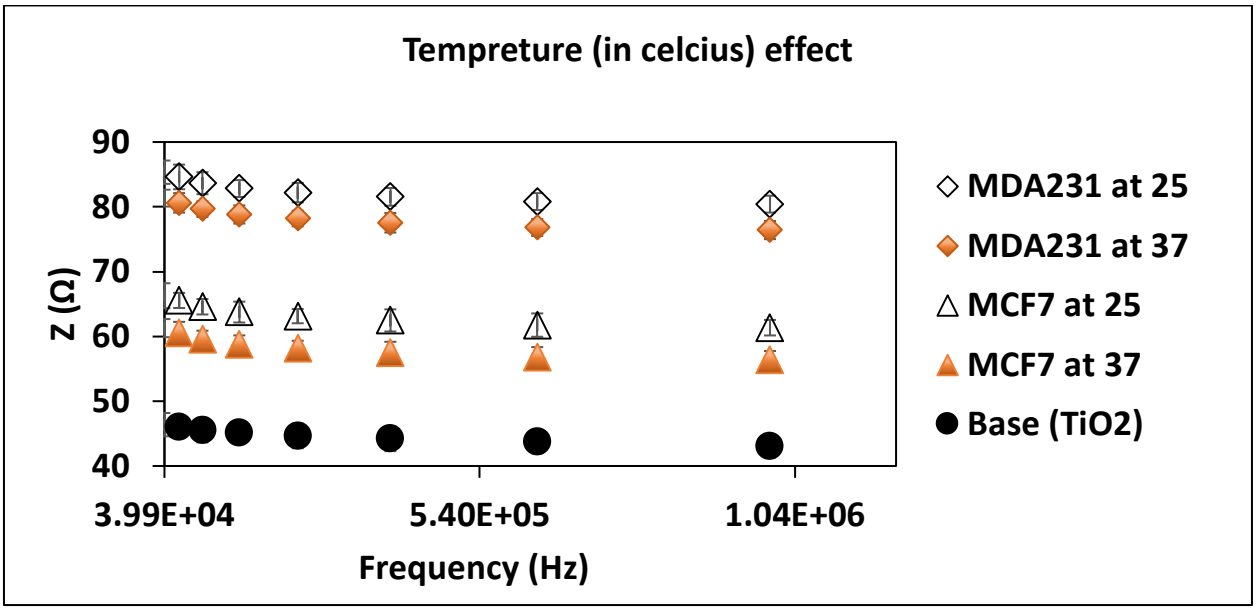

Figure 6.18: Impedance level of MCF7 and MDA 231 at 37℃

6.2.6 1st impedance test for the doxorubicin drug effect on the breast cancer cell lines

Doxorubicin (DOX, in a chemical formula of $C_{27}H_{29}NO_{11}$), also called Adriamycin^{TM}, is a popular chemotherapy drug for treating several types of cancer including breast cancer via triggering the cancer cell death. This drug was used to quantify the drug effect on breast cancer cells' metabolism in response to stresses from different dosages of the DOX, via monitoring the impedance signal change from the cancer cells before and after the DOX treatment. The drug cytotoxicity was assessed to determine the concentration of 2.0 (μM), which the cancer cells start to die in a proper pace that can enable us to quantitatively characterize the DOX effect on the cancer cell's metabolism and apoptosis directly on the smart bioscaffold **(Fig. 6.19)**.

The DOX is supposed to decrease the MCF 7 impedance due to cell's resistance to the DOX.[163, 164] This is because the overexpressed P-glycoprotein 1 (P-gp), also called multidrug resistance protein 1 (MDR1) or ATP-binding cassette sub-family B member 1 (ABCB1) or cluster of differentiation 243 (CD243), can pump the foreign molecules out of the MCF 7 cell.[165]

Due to MCF7 cell's resistance to DOX, incubating MCF7 with glucose helped MCF7 cell to flush the pre-absorbed DOX out to the extracellular solution, which should result in a higher impedance on the bioscaffold at low frequency due to the DOX negative in charge at physiological pH 7.4 (**Fig. 6.20**). In contrast, the MDA 231 cells, with a much lower resistance to DOX, should show a lower impedance under the same condition, and no significant response to glucose after being pre-treated with DOX (**Fig. 6.21**).

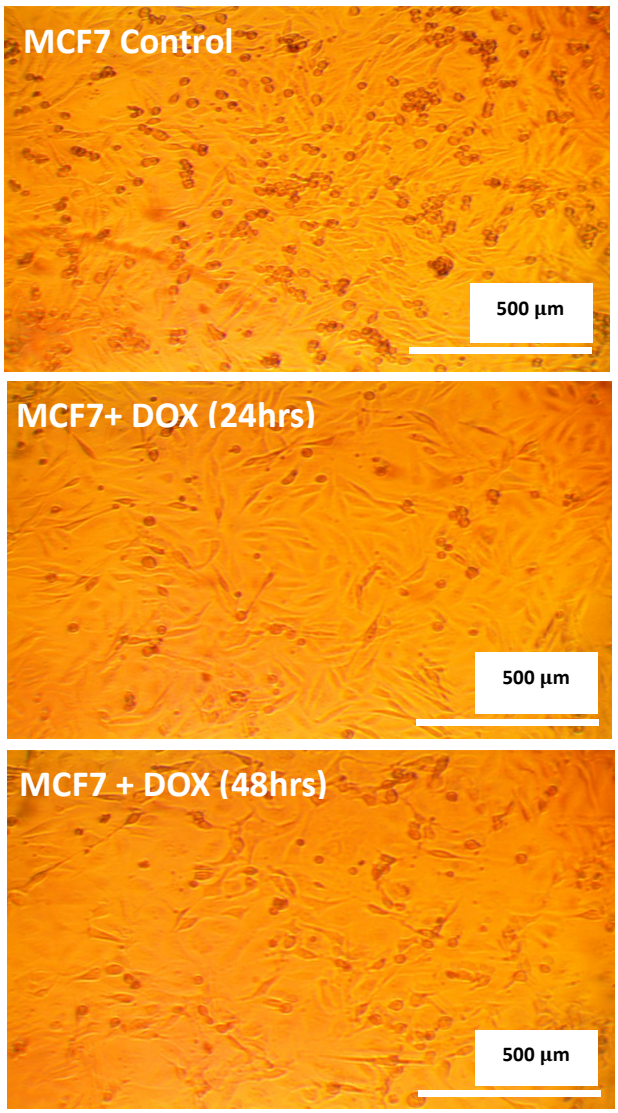

Figure 6.19: Microscopic image to drug treated MCF7 in cell culture compared to control.

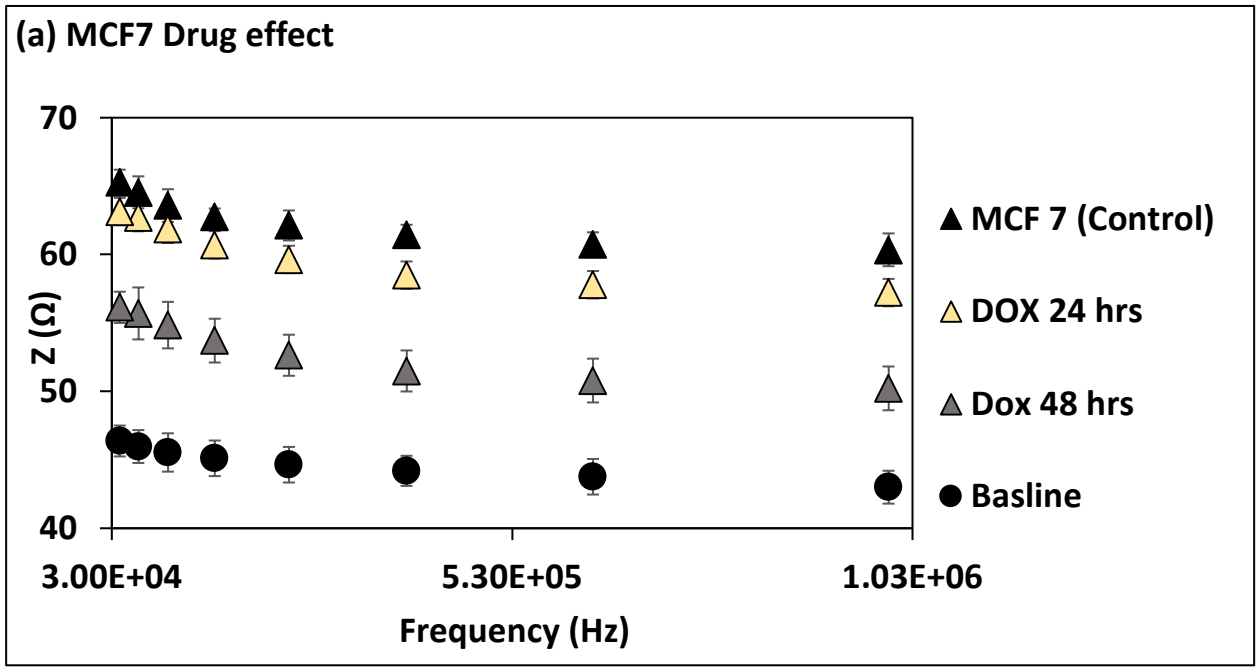

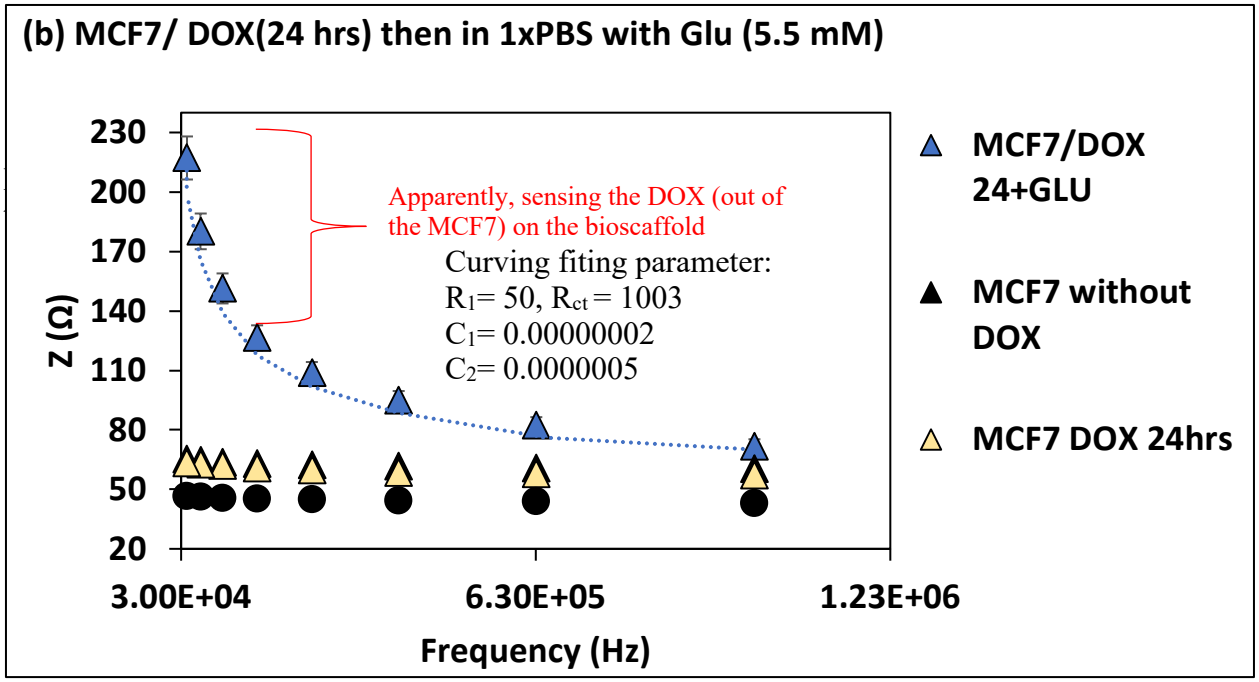

Figure 6.20: (a) Impedance test for MCF7 treated with DOX for 24 and 48 hours. (b) Impedance test for MCF7 treated with DOX for 24 hrs and then incubated with glucose for 35 minutes before performing the test.

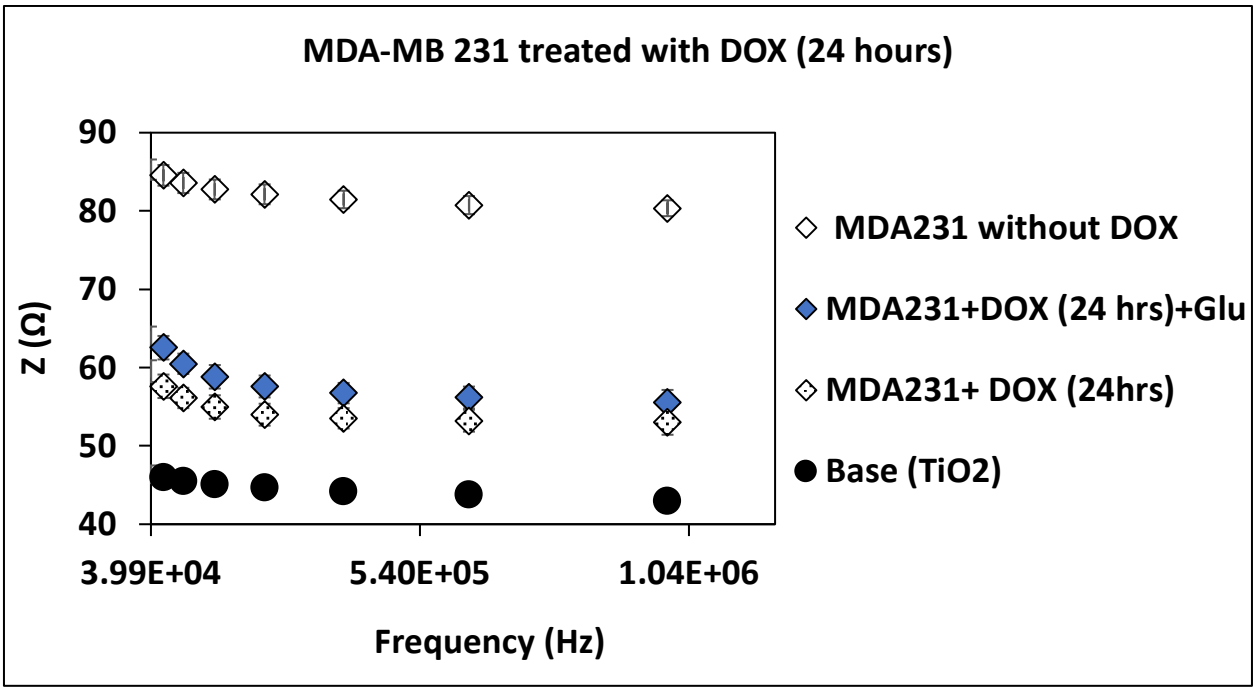

Figure 6.21: Impedance test of MDA-MB231 treated with DOX for 24hours and being incubated with glucose before the test.

6.3 Checking the cell attachment under the optical microscope

Before and after the impedance, the normal and cancerous cells on the bioscaffold were checked under the optical microscope. As can be seen in the **Fig. 6.23**, the cells population change on the bioscaffold was negligible, which supports why the impedance cell-sensing was kept within the 35 minutes.

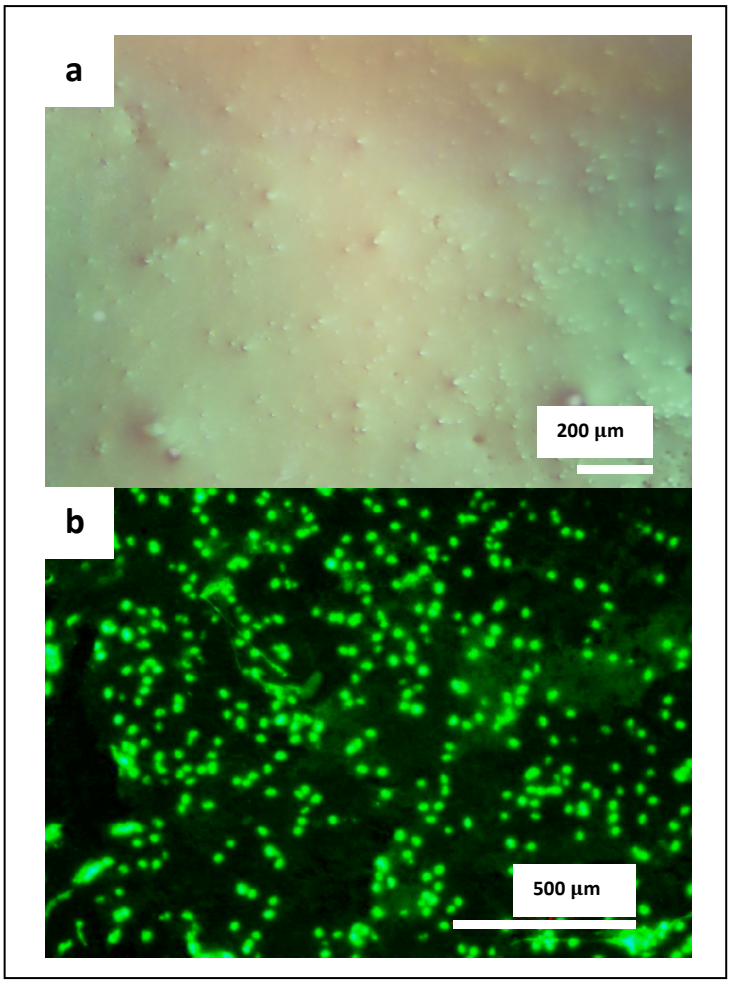

Figure 6.22: Optical microscopic images of the cells on bioscaffold. (a). without stain; (b). with fluorescent stain (b).

Chapter 7. Conclusion

The bioscaffold sensor can differentiate the pathological stage for the benign and malignant cancer cells. The different cancer cells from different origins (e.g. colon cancer vs. breast cancer) showed different impedance responses upon binding and metabolizing to the nanowire surface, to date never reported in literature, which will help collect new data for advancing the cancer biology. Mixing cancer cells with normal cells over a wide range has further validated this new cell-sensing technology. Quantifying the cancer drug's efficacy has been ongoing using other drugs old and new to the market. The sensing for the glucose effect showed a partial reversibility of the cancer-drug effect different for different types of the cancer cells. On this basis, the characteristic fingerprints of cancer cells have been concluded in the **Fig.7.1** for MCF7 cells, and in the **Fig.7.2** for the MDA-MB231, which may change the game in today's cancer-pathology labs, via thus-sensing other cells on the smart-bioscaffold.

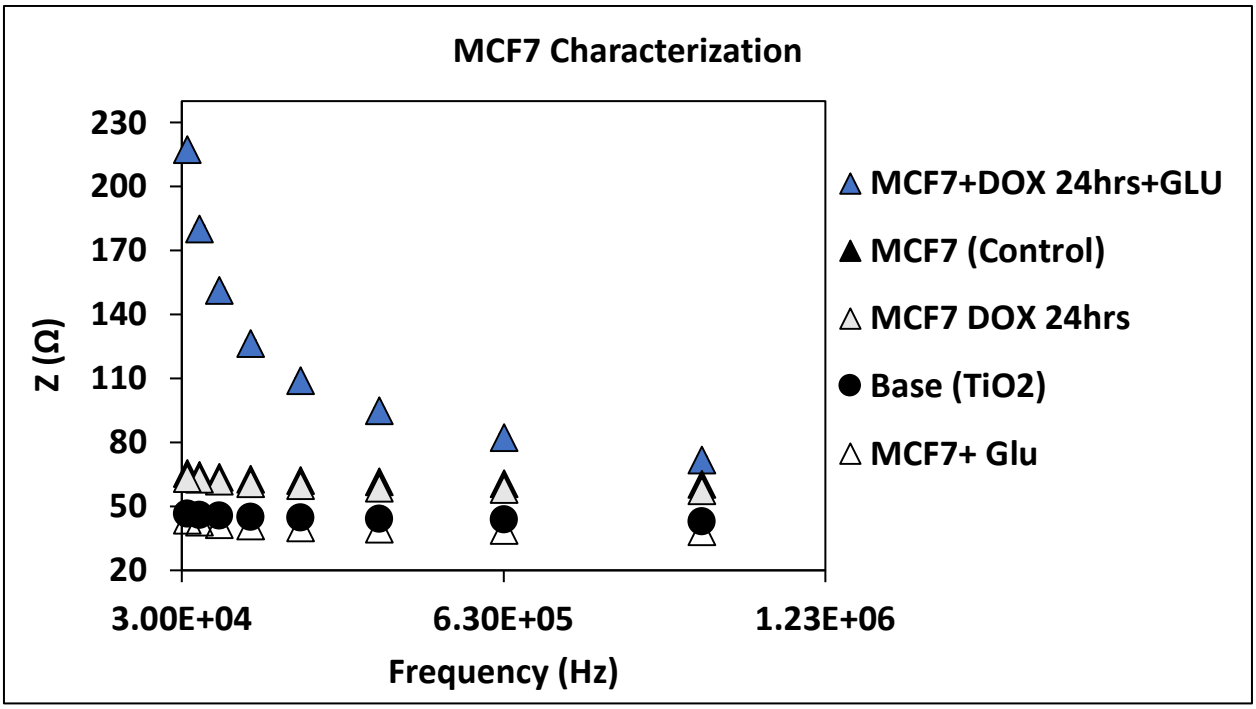

Figure 7.1: MCF7 characterization

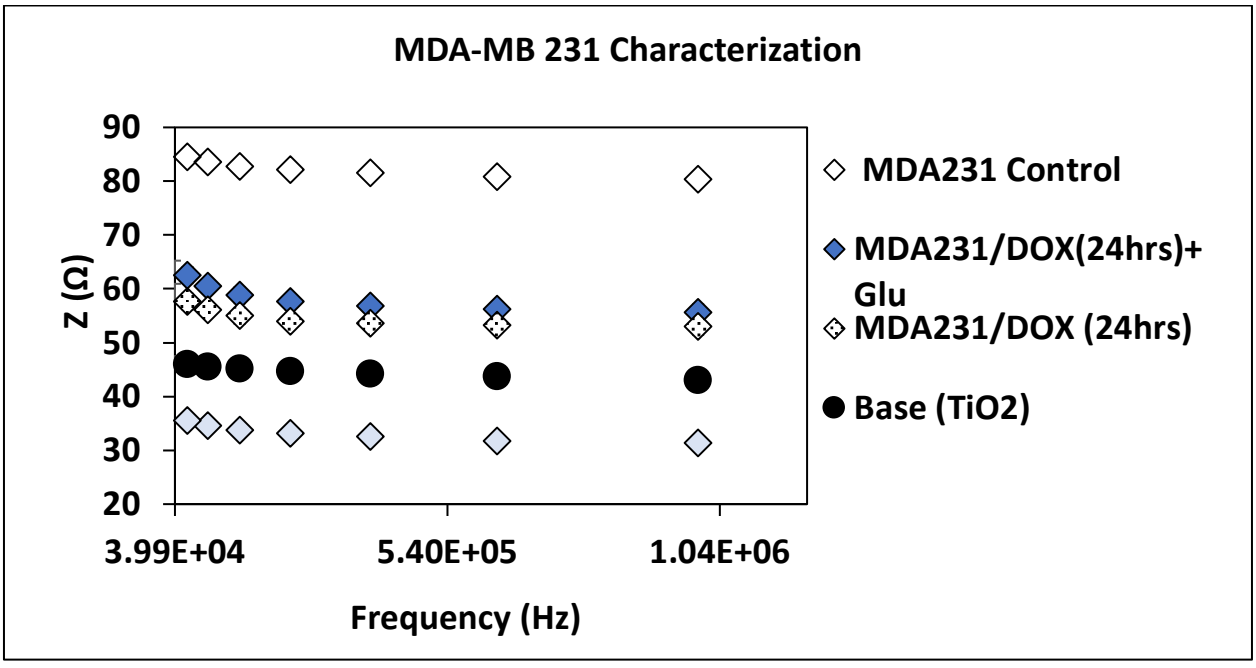

Figure 7.2: MDA-MB231 characterization.

Chapter 8. Future work

The findings from the experiments that are summarized in this dissertation have urged us to propose some low-risk, high-gain future work in the following:

1- To determine the impedance of more shapes, sizes and types on the smart bioscaffold.

2- To improve the sensitivity of the bioscaffold to the highest toward detecting single (or single digit) cell(s).

3- To expand the impedance sensing technology to covering all kinds of charge species besides the biological cells.

4- To study the impedance of tissues, bacteria, virus, eggs, and live insects on the bioscaffolds.

References

1. NewsCAP: American Cancer Society predicts new cancer cases and cancer deaths. *American Journal of Nursing* **118** (2018).
2. Destounis, S.V. et al. Can computer-aided detection with double reading of screening mammograms help decrease the false-negative rate? Initial experience. *Radiology* **232**, 578-584 (2004).
3. Cristofanilli, M. et al. Circulating tumor cells, disease progression, and survival in metastatic breast cancer. *New England Journal of Medicine* **351**, 781-791 (2004).
4. Wanekaya, A.K., Chen, W., Myung, N.V. & Mulchandani, A. Nanowire-based electrochemical biosensors. *Electroanalysis* **18**, 533-550 (2006).
5. Dong, W. et al. Multifunctional nanowire bioscaffolds on titanium. *Chemistry of Materials* **19**, 4454-4459 (2007).
6. Mader, S.S., Windelspecht, M. & Preston, L. *Essentials of biology*, Edn. 5th. (McGraw-Hill, NY; 2017).
7. Hardin, J., Bertoni, G., Kleinsmith, L.J. & Becker, W.M. Becker's world of the cell. (Benjamin, Boston 2012).
8. Lodish, H. et al. Molecular Cell Biology, Edn. 8. (Macmillan Learning, NewYork,NY; 2016).
9. Schaefer, T.J. & Wolford, R.W. Disorders of potassium. *Emergency Medicine Clinics of North America* **23**, 723-+ (2005).
10. Hsu, P.P. & Sabatini, D.M. Cancer cell metabolism: Warburg and beyond. *Cell* **134**, 703-707 (2008).
11. DeBerardinis, R.J., Lum, J.J., Hatzivassiliou, G. & Thompson, C.B. The biology of cancer: Metabolic reprogramming fuels cell growth and proliferation. *Cell Metabolism* **7**, 11-20 (2008).
12. Warburg, O. On the Origin of Cancer Cells. *Science* **123**, 309-314 (1956).
13. Gatenby, R.A. & Gillies, R.J. Why do cancers have high aerobic glycolysis? *Nature Reviews Cancer* **4**, 891-899 (2004).
14. Ortega, A.D. et al. Glucose avidity of carcinomas. *Cancer Letters* **276**, 125-135 (2009).
15. Moreno-Sanchez, R., Rodriguez-Enriquez, S., Marin-Hernandez, A. & Saavedra, E. Energy metabolism in tumor cells. *Febs Journal* **274**, 1393-1418 (2007).
16. Altenberg, B. & Greulich, K.O. Genes of glycolysis are ubiquitously overexpressed in 24 cancer classes. *Genomics* **84**, 1014-1020 (2004).
17. Lu, Y. et al. Common Human Cancer Genes Discovered by Integrated Gene-Expression Analysis. *Plos One* **2** (2007).
18. Amann, T. et al. GLUT1 Expression Is Increased in Hepatocellular Carcinoma and Promotes Tumorigenesis. *American Journal of Pathology* **174**, 1544-1552 (2009).

19. Meadows, A.L. et al. Metabolic and morphological differences between rapidly proliferating cancerous and normal breast epithelial cells. *Biotechnology Progress* **24**, 334-341 (2008).

20. Boag, J.M. et al. Altered glucose metabolism in childhood pre-B acute lymphoblastic leukaemia. *Leukemia* **20**, 1731-1737 (2006).

21. Marin-Hernandez, A., Gallardo-Perez, J.C., Ralph, S.J., Rodriguez-Enriquez, S. & Moreno-Sanchez, R. HIF-1 alpha Modulates Energy Metabolism in Cancer Cells by Inducing Over-Expression of Specific Glycolytic Isoforms. *Mini-Reviews in Medicinal Chemistry* **9**, 1084-1101 (2009).

22. Zancan, P., Sola-Penna, M., Furtado, C.M. & Da Silva, D. Differential expression of phosphofructokinase-1 isoforms correlates with the glycolytic efficiency of breast cancer cells. *Molecular Genetics and Metabolism* **100**, 372-378 (2010).

23. Korotchkina, L.G. & Patel, M.S. Site specificity of four pyruvate dehydrogenase kinase isoenzymes toward the three phosphorylation sites of human pyruvate dehydrogenase. *Journal of Biological Chemistry* **276**, 37223-37229 (2001).

24. Korotchkina, L.G., Sidhu, S. & Patel, M.S. Characterization of testis-specific isoenzyme of human pyruvate dehydrogenase. *Journal of Biological Chemistry* **281**, 9688-9696 (2006).

25. Bartrons, R. & Caro, J. Hypoxia, glucose metabolism and the Warburg's effect. *Journal of Bioenergetics and Biomembranes* **39**, 223-229 (2007).

26. Rankin, E.B. & Giaccia, A.J. The role of hypoxia-inducible factors in tumorigenesis. *Cell Death and Differentiation* **15**, 678-685 (2008).

27. Chiche, J., Brahimi-Horn, M.C. & Pouyssegur, J. Tumour hypoxia induces a metabolic shift causing acidosis: a common feature in cancer. *Journal of Cellular and Molecular Medicine* **14**, 771-794 (2010).

28. Helmlinger, G., Schell, A., Dellian, M., Forbes, N.S. & Jain, R.K. Acid production in glycolysis-impaired tumors provides new insights into tumor metabolism. *Clinical Cancer Research* **8**, 1284-1291 (2002).

29. Sonveaux, P. et al. Targeting lactate-fueled respiration selectively kills hypoxic tumor cells in mice. *Journal of Clinical Investigation* **118**, 3930-3942 (2008).

30. Laconi, E. The evolving concept of tumor microenvironments. *Bioessays* **29**, 738-744 (2007).

31. Gort, E.H., Groot, A.J., van der Wall, E., van Diest, P.J. & Vooijs, M.A. Hypoxic regulation of metastasis via hypoxia-inducible factors. *Current Molecular Medicine* **8**, 60-67 (2008).

32. Heddleston, J.M. et al. Hypoxia inducible factors in cancer stem cells. *British Journal of Cancer* **102**, 789-795 (2010).

33. Airley, R.E. & Mobasheri, A. Hypoxic regulation of glucose transport, anaerobic metabolism and angiogenesis in cancer: Novel pathways and targets for anticancer therapeutics. *Chemotherapy* **53**, 233-256 (2007).

34. Luo, W.B. et al. Pyruvate Kinase M2 Is a PHD3-Stimulated Coactivator for Hypoxia-Inducible Factor 1. *Cell* **145**, 732-744 (2011).

35. Moellering, R.E. et al. Acid treatment of melanoma cells selects for invasive phenotypes. *Clinical & Experimental Metastasis* **25**, 411-425 (2008).

36. Daniels, J.S. & Pourmand, N. Label-free impedance biosensors: Opportunities and challenges. *Electroanalysis* **19**, 1239-1257 (2007).

37. Huang, X.Q., Nguyen, D., Greve, D.W. & Domach, M.M. Simulation of microelectrode impedance changes due to cell growth. *Ieee Sensors Journal* **4**, 576-583 (2004).

38. Dean, D.A., Ramanathan, T., Machado, D. & Sundararajan, R. Electrical impedance spectroscopy study of biological tissues. *Journal of Electrostatics* **66**, 165-177 (2008).

39. Foster, K.R. & Schepps, J.L. DIELECTRIC-PROPERTIES OF TUMOR AND NORMAL-TISSUES AT RADIO THROUGH MICROWAVE-FREQUENCIES. *Journal of Microwave Power and Electromagnetic Energy* **16**, 107-119 (1981).

40. Blad, B. & Baldetorp, B. Impedance spectra of tumour tissue in comparison with normal tissue; A possible clinical application for electrical impedance tomography. *Physiological Measurement* **17**, A105-A115 (1996).

41. O'Rourke, A.P. et al. Dielectric properties of human normal, malignant and cirrhotic liver tissue: in vivo and ex vivo measurements from 0.5 to 20 GHz using a precision open-ended coaxial probe. *Physics in Medicine and Biology* **52**, 4707-4719 (2007).

42. Glickman, Y.A. et al. Electrical impedance scanning: a new approach to skin cancer diagnosis. *Skin Research and Technology* **9**, 262-268 (2003).

43. Lisdat, F. & Schafer, D. The use of electrochemical impedance spectroscopy for biosensing. *Analytical and Bioanalytical Chemistry* **391**, 1555-1567 (2008).

44. Chang, B.Y. & Park, S.M. Electrochemical Impedance Spectroscopy. *Annual Review of Analytical Chemistry, Vol 3* **3**, 207-229 (2010).

45. Park, S.M., Yoo, J.S., Chang, B.Y. & Ahn, E.S. Novel instrumentation in electrochemical impedance spectroscopy and a full description of an electrochemical system. *Pure and Applied Chemistry* **78**, 1069-1080 (2006).

46. Pethig, R. Dielectric-properties of biological-materials - biophysical and medical applications. *Ieee Transactions on Electrical Insulation* **19**, 453-474 (1984).

47. Davies, R.J. Underlying Mechanisms Involved in Surface Electrical Potential Measurements for the Diagnosis of Breast Cancer: An Electrophysiological Approach to Cancer Diagnosis. (Springer, Berlin, Heidelberg; 1996).

48. Goller, D.A., Weidema, W.F. & Davies, R.J. Transmural electrical potential difference as an early marker in colon cancer. *Archives of Surgery* **121**, 345-350 (1986).

49. Morimoto, T. et al. Measurement of the electrical bioimpedance of breast-tumors. *European Surgical Research* **22**, 86-92 (1990).

50. Jossinet, J. Variability of impedivity in normal and pathological breast tissue. *Medical & Biological Engineering & Computing* **34**, 346-350 (1996).

51. Jossinet, J. The impedivity of freshly excised human breast tissue. *Physiological Measurement* **19**, 61-75 (1998).

52. Foster, K.R. & Schwan, H.P. Dielectric-properties of tissues and biological-materials - a critical-review. *Critical Reviews in Biomedical Engineering* **17**, 25-104 (1989).

53. Schwan, H.P. Electrical properties of tissue and cell suspensions. *Advances in biological and medical physics* **5**, 147-209 (1957).

54. Giaever, I. & Keese, C.R. Monitoring fibroblast behavior in tissue-culture with an applied electric-field. *Proceedings of the National Academy of Sciences of the United States of America-Biological Sciences* **81**, 3761-3764 (1984).

55. Ng, E.Y.K., Sree, S.V., Ng, K.H. & Kaw, G. The use of tissue electrical characteristics for breast cancer detection: A perspective review. *Technology in Cancer Research & Treatment* **7**, 295-308 (2008).

56. Pethig, R. Dielectric properties of body tissues. *Clinical physics and physiological measurement : an official journal of the Hospital Physicists' Association, Deutsche Gesellschaft fur Medizinische Physik and the European Federation of Organisations for Medical Physics* **8 Suppl A**, 5-12 (1987).

57. Polk, C. & Postow, E. CRC handbook of biological effects of electromagnetic fields. *CRC handbook of biological effects of electromagnetic fields.*, i-xiii, 1-503 (1986).

58. Srinivasaraghavan, V., Strobl, J. & Agah, M. Bioimpedance rise in response to histone deacetylase inhibitor is a marker of mammary cancer cells within a mixed culture of normal breast cells. *Lab on a Chip* **12**, 5168-5179 (2012).

59. Wang, L., Wang, H., Mitchelson, K., Yu, Z.Y. & Cheng, J. Analysis of the sensitivity and frequency characteristics of coplanar electrical cell-substrate impedance sensors. *Biosensors & Bioelectronics* **24**, 14-21 (2008).

60. Han, A., Yang, L. & Frazier, A.B. Quantification of the heterogeneity in breast cancer cell lines using whole-cell impedance spectroscopy. *Clinical Cancer Research* **13**, 139-143 (2007).

61. Yang, L.J., Arias, L.R., Lane, T.S., Yancey, M.D. & Mamouni, J. Real-time electrical impedance-based measurement to distinguish oral cancer cells and non-cancer oral epithelial cells. *Analytical and Bioanalytical Chemistry* **399**, 1823-1833 (2011).

62. Qiao, G.F. et al. Bioimpedance Analysis for the Characterization of Breast Cancer Cells in Suspension. *Ieee Transactions on Biomedical Engineering* **59**, 2321-2329 (2012).

63. Nwankire, C.E. et al. Label-free impedance detection of cancer cells from whole blood on an integrated centrifugal microfluidic platform. *Biosensors & Bioelectronics* **68**, 382-389 (2015).

64. Ehret, R. et al. Monitoring of cellular behaviour by impedance measurements on interdigitated electrode structures. *Biosensors & Bioelectronics* **12**, 29-41 (1997).

65. Asphahani, F. et al. Influence of cell adhesion and spreading on impedance characteristics of cell-based sensors. *Biosensors & Bioelectronics* **23**, 1307-1313 (2008).

66. Mitra, P., Keese, C.R. & Giaever, I. Electric measurements can be used to monitor the attachment and spreading of cells in tissue-culture. *Biotechniques* **11**, 504-& (1991).

67. Wegener, J., Keese, C.R. & Giaever, I. Electric cell-substrate impedance sensing (ECIS) as a noninvasive means to monitor the kinetics of cell spreading to artificial surfaces. *Experimental Cell Research* **259**, 158-166 (2000).

68. Ghenim, L. et al. Monitoring impedance changes associated with motility and mitosis of a single cell. *Lab on a Chip* **10**, 2546-2550 (2010).

69. Giaever, I. & Keese, C.R. Micromotion of mammalian-cells measured electrically. *Proceedings of the National Academy of Sciences of the United States of America* **88**, 7896-7900 (1991).

70. Wang, L., Zhu, J., Deng, C., Xing, W.L. & Cheng, J. An automatic and quantitative on-chip cell migration assay using self-assembled monolayers combined with real-time cellular impedance sensing. *Lab on a Chip* **8**, 872-878 (2008).

71. Vistejnova, L. et al. The comparison of impedance-based method of cell proliferation monitoring with commonly used metabolic-based techniques. *Neuroendocrinology Letters* **30**, 121-127 (2009).

72. Asphahani, F. et al. Single-cell bioelectrical impedance platform for monitoring cellular response to drug treatment. *Physical Biology* **8** (2011).

73. Male, K.B., Lachance, B., Hrapovic, S., Sunahara, G. & Luong, J.H.T. Assessment of cytotoxicity of quantum dots and gold nanoparticles using cell-based. impedance spectroscopy. *Analytical Chemistry* **80**, 5487-5493 (2008).

74. Opp, D. et al. Use of electric cell-substrate impedance sensing to assess in vitro cytotoxicity. *Biosensors & Bioelectronics* **24**, 2625-2629 (2009).

75. Ramasamy, S., Bennet, D. & Kim, S. Drug and bioactive molecule screening based on a bioelectrical impedance cell culture platform. *International Journal of Nanomedicine* **9**, 5789-5809 (2014).

76. Kuo, Y.C. et al. Transforming growth factor-beta induces CD44 cleavage that promotes migration of MDA-MB-435s cells through the up-regulation of membrane type 1-matrix metalloproteinase. *International Journal of Cancer* **124**, 2568-2576 (2009).

77. Stanica, L. et al. Electric Cell-Substrate Impedance Sensing of Cellular Effects under Hypoxic Conditions and Carbonic Anhydrase Inhibition. *Journal of Sensors* (2017).

78. Sun, Q., Wang, Q., Rao, B.K. & Jena, P. Electronic structure and bonding of Au on a SiO2 cluster: A nanobullet for tumors. *Physical Review Letters* **93** (2004).

79. Mauck, R.L. et al. Engineering on the Straight and Narrow: The Mechanics of Nanofibrous Assemblies for Fiber-Reinforced Tissue Regeneration. *Tissue Engineering Part B-Reviews* **15**, 171-193 (2009).

80. Lee, J., Cuddihy, M.J. & Kotov, N.A. Three-dimensional cell culture matrices: State of the art. *Tissue Engineering Part B-Reviews* **14**, 61-86 (2008).

81. Ma, P.X. & Zhang, R.Y. Synthetic nano-scale fibrous extracellular matrix. *Journal of Biomedical Materials Research* **46**, 60-72 (1999).

82. Ellis-Behnke, R.G. et al. Nano neuro knitting: Peptide nanofiber scaffold for brain repair and axon regeneration with functional return of vision. *Proceedings of the National Academy of Sciences of the United States of America* **103**, 5054-5059 (2006).

83. Koh, H.S., Yong, T., Chan, C.K. & Ramakrishna, S. Enhancement of neurite outgrowth using nano-structured scaffolds coupled with laminin. *Biomaterials* **29**, 3574-3582 (2008).

84. He, H.X., Li, C.Z. & Tao, N.J. Conductance of polymer nanowires fabricated by a combined electrodeposition and mechanical break junction method. *Applied Physics Letters* **78**, 811-813 (2001).

85. Doshi, J. & Reneker, D.H. Electrospinning process and applications of electrospun fibers. *Journal of Electrostatics* **35**, 151-160 (1995).

86. Reneker, D.H., Yarin, A.L., Fong, H. & Koombhongse, S. Bending instability of electrically charged liquid jets of polymer solutions in electrospinning. *Journal of Applied Physics* **87**, 4531-4547 (2000).

87. Barnes, C.P., Sell, S.A., Boland, E.D., Simpson, D.G. & Bowlin, G.L. Nanofiber technology: Designing the next generation of tissue engineering scaffolds. *Advanced Drug Delivery Reviews* **59**, 1413-1433 (2007).

88. Patel, S. et al. Bioactive nanofibers: Synergistic effects of nanotopography and chemical signaling on cell guidance. *Nano Letters* **7**, 2122-2128 (2007).

89. Kameoka, J. & Craighead, H.G. Fabrication of oriented polymeric nanofibers on planar surfaces by electrospinning. *Applied Physics Letters* **83**, 371-373 (2003).

90. Kameoka, J. et al. A scanning tip electrospinning source for deposition of oriented nanofibres. *Nanotechnology* **14**, 1124-1129 (2003).

91. Liu, H.Q., Kameoka, J., Czaplewski, D.A. & Craighead, H.G. Polymeric nanowire chemical sensor. *Nano Letters* **4**, 671-675 (2004).

92. Theron, A., Zussman, E. & Yarin, A.L. Electrostatic field-assisted alignment of electrospun nanofibres. *Nanotechnology* **12**, 384-390 (2001).

93. Li, D., Wang, Y.L. & Xia, Y.N. Electrospinning of polymeric and ceramic nanofibers as uniaxially aligned arrays. *Nano Letters* **3**, 1167-1171 (2003).

94. Zong, X.H. et al. Structure and morphology changes during in vitro degradation of electrospun poly(glycolide-co-lactide) nanofiber membrane. *Biomacromolecules* **4**, 416-423 (2003).

95. Sell, S.A., McClure, M.J., Garg, K., Wolfe, P.S. & Bowlin, G.L. Electrospinning of collagen/biopolymers for regenerative medicine and cardiovascular tissue engineering. *Advanced Drug Delivery Reviews* **61**, 1007-1019 (2009).

96. Jang, J.H., Castano, O. & Kim, H.W. Electrospun materials as potential platforms for bone tissue engineering. *Advanced Drug Delivery Reviews* **61**, 1065-1083 (2009).

97. Xie, J.W. et al. The differentiation of embryonic stem cells seeded on electrospun nanofibers into neural lineages. *Biomaterials* **30**, 354-362 (2009).

98. Pedrotty, D.M. et al. Engineering skeletal myoblasts: roles of three-dimensional culture and electrical stimulation. *American Journal of Physiology-Heart and Circulatory Physiology* **288**, H1620-H1626 (2005).

99. Teasdale, P.R. & Wallace, G.G. Molecular recognition using conducting polymers - basis of an electrochemical sensing technology. *Analyst* **118**, 329-334 (1993).

100. Bangar, M.A., Shirale, D.J., Chen, W., Myung, N.V. & Mulchandani, A. Single Conducting Polymer Nanowire Chemiresistive Label-Free Immunosensor for Cancer Biomarker. *Analytical Chemistry* **81**, 2168-2175 (2009).

101. Pan, J.H. et al. Self-Template Synthesis of Porous Perovskite Titanate Solid and Hollow Submicrospheres for Photocatalytic Oxygen Evolution and Mesoscopic Solar Cells. *Acs Applied Materials & Interfaces* **7**, 14859-14869 (2015).

102. Kobayashi, Y., Iizuka, Y., Tanase, T. & Konno, M. Low-temperature synthesis of single-phase barium strontium titanate thin film with a nm-seeding technique and its dielectric properties. *Journal of Sol-Gel Science and Technology* **33**, 315-321 (2005).

103. Pan, H.F. et al. Construction of layer-by-layer assembled chitosan/titanate nanotubes based nanocoating on cotton fabrics: flame retardant performance and combustion behavior. *Cellulose* **22**, 911-923 (2015).

104. Li, D. & Xia, Y.N. Fabrication of titania nanofibers by electrospinning. *Nano Letters* **3**, 555-560 (2003).

105. Wu, D. et al. Sequence of events for the formation of titanate nanotubes, nanofibers, nanowires, and nanobelts. *Chemistry of Materials* **18**, 547-553 (2006).

106. Miao, Z. et al. Electrochemically induced sol-gel preparation of single-crystalline TiO2 nanowires. *Nano Letters* **2**, 717-720 (2002).

107. Sander, M.S., Cote, M.J., Gu, W., Kile, B.M. & Tripp, C.P. Template-assisted fabrication of dense, aligned arrays of titania nanotubes with well-controlled dimensions on substrates. *Advanced Materials* **16**, 2052-+ (2004).

108. Shchukin, D.G. et al. Layer-by-layer assembled nanocontainers for self-healing corrosion protection. *Advanced Materials* **18**, 1672-+ (2006).

109. Ruan, C.M., Paulose, M., Varghese, O.K., Mor, G.K. & Grimes, C.A. Fabrication of highly ordered TiO2 nanotube arrays using an organic electrolyte. *Journal of Physical Chemistry B* **109**, 15754-15759 (2005).

110. Tian, Z.R.R., Voigt, J.A., Liu, J., McKenzie, B. & Xu, H.F. Large oriented arrays and continuous films of TiO2-based nanotubes. *Journal of the American Chemical Society* **125**, 12384-12385 (2003).

111. Huang, H.H., Pan, S.J. & Lu, F.H. Surface electrochemical impedance in situ monitoring of cell-cultured titanium with a nano-network surface layer. *Scripta Materialia* **53**, 1037-1042 (2005).

112. Dong, W. et al. Biocompatible nanofiber scaffolds on metal for controlled release and cell colonization. *Nanomedicine-Nanotechnology Biology and Medicine* **2**, 248-252 (2006).

113. Lakadamyali, F. & Reisner, E. Photocatalytic H-2 evolution from neutral water with a molecular cobalt catalyst on a dye-sensitised TiO2 nanoparticle. *Chemical Communications* **47**, 1695-1697 (2011).

114. Xia, Y.B. & Yin, L.W. Core-shell structured alpha-Fe2O3@TiO2 nanocomposites with improved photocatalytic activity in the visible light region. *Physical Chemistry Chemical Physics* **15**, 18627-18634 (2013).

115. Tanaka, A., Fuku, K., Nishi, T., Hashimoto, K. & Kominami, H. Functionalization of Au/TiO2 Plasmonic Photocatalysts with Pd by Formation of a Core-Shell Structure for Effective Dechlorination of Chlorobenzene under Irradiation of Visible Light. *Journal of Physical Chemistry C* **117**, 16983-16989 (2013).

116. Fang-Xing, X. et al. Metal-Cluster-Decorated TiO2 Nanotube Arrays: A Composite Heterostructure toward Versatile Photocatalytic and Photoelectrochemical Applications. *Small* **11**, 554-567 (2015).

117. Quan, L.N. et al. Soft-template-carbonization route to highly textured mesoporous carbon-TiO2 inverse opals for efficient photocatalytic and photoelectrochemical applications. *Physical Chemistry Chemical Physics* **16**, 9023-9030 (2014).

118. Zhang, N., Yang, M.Q., Tang, Z.R. & Xu, Y.J. Toward Improving the Graphene-Semiconductor Composite Photoactivity via the Addition of Metal Ions as Generic Interfacial Mediator. *Acs Nano* **8**, 623-633 (2014).

119. Banerjee, A. The design, fabrication, and photocatalytic utility of nanostructured semiconductors: focus on TiO2-based nanostructures. **4**, 35-65 (2011).

120. Casarin, M., Vittadini, A. & Selloni, A. First Principles Study of Hydrated/Hydroxylated TiO2 Nanolayers: From Isolated Sheets to Stacks and Tubes. *Acs Nano* **3**, 317-324 (2009).

121. Ide, Y., Nakasato, Y. & Ogawa, M. Molecular Recognitive Photocatalysis Driven by the Selective Adsorption on Layered Titanates. *Journal of the American Chemical Society* **132**, 3601-3604 (2010).

122. Bavykin, D.V. & Walsh, F.C. Elongated Titanate Nanostructures and Their Applications. *European Journal of Inorganic Chemistry*, 977-997 (2009).

123. Fujishima, A. & Honda, K. Electrochemical photolysis of water at a semiconductor electrode. *Nature* **238**, 37-+ (1972).

124. Paz, Y. Application of TiO2 photocatalysis for air treatment: Patents' overview. *Applied Catalysis B-Environmental* **99**, 448-460 (2010).

125. Kim, Y.I., Salim, S., Huq, M.J. & Mallouk, T.E. Visible-light photolysis of hydrogen iodide using sensitized layered semiconductor particles. *Journal of the American Chemical Society* **113**, 9561-9563 (1991).

126. Sasaki, T., Watanabe, M., Hashizume, H., Yamada, H. & Nakazawa, H. Macromolecule-like aspects for a colloidal suspension of an exfoliated titanate. Pairwise association of nanosheets and dynamic reassembling process initiated from it. *Journal of the American Chemical Society* **118**, 8329-8335 (1996).

127. Sukpirom, N. & Lerner, M.M. Preparation of organic-inorganic nanocomposites with a layered titanate. *Chemistry of Materials* **13**, 2179-2185 (2001).

128. Grieshaber, D., MacKenzie, R., Voros, J. & Reimhult, E. Electrochemical biosensors - Sensor principles and architectures. *Sensors* **8**, 1400-1458 (2008).

129. McNamara, K. & Tofail, S.A.M. Nanoparticles in biomedical applications. *Advances in Physics-X* **2**, 54-88 (2017).

130. Bhalla, N., Jolly, P., Formisano, N. & Estrela, P. Introduction to biosensors. *Biosensor Technologies for Detection of Biomolecules* **60**, 1-8 (2016).

131. Adams, K.L., Puchades, M. & Ewing, A.G. In Vitro Electrochemistry of Biological Systems. *Annual Review of Analytical Chemistry* **1**, 329-355 (2008).

132. Zhang, Y.H., Zhang, B. & White, H.S. Electrochemistry of nanopore electrodes in low ionic strength solutions. *Journal of Physical Chemistry B* **110**, 1768-1774 (2006).

133. Cui, Y., Wei, Q.Q., Park, H.K. & Lieber, C.M. Nanowire nanosensors for highly sensitive and selective detection of biological and chemical species. *Science* **293**, 1289-1292 (2001).

134. Zheng, G.F., Patolsky, F., Cui, Y., Wang, W.U. & Lieber, C.M. Multiplexed electrical detection of cancer markers with nanowire sensor arrays. *Nature Biotechnology* **23**, 1294-1301 (2005).

135. Kim, A. et al. Ultrasensitive, label-free, and real-time immunodetection using silicon field-effect transistors. *Applied Physics Letters* **91** (2007).

136. Zhang, G.J., Chua, J.H., Chee, R.E., Agarwal, A. & Wong, S.M. Label-free direct detection of MiRNAs with silicon nanowire biosensors. *Biosensors & Bioelectronics* **24**, 2504-2508 (2009).

137. Nelson, P.T. et al. Microarray-based, high-throughput gene expression profiling of microRNAs. *Nature Methods* **1**, 155-161 (2004).

138. Abdolahad, M., Shashaani, H., Janmaleki, M. & Mohajerzadeh, S. Silicon nanograss based impedance biosensor for label free detection of rare metastatic cells among primary cancerous colon cells, suitable for more accurate cancer staging. *Biosensors & Bioelectronics* **59**, 151-159 (2014).

139. Shashaani, H. et al. Silicon nanowire based biosensing platform for electrochemical sensing of Mebendazole drug activity on breast cancer cells. *Biosensors & Bioelectronics* **85**, 363-370 (2016).

140. Alikhani, A., Gharooni, M., Abiri, H., Farokhmanesh, F. & Abdolahad, M. Tracing the pH dependent activation of autophagy in cancer cells by silicon nanowire-based impedance biosensor. *Journal of Pharmaceutical and Biomedical Analysis* **154**, 158-165 (2018).

141. Zhang, X.Y. et al. Synthesis of ordered single crystal silicon nanowire arrays. *Advanced Materials* **13**, 1238-1241 (2001).

142. Liu, S.Q. & Chen, A.C. Coadsorption of horseradish peroxidase with thionine on TiO2: Nanotubes for biosensing. *Langmuir* **21**, 8409-8413 (2005).

143. Xie, Y.B., Zhou, L.M. & Huang, H.T. Bioelectrocatalytic application of titania nanotube array for molecule detection. *Biosensors & Bioelectronics* **22**, 2812-2818 (2007).

144. Shi, Y.T., Yuan, R., Chai, Y.Q., Tang, M.Y. & He, X.L. Amplification of antigen-antibody interactions via back-filling of HRP on the layer-by-layer self-assembling of thionine and gold nanoparticles films on titania nanoparticles/gold nanoparticles-coated Au electrode. *Journal of Electroanalytical Chemistry* **604**, 9-16 (2007).

145. Yuan, S., Peng, D.H., Song, D.D. & Gong, J.M. Layered titanate nanosheets as an enhanced sensing platform for ultrasensitive stripping voltammetric detection of mercury(II). *Sensors and Actuators B-Chemical* **181**, 432-438 (2013).

146. Doong, R.A. & Shih, H.M. Glutamate optical biosensor based on the immobilization of glutamate dehydrogenase in titanium dioxide sol-gel matrix. *Biosensors & Bioelectronics* **22**, 185-191 (2006).

147. Li, J.L., Han, T., Wei, N.N., Du, J.Y. & Zhao, X.W. Three-dimensionally ordered macroporous (3DOM) gold-nanoparticle-doped titanium dioxide (GTD) photonic crystals modified electrodes for hydrogen peroxide biosensor. *Biosensors & Bioelectronics* **25**, 773-777 (2009).

148. Yin, Z.F., Wu, L., Yang, H.G. & Su, Y.H. Recent progress in biomedical applications of titanium dioxide. *Physical Chemistry Chemical Physics* **15**, 4844-4858 (2013).

149. Wang, R.H., Ruan, C.M., Kanayeva, D., Lassiter, K. & Li, Y.B. TiO2 nanowire bundle microelectrode based impedance immunosensor for rapid and sensitive detection of Listeria monocytogenes. *Nano Letters* **8**, 2625-2631 (2008).

150. Luo, Y.P., Liu, H.Q., Rui, Q. & Tian, Y. Detection of Extracellular H2O2 Released from Human Liver Cancer Cells Based on TiO2 Nanoneedles with Enhanced Electron Transfer of Cytochrome c. *Analytical Chemistry* **81**, 3035-3041 (2009).

151. Nicolini, J.V., Ferraz, H.C. & de Resende, N.S. Immobilization of horseradish peroxidase on titanate nanowires for biosensing application. *Journal of Applied Electrochemistry* **46**, 17-25 (2016).

152. Brad, A.J. & Faulkner, L.R. Electrochemical Methods: Fundamentals and Applications, Edn. 2. (Wiley, USA; 2000).

153. Park, J. & Regalbuto, J.R. Simple, accurate determination of oxide pzc and the strong buffering effect of oxide surfaces at incipient wetness. *Journal of Colloid and Interface Science* **175**, 239-252 (1995).

154. Lovitt, C.J., Shelper, T.B. & Avery, V.M. Doxorubicin resistance in breast cancer cells is mediated by extracellular matrix proteins. *Bmc Cancer* **18** (2018).

155. Chen, F. in Chemistry and biochemistry, Vol. P.hD 91 (University of Arkansas, Theses and Dissertations 2011).

156. Dobrzynska, I., Skrzydlewska, E. & Figaszewski, Z.A. Changes in Electric Properties of Human Breast Cancer Cells. *Journal of Membrane Biology* **246**, 161-166 (2013).

157. Ziegler, Y.S., Moresco, J.J., Tu, P.G., Yates, J.R. & Nardulli, A.M. Plasma Membrane Proteomics of Human Breast Cancer Cell Lines Identifies Potential Targets for Breast Cancer Diagnosis and Treatment. *Plos One* **9** (2014).

158. He, M.W., Guo, S. & Li, Z.L. In situ characterizing membrane lipid phenotype of breast cancer cells using mass spectrometry profiling. *Scientific Reports* **5** (2015).

159. Szachowicz-Petelska, B., Dobrzynska, I., Sulkowski, S. & Figaszewski, Z. Characterization of the cell membrane during cancer transformation. *Journal of Environmental Biology* **31**, 845-850 (2010).

160. Sakai, K. et al. Composition and turnover of phospholipids and neutral lipids in human breast-cancer and reference tissues. *Carcinogenesis* **13**, 579-584 (1992).

161. Teoh, S.T., Ogrodzinski, M.P., Ross, C., Hunter, K.W. & Lunt, S.Y. Sialic Acid Metabolism: A Key Player in Breast Cancer Metastasis Revealed by Metabolomics. *Frontiers in Oncology* **8** (2018).

162. Halama, A. et al. Metabolic signatures differentiate ovarian from colon cancer cell lines. *Journal of Translational Medicine* **13** (2015).

163. Tacar, O., Sriamornsak, P. & Dass, C.R. Doxorubicin: an update on anticancer molecular action, toxicity and novel drug delivery systems. *Journal of Pharmacy and Pharmacology* **65**, 157-170 (2013).

164. Kovalchuk, O. et al. Involvement of microRNA-451 in resistance of the MCF-7 breast cancer cells to chemotherapeutic drug doxorubicin. *Molecular Cancer Therapeutics* **7**, 2152-2159 (2008).

165. Ren, W.Z. et al. Enhanced doxorubicin transport to multidrug resistant breast cancer cells via TiO2 nanocarriers. *Rsc Advances* **3**, 20855-20861 (2013).